

Ministry of Education and Science of Ukraine

Sumy National Agrarian University

Qualifying scientific
work on the rights of the manuscript

Du Xin

UDC621.8:621.09.048

DISSERTATION

**Technological support of strength and durability at the manufacture
and repair of component parts for branch mechanical engineering**

133 – Industrial machinery engineering

13 – Mechanical engineering

Applies for the degree of the doctor of philosophy

The dissertation contains the results of own research. The use of other authors'
ideas, results and texts link to the source_____ **Du Xin**

Scientific supervisor: Viacheslav Tarellyk,

Professor, Doctor of Technical Sciences,

Academician of the Academy of Sciences of Ukraine.

Sumy – 2023

ANNOTATION

Du Xin Technological support of strength and durability at the manufacture and repair of component parts for branch mechanical engineering. -The qualifying scientific work based on the manuscript.

The dissertation on competition of a scientific degree of the doctor of philosophy in the field of knowledge 13-Mechanical engineering on a specialty 133-Branch mechanical engineering. -Sumy National Agrarian University, Sumy, 2023

This dissertation is dedicated to solving practical scientific and technological problems in the branch mechanical engineering field: Friction causes a large number of mechanical products to be damaged.

Human beings have been exploring theories and methods to prolong the life of mechanical equipment and parts. The research of wear mechanism has positive significance for improving the life of mechanical parts and repairing parts. Wear is generated on the surface of mechanical equipment. The failed parts can be repaired by surface processing technology. Surface processing technology has been used in remanufacturing engineering. The research of wear and wear-resistant materials has always been the most active field of tribology research. The development of new materials and processes has been the hotspot of wear application research. The application research of surface coating and surface modification has become the most active field of tribology research.

The present research focuses on wear caused by linear reciprocating motion in an open environment. It explores the theory and methodology of using remanufacturing technology to continuously improve the wear resistance and enhance the life of parts.

One of the difficulties in wear research is the research on the anti-wear and anti-friction properties of coatings under extreme conditions.

With the rapid development of composite surface coating theory, new coating theories appear. It is of great significance to redesign the anti-wear and anti-friction coating by using the new theory.

Since electro-spark deposition (tantamount to electro-spark alloying) has the characteristics of energy saving and environmental protection, low use cost and convenient operation, it is of positive significance to combine ESD technology with composite coating theory to explore new coatings. In this study, high toughness materials, high wear-resistant materials, and friction-reducing materials are used for composite, in order to explore new friction-reducing and wear-resistant coatings.

The development of pneumatic impact deposition technology can improve the traditional deposition process and greatly improve the quality of friction-reducing coating, which is a new attempt in science.

This new composite coating solution reduces energy consumption and pollution, which is important for low wear and high service life of mechanical equipment. It has promotional value for parts with the same wear mechanism. It is also very important to save a lot of resources and reduce a lot of business money.

The object of research is a technological process for forming functional coatings on the pin shaft of the locking mechanism for the lifting device.

The subject of research is the regularities of the technological process for forming a surface with specified performance properties, which ensure the necessary quality (durability, wear resistance, workability) of the pin shaft surface of the locking mechanism for the lifting device.

The purpose of the study is to improve the quality of the surface layers at manufacturing and remanufacturing the pin shaft of the locking mechanism for the lifting device of an electric car battery by forming the composite multilayer coatings of the SKH51+WC+B83 composition on its wear surfaces with the use of the method of electro-spark deposition.

To achieve this goal, it is necessary to solve the following **tasks**:

1. To conduct an analysis of the existing modern methods and technologies for repairing component parts for branch mechanical engineering in accordance with the ESD characteristics.

2. To conduct an analysis of modern materials for electrode – tools to provide for a comprehensive assessment of the properties of the surface coatings applied to improve the overall technical characteristics of the surface.

3. To conduct a research on the formation of wear-resistant composite coatings and compare various surface properties.

4. To conduct a research of the defects of low-temperature soft metal deposition and improve the existing repair technology.

5. To investigate the effect of the ESD coating repair technology on the accuracy of the surface obtained.

6. To introduce the research results into the engineering practice of enterprise remanufacturing.

In the introduction, the topic and scientific task of the thesis are described, the aims and tasks of the research are formulated, and the scientific novelty and practical value of the received results are specified, as well as information on the approval, structure and scope of work.

In the First Chapter, the development of remanufacturing engineering was introduced, and several major remanufacturing common processes were compared. Because of the cost and convenience, electro-spark deposition technology was emphasized. This chapter provided an overview of the history of ESD deposition, the recent research progress and optimization of the ESD process.

In the Second Chapter, the basic theories and research methods were mainly introduced. The working principle of the ESD deposition method was introduced. Three different principles of vibrating electrodes were presented. The basic theory of coating formation by the ESD method was analyzed. It included corrosion mechanism of ESD, pulse energy theory, the metal melting theory and heat transfer simplified model. Also in the chapter, there was presented the surface property testing equipment, which could perform surface morphology, elemental composition, roughness, hardness and tribological properties. Finally, experimental methods and coating deposition processes were described.

In the Third Chapter, there were described the methods for increasing surface abrasion resistance coating, which have been being constantly improved. (1) Graphite deposited on the surface of 45 steel can improve the abrasion resistance of the material surface. According to abrasion width, Taguchi orthogonal method was used to find out the optimum process on the graphite deposition. Thereby, the optimum parameters of ESD process were determined, which were efficiency, voltage, current frequency and work time. Since the surface had hard phase Fe_3C , the carburized surface was 59.96% less abrasion mark width than the non-carburized surface. The surface wear resistance of the substrate was increased.

(2) The high-speed steel SKH51 was used for electro-spark deposition on the surface of 45 steel. The SKH51 material has good wear resistance and excellent impact

toughness, which is better than that of carburized 45 steel. Therefore, the SKH51 material was used as a transition layer, so that the more wear resistant material WC can be deposited later to form a gradient coating. The normalization method and weighting factor method were used to evaluate the different performance parameters of the coating, and the optimal coating deposition process parameters were obtained.

(3) Titanium and titanium alloys, Nb, and Zr were carburized on the surface, and hard phases such as TiC, ZrC, and NbC were formed in situ. The graphene oxide gel coatings were obtained by coating materials. By comparing these coatings, it was found that SKH51+WC+B83 composite coating had better coating performance.

(4) For low-temperature soft metals, a new deposition process was created to enhance the surface quality. Continuous deposition was carried out with the use of pneumatic impact deposition and RC low-energy circuits. Considering graphite powder for lubrication, it tends to come off easily.

(5) GO gel and sodium silicate coatings were utilized. Because graphite powder and sodium silicate composite coatings had the poor abrasion resistance, GO gel coating had good wear resistance. It can improve surface accuracy and reduce friction.

In the Fourth Chapter, there was described the ESD process, which was applied in the battery replacement equipment of electric vehicle. The test results of the coating for the four versions of solutions were summarized and analyzed, and the best industrial application solution was determined based on the wear resistance test.

Because some of the locking device normal cannot return, a composite coating solution was proposed on the pin shafts. The formed coating not only met the requirements of wear resistance, but also had a smaller friction and a certain degree of corrosion resistance. The solution of SKH51+WC+B83 can effectively reduce the cost,

reduce the pollution in the electroplating process, and additionally, it can realize the long life of the parts.

In the Fifth Chapter, the research work of the PhD is summarized, conclusions are drawn and recommendations for future research are made.

According to the set purpose and tasks in work the following **results** have been obtained:

1. When using Taguchi's orthogonal method, according to the abrasion width, the optimal parameters of the surface carburizing process of steel 45 have been set: the efficiency of 50%, the voltage of 35 V, the current frequency of 180 Hz, and the operating time of 360 s. As a result, the average wear width was 268.206 μm , and the wear depth was 2.999 μm , which is 59.96% less than for steel 45 without carburizing.

2. Using the method of normalization and the method of weighting coefficients to estimate the operating parameters of the coating at the maximum value of the objective function of 0.687887, the optimal parameters of the process of electro-spark deposition of the SKH51 coating on the surface of steel 45, namely, the current frequency of 300 Hz, the voltage of 44 V, the efficiency of 30%, and the rotation speed of 150 rpm have been determined.

3. While comparing the composite coatings of different composition, as an optimal solution, there has been recognized the composite coating formed according to the scheme of SKH51+WC+B83. With the gradient coating of SKH51+ WC, the value of the coating had a gradient wear resistance, the coating of SKH51 had a better morphology and lower roughness ($R_a = 1,086 \mu\text{m}$.) The WC coating had the best wear resistance among all the schemes, and the wear width was 586.12 μm . The B83 coating had a very stable friction coefficient of 0.12, which was 48% lower than that of the WC coating.

Coating SKH 51+WC+B83 has a good wear resistance and low coefficient of friction, long service life and high reliability. Since the material of B83 is the outer layer of the composite coating of SKH51+ WC+B83, the wear mechanism of the optimal coating is mainly plastic deformation accompanied by slightly polishing.

4. To obtain a better surface quality when providing for a deposition of a soft low-temperature metal by the ESD method, it is necessary to use an RC-discharge circuit and the technology of gas-vibration processing, which makes it possible to control the discharge energy, not to cool the electrode for a long period of time, and to carry out a continuous process of applying a deposition. When the discharge energy is getting greater than the melting energy, the ESD coating would be able to deposit. When the discharge energy is getting less than the melting energy, the electrode performs reciprocating friction on the deposited surface. While processing, the air pressure is in the range of 0.45~0.62MPa, the proper distance of the electrode is to be guaranteed. In this case, a stable vibration frequency is of 310~350 Hz. The pneumatic impact is more stable, and a better deposition effect can be obtained. The mechanism of pneumatic deposition is to control energy through the number of impact discharges per unit time, which reduces the traditional electrode impact force and reduces the deformation of the low-temperature soft metal electrodes. In such a manner, it can enhance the quality of the surface deposition.

5. Graphene oxide gel coating can reduce coating friction and surface roughness. It has a certain wear resistance. It is a new research to modify the surface of ESD coatings with Nano-materials. It was low in cost, very effective in improving surface quality, and easily recognized by the industry. Through the research on the performance of graphene oxide gel, it has been found that the friction coefficient is 0.17, the grinding

width is 1283.02 μm , the surface quality is the lowest, and the bonding force is of 16.57~20.35N.

6. The ESD process has been applied in the automotive industry to discharge batteries of electric vehicles. Since some locking devices cannot return normally, a solution of SKH51+WC+B83 composite coating on the pin shaft surface of the locking mechanism for the lifting device of a battery for an electric car was proposed. It can effectively reduce costs, reduce pollution during the electro-spark deposition coating process and to ensure a long service life of the remanufactured parts. This method is cheap, easy to operate and easy to maintain, and it is recognized by enterprises. This is expected to save the company 115,000 UAH per year.

Scientific novelty of the obtained results:

1. For the first time, high-speed steel SKH51 was studied as a transitional layer of the coating. In this case, the high-speed steel SKH51 has both high wear resistance and impact toughness. During the deposition process, there are almost no micro-cracks on the surface. At the same time, it has a good compatibility with WC coating and can increase the thickness of a composite coating.

2. For the first time, abrasion width method was used to research the wear resistance of ESD coatings. Due to uneven micro-textures of the ESD coating, the abrasive particles can be easily embedded in the micro-texture, which will bring large errors to measure the wear quality of the coating. The wear width is measured by the microscope, which can measure values more conveniently and accurately.

3. For the first time, the evaluation model of normalization method and weighting factors were used for comprehensive evaluation of ESD coating. Deposition quality, coating thickness, roughness, Vickers hardness and wear-resistant width were normalized. Corresponding weighting factors were determined and the total score of

each candidate solution was obtained. The test solutions were evaluated to arrive at the optimal solution.

The practical significance of the obtained results is to provide technical suggestions for remanufacturing of the core parts of the chassis swap battery box. The given coating scheme solves the technical problem of parts remanufacturing in mechanical engineering with a lower cost.

This technical solution is expected to save the enterprise 115 thousand UAH every year.

Keywords: electrospark alloying, coating, combined electro-spark coatings, surface layer, alloy, steel, bronze, mechanical properties, hardness, microhardness, wear resistance, coefficient of friction, ecology, technogenic safety, remanufacture ,Taguchi OA experiment , comprehensive evaluation ,low-temperature soft metal, mechanical part

АНОТАЦІЯ

Ду Сінь. Технологічне забезпечення міцності та довговічності при виготовленні та ремонті деталей галузевого машинобудування. – Кваліфікаційна наукова робота на основі рукопису.

Дисертація на здобуття наукового ступеня доктора філософії в галузі знань 13 – Машинобудування за спеціальністю 133 – Галузеве машинобудування.
- Сумський національний аграрний університет, Суми, 2023.

Ця дисертація присвячена вирішенню практичних науково-технологічних задач у галузі машинобудування. Тертя викликає пошкодження багатьох механічних виробів. Людина досліджує теорії та методи продовження терміну служби механічного обладнання та виробів. Дослідження механізму зношування сприяє прогресу у підвищенні терміну служби механічних деталей та удосконалює

їх ремонт. Поверхні механічного обладнання піддаються зносу. Деталі, що вийшли з ладу, можна відремонтувати, застосовуючи технологію обробки поверхні. Технологія обробки поверхні використовується у техніці відновлювального ремонту. Дослідження зносу та зносостійких матеріалів завжди було найактивнішою сферою трибологічних досліджень. Розробка нових матеріалів і процесів завжди залишається у центрі уваги досліджень зносу. Дослідження застосування поверхневих покриттів і модифікації поверхні стали найактивнішою сферою трибологічних досліджень.

Дійсне дослідження зосереджено на зносі, викликаному лінійним зворотно-поступальним рухом у відкритому середовищі. Воно зосереджене на дослідженні теорії та методології використання технології відновлювального ремонту для постійного покращення зносостійкості та збільшення терміну служби деталей. Однією з труднощів дослідження зносу є дослідження протизносних і антифрикційних властивостей покриттів в екстремальних умовах. Зі швидким розвитком теорії композитних поверхневих покриттів з'являються нові теорії, пов'язані з покриттями. Дуже важливо сформулювати новий підхід до створення протизносних та антифрикційних покриттів, спираючись на нові теоретичні дослідження. Оскільки електроіскрове осадження (те ж, що і електроіскрове легування) має характеристики енергозбереження та захисту навколишнього середовища, низьку вартість використання та зручність експлуатації, поєднання технології ESD із теорією композитних покриттів має позитивне значення для дослідження нових покриттів. У цьому дослідженні матеріали з високою в'язкістю, високою зносостійкістю та матеріали, що зменшують тертя, використовуються для виготовлення композитного матеріалу, щоб досліджувати нові покриття, які зменшують тертя та є зносостійкими. Розвиток технології пневматичного ударного

напилення може покращити традиційний процес напилення та значно покращити якість антифрикційного покриття, що є новим досягненням у розвитку наукової думки.

Таке нове композитне покриття сприяє зменшенню споживання енергії та зниженню забруднення навколишнього середовища, що важливо для забезпечення низького зносу та тривалого терміну служби механічного обладнання. Воно має рекламну цінність як фактор стимулювання для деталей з однаковим механізмом зносу. Також дуже важливим у цьому відношенні є можливість заощадження ресурсів та зменшення витрат для бізнесу.

Об'єкт дослідження – технологічний процес формування функціональних покриттів на поверхні валу штифта замкового механізму підйомного пристрою.

Предмет дослідження – закономірності технологічного процесу формоутворення поверхні із заданими експлуатаційними властивостями, що забезпечує необхідну якість (довговічність, зносостійкість, працездатність) поверхні валу штифта замкового механізму підйомного пристрою.

Метою роботи є підвищення якості поверхневих шарів при виготовленні і відновленні валу штифта замкового механізму підйомного пристрою акумуляторної батареї електромобіля, шляхом формування на його поверхнях, що зношуються, методом електроіскрового осадження композиційних багат шарових покриттів складу SKH51+WC+B83.

Для досягнення поставленої мети необхідно вирішити наступні **задачі**:

1. Провести аналіз існуючих сучасних технологій ремонту деталей галузевого машинобудування відповідно до характеристик ESD.

2. Провести аналіз сучасних матеріалів електродів – інструментів для комплексної оцінки властивостей поверхневих покриттів, нанесених для покращення загальної технічної характеристики поверхні.

3. Провести дослідження формування зносостійких композитних градієнтних покриттів і порівняння різних властивостей поверхні.

4. Проаналізувати дефекти низькотемпературного напилення м'яких металів та вдосконалити існуючу технологію ремонту.

5. Дослідити вплив технології ремонту нанесенням покриття методом ESD на точність отриманої поверхні.

6. Запровадження результатів дослідження в інженерну практику відновлювального ремонту (повної модернізації) на підприємстві.

У **Вступі** викладено тему та наукове завдання дисертації, сформульовано цілі та задачі дослідження, визначено наукову новизну та практичну цінність отриманих результатів, а також відомості про її апробацію, структуру та обсяг роботи.

У **першому розділі** було представлено розвиток інжинірінга відновлювального ремонту (модернізації) та виконано порівняння кількох основних загальних процесів відновлювального ремонту (модернізації). Беручи до уваги вартість і зручність, наголошувалося на технології електроіскрового напилення. Наведено огляд історії розвитку методу електроіскрового напилення ESD, останніх досліджень та оптимізації ESD процесу.

У **другому розділі**, були наведені основні теорії та методи дослідження. Представлено робочий принцип методу ESD. Були показані три різновиди функціонування вібруючих електродів. Було проаналізовано основну теорію формування покриттів методом ESD, яка включала механізм корозії ESD, теорію

енергії імпульсу, теорію плавлення металу та спрощену модель теплопередачі. Також у розділі представлено обладнання для перевірки властивостей поверхні, яке може визначати морфологію поверхні, елементний склад, фазовий аналіз, твердість і трибологічні властивості. Нарешті описано експериментальні методи та процеси напилювання покриття.

У **третьому розділі** описано постійне вдосконалення методів, нанесення поверхневих покриттів з підвищеною стійкістю до стирання (1). Графіт, нанесений на поверхню сталі 45, може покращити стійкість поверхні матеріалу до стирання. У відповідності з шириною стирання, ортогональний метод Тагучі використовувався для визначення оптимального процесу відносно напилення графіту. У такий спосіб визначено оптимальні параметри процесу ESD, а саме ККД, напругу, частоту струму та час роботи. Оскільки поверхня містить тверду фазу Fe_3C , цементована поверхня мала на 59,96% меншу ширину сліду стирання, ніж не цементована поверхня. Поверхнева зносостійкість підкладки була підвищена (2). Швидкорізальна сталь CX51 використовувалася для електроіскрового напилення на поверхню сталі 45. Матеріал CX51 має високу зносостійкість і відмінну ударну в'язкість, яка краща, ніж у цементованої сталі 45. Тому матеріал CX51 використовували як перехідний шар, щоб більш зносостійкий матеріал WC можна було нанести пізніше для формування градієнтного покриття. Метод нормалізації та метод вагового коефіцієнта були використані для оцінки різних робочих параметрів покриття, при цьому були отримані оптимальні параметри процесу напилення покриття (3). Титан і титанові сплави, Nb і Zr були цементовані на поверхні, а тверді фази, такі як TiC , ZrC і NbC , були сформовані на виробничій площадці *in situ*. Гелеві покриття з оксиду графену були отримані шляхом нанесення полімерних матеріалів. Порівнюючи різні покриття, було виявлено, що

градієнтне композитне покриття CX51+WC+B83 має кращі робочі характеристики. Оскільки вміст твердої фази в цьому покритті був вищим, ніж в інших розчинах (4). Для низькотемпературних м'яких металів було розроблено новий процес напилення для покращення якості поверхні. Безперервне напилення проводили із застосуванням технології пневматичного ударного напилення та низькоенергетичних схем RC. Враховуючи те, що графітовий порошок для мастила, як правило, легко відділяється (5). Використовувалися самозмащувальні покриття. Оскільки графітові енергетичні та полімерні композитні покриття мали низьку стійкість до стирання, було запропоновано нанополімерне самозмащувальне покриття, яке являло собою гелеве покриття з оксиду графену.

У **четвертому розділі** описано процес ESD, який було застосовано при заміні акумуляторних батарей електромобілів в атомобільній галузі. Результати випробувань покриття для чотирьох варіантів рішень проблеми були узагальнені та проаналізовані, і на основі випробувань на зносостійкість було визначено найкраще рішення для промислового застосування. Оскільки деякі пристрої автоматичного блокування не можуть повернутися до нормального (перпендикулярного) стану, було запропоновано градієнтне композитне покриття на фіксаторі (валу штифта замкового механізму підйомного пристрою акумуляторної батареї електромобіля). Сформоване покриття не тільки відповідало вимогам зносостійкості, але також мало нижчу ступінь тертя та певну антикорозійну стійкість. Рішення, що відповідає схемі CX51+WC+B83 може ефективно знизити витрати, зменшити забруднення навколишнього середовища у процесі нанесення покриття методом електроосадження та забезпечити більш тривалий термін служби деталей.

Відповідно до поставленої мети та задач, що підлягають вирішенню, у роботі отримано такі результати:

1. При використанні ортогонального методу Тагучі, відповідно до ширини стирання, встановлені оптимальні параметри процесу поверхневої цементації сталі 45: ефективність 50%, напруга 35 В, частота струму 180 Гц і час роботи 360 с. У результаті середнє значення ширини стирання склало 268,206 мкм, а глибина стирання – 2,999 мкм, що на 59,96% менше, ніж для сталі 45 без цементації.

2. За допомогою методу нормалізації та методу вагових коефіцієнтів для оцінки робочих параметрів покриття при максимальному значенні цільової функції 0,687887, визначенні оптимальні параметри процесу електроіскрового напилення покриття CX51 на поверхню сталі 45: частота струму 300 Гц, напруга 44 В, ККД 30 % і швидкість обертання 150 об/хв.

3. При порівнянні композитних покриттів різного складу, оптимальним визнане композитне покриття, сформоване за схемою CX51+WC+B83. Використовуючи градієнтне покриття CX51+ WC, показник покриття мав градієнтну зносостійкість, покриття CX51 мало кращу морфологію та меншу шорсткість ($R_a = 1,086$ мкм). Покриття WC мало найкращу зносостійкість серед усіх схем, а ширина його зносу становила 586,12 мкм. Покриття B83 мало дуже стабільний коефіцієнт тертя 0,12, що на 48% нижче, ніж у покриття WC. Покриття CX51+ WC+B83 має хорошу зносостійкість і низький коефіцієнт тертя, довгий термін служби і високу надійність. Оскільки матеріал B83 є зовнішнім шаром композитного покриття CX51+ WC+B83, механізм зносу оптимального покриття полягає в основному в пластичній деформації, що супроводжується незначним поліруванням.

4. Для отримання кращої якості поверхні при напиленні м'якого низькотемпературного металу методом ESD потрібно застосовувати RC-розрядний ланцюг та технологію газо-вібраційної обробки, що дозволяє контролювати

енергію розряду, не охолоджувати протягом тривалого періоду часу електрод і проводити безперервний процес напилення. Коли енергія розряду стає більшою за енергію плавлення, діє процес напилення ESD покриття, в протилежному випадку електрод здійснює зворотно-поступальне тертя по напиленій поверхні. Під час здійснення процесу тиск повітря знаходиться в діапазоні 0,45 ~ 0,62 МПа, належна відстань електрода повинна бути гарантована, генерування стабільної частоти вібрації складає 310 ~ 350 Гц. Механізм пневматичного напилення полягає в управлінні енергією через кількість ударних розрядів за одиницю часу, що зменшує традиційну ударну силу електрода та зменшує деформацію низькотемпературних м'яких металевих електродів і таким чином підвищує якість поверхневого напилення.

5. Гелеве покриття з оксиду графену зменшує тертя покриття та шорсткість поверхні. Воно має певну зносостійкість. Це нове дослідження, спрямоване на модифікацію поверхні ESD покриттів полімерними наноматеріалами. Воно виявилось дешевим, дуже ефективним для покращення якості поверхні та легко отримало визнання в галузі. Завдяки дослідженню робочих характеристик гелю оксиду графену, було встановлено, що його коефіцієнт тертя становить 0,17, ширина шліфування - 1283,02 мкм, якість поверхні - найнижча, а сила зчеплення - 16,57 ~ 20,35 Н.

6. Процес ESD був застосований у автомобільній промисловості для розрядження акумуляторів електромобілів. Оскільки деякі автоматичні замикаючі пристрої не можуть повертатися до нормального стану, було запропоновано рішення з градієнтним композитним покриттям на фіксаторах (валу штифта замкового механізму підйомного пристрою акумуляторної батареї електромобіля), яке було виготовлене за схемою CX51+WC+B83. Воно може ефективно знизити

витрати, зменшити забруднення при проведенні процесу нанесення покриття електроіскровим осадженням та забезпечити тривалий термін служби відновлених деталей. Цей метод є дешевим, простим у експлуатації та обслуговуванні. Очікується, що він може заощадити компанії 115 000 грн. у рік.

Наукова новизна отриманих результатів:

1. Вперше в якості перехідного шару покриття досліджено швидкорізальну сталь CX51, яка має як високу зносостійкість, так і ударну в'язкість. У процесі напилення мікротріщини на поверхні практично відсутні. У той же час вона має хорошу сумісність з покриттям WC і може збільшити товщину градієнтного покриття.

2. Вперше метод ширини стирання було застосовано для дослідження зносостійкості ESD - покриттів. Через нерівномірну мікротекстуру ESD - покриття, абразивні частинки можуть легко вбудовуватися в мікротекстуру, що обов'язково призведе до великих похибок щодо якості покриття на зносостійкість. Ширина зносу вимірюється мікроскопом, який здатний вимірювати більш зручно та точно.

3. Вперше для комплексної оцінки ESD - покриття використано оціночну модель методу нормалізації. Було нормалізовано якість осадження, товщину покриття, шорсткість, твердість за Віккерсом та ширину зносостійкої ділянки. Було визначено відповідні вагові коефіцієнти та отримано загальну оцінку кожного рішення-кандидата. Досліджувані рішення були оцінені для досягнення оптимального рішення поставленої задачі.

Практичне значення отриманих результатів полягає в наданні технологічних пропозицій щодо відновлення основних деталей змінного акумуляторного блоку шасі. Наведена схема покриття вирішує технічну задачу

відновлення деталей у машинобудуванні з меншими затратами. Очікується, що таке технічне рішення буде щорічно економити підприємству 115 тисяч гривень.

Ключові слова: електроіскрове легування, покриття, комбіновані електроіскрові покриття, поверхневий шар, сплав, сталь, бронза, механічні властивості, твердість, мікротвердість, зносостійкість, коефіцієнт тертя, екологія, техногенна безпека, відновлення, експерименти методами Тагучі О.А., комплексна оцінка, м'який низькотемпературний метал, механічна деталь.

LIST OF THE APPLICANT'S PUBLICATIONS ON THE TOPIC OF THE DISSERTATION

Articles in scientific professional publications of Ukraine

1. **Du Xin**, Konoplianchenko Ie., Tarellyk V. Electrosark deposition in remanufacturing engineering, prospect of development and application Mechanization and Automation of Production Processes.2021, 1 (43),8-12, DOI: <https://doi.org/10.32845/msnau.2021.1.2>(PhD participant in carrying out of investigation, review and editing, preparation of article for printing).

2. **Du Xin**, Research on wear resistance of carbonized 45 steel by electro-spark deposition technology , Bulletin of Sumy National Agrarian University. The series: Mechanization and Automation of Production Processes.2022, 3 (49),11-18.DOI: <https://doi.org/10.32845/msnau.2022.3.2> (PhD participant in carrying out of experimental researches, processing of results, preparation of article for printing).

3. Zhengchuan, Z., Konoplianchenko E. B., Tarellyk B. B., Guanjun, L., **Xin, D.**, Yao, J., & Zhaoyang, S. (2022). Industry Application of the Coatings on the Bearing Bush by Electro Spark Alloying Technology. Scientific Bulletin of Ivano-Frankivsk National Technical University of Oil and Gas, 2022,1(52), 15–23. DOI: [https://doi.org/10.31471/1993-9965-2022-1\(52\)-15-23](https://doi.org/10.31471/1993-9965-2022-1(52)-15-23) (PhD participant in carrying out of experimental researches, processing of results).

4. Zhang Zhengchuan, Liu Guanjun, Ie. Konoplianchenko, V. Tarellyk, Ge Zhiqin, **Du Xin**. A review of the electro-spark deposition technology. Bulletin of Sumy National Agrarian University, The Series: Mechanization and Automation of Production Processes. 2021, 2(44), 45-53.DOI:<https://doi.org/10.32845/msnau.2021>. (PhD participant in carrying out of investigation, review and editing).

Articles in others scientific journals

5. **Xin D**, Tarelyk V. Konoplianchenko Ie. Research on SKH51+WC+B83 composite gradient coating by ESD method, Sciences Of Europe. 2023, 127, 102-110. DOI: [https://doi.org/ 10.5281/zenodo.10039444](https://doi.org/10.5281/zenodo.10039444) (PhD participant in carrying out of investigation, review and editing, preparation of article for printing).

6. **Xin D**, Tarelyk V. Performance analysis of GO gel composite coating on electro-spark deposited surfaces, International Science Journal of Engineering & Agriculture.2023, 2(5), 20-30.DOI:[https://doi.org/ 10.46299/j.isjea.20230205.03](https://doi.org/10.46299/j.isjea.20230205.03)(PhD participant in carrying out of investigation, review and editing, preparation of article for printing).

Articles in scientific journals indexed by Scopus or Web of Science Core Collection

7. Zhang Zhengchuan, Ievgen Konoplianchenko, Viacheslav Tarelyk, Liu Guanjun, **Du Xin**, Yu Hua. The Characterization of Soft Antifriction Coating on the Tin Bronze by Electro-spark Alloying. Materials Science (Medžiagotyra). 2023, 29(1), 40-47. (PhD participant in carrying out of experimental researches, processing of results).

DOI:<http://dx.doi.org/10.5755/j02.ms.30610> (**Scopus Q4, Web of Science**)

8. Zhang Zhengchuan, Viacheslav Tarelyk, Ievgen Konoplianchenko, Liu Guanjun, **Du Xin**, Ju Yao. The Characterization of Tin Bronze Substrates Coated by Ag+B83 through Electro-spark Deposition Method. Surface Engineering and Applied Electrochemistry. 2023, 59(2), 220-230. (PhD participant in carrying out of experimental researches, processing of results).

DOI:<https://doi.org/10.3103/S1068375523020187> (**Scopus Q3, Web of Science**)

9. Zhang Zhengchuan, Viacheslav Tarelyk, Ievgen Konoplianchenko, Liu Guanjun, Wang Hongyue, **Du Xin**, Ju Yao, Li Zongxi. New evaluation method for the

characterization of coatings by electroerosive alloying. *Materials Research Express*. 2023, 10(3), 036401. (PhD participant in carrying out of experimental researches, processing of results).

DOI:<https://doi.org/10.1088/2053-1591/acc15b> (**Scopus Q1, Web of Science**)

10. Zhang Zhengchuan, Ievgen Konoplianchenko, Viacheslav Tarellyk, Liu Guanjun, **Du Xin**, Yu Hua. The Characterization of Running-In Coatings on the Surface of Tin Bronze by Electro-spark Deposition. *Coatings*. 2022, 12(7), 930-945. (PhD participant in carrying out of experimental researches, processing of results, preparation of article for printing).

DOI:<https://doi.org/10.3390/coatings12070930> (**Web of Science Q2, Scopus Q3**)

Theses of scientific reports

11. **Du Xin**, Tarellyk V. Study on the properties of electro-spark deposited SKH51+WC gradient coating on 45 steel. Proceedings of the 2nd International scientific and practical conference. CPN Publishing Group. Tokyo, Japan. 2023. 207-213. ISBN 978-4-9783419-2-1. (PhD participant in carrying out of experimental researches, processing of results)

12. **Du Xin**, Tarellyk V., Konoplianchenko Ie. Study on the deposition property of SKH51 transitional coatings by TAGUCHI orthogonal array method, Proceedings of the 10th International scientific and practical conference, Barca Academy Publishing. Madrid, Spain. 2023. 117-122. ISBN978-84-15927-34-1 (PhD participant in carrying out of experimental researches, processing of results)

13. **Du Xin**, Tarellyk V. Research on performance of SKH51+WC+B83 composite coatings in locking mechanism of electric vehicle, Proceedings of the 10th International scientific and practical conference, Barca academy publishing, Madrid, Spain. 2023.

123-128. ISBN 978-84-15927-34-1 (PhD participant in carrying out of experimental researches, processing of results)

14. **Du Xin**, Ievgen Konoplianchenko, Viacheslav Tarellyk, Development directions and perspectives of ESD technologies. The 27th International Scientific and Practical Conference, Sumy, Ukraine. 2021. 214-217. (PhD participant in carrying out of experimental researches, processing of results)

15. **Xin D**, Tarellyk V., Konoplianchenko Ie., Zhaoyang Song. The orthogonal design of wc-8co reinforcement thickness on experimental analysis. The 10th International scientific and practical conference (December 25-27, 2022), Lviv, Ukraine. 2022. 347-352. ISBN 978-966-8219-86-3 (PhD participant in carrying out of experimental researches, processing of results, preparation of article for printing)

16. **Xin D**. Technology of deposition of power lines of road transport systems. Збірник тез доповідей VI Міжнародної науково-практичної конференції «Автомобільний транспорт та інфраструктура» (19–21 квітня 2023 року). Національний університет біоресурсів і природокористування України. Київ. 2023. 144-145. ISBN 978-617-8102-96-8. (PhD participant in carrying out of experimental researches)

17. **Du Xin**, Viachesla Tarellyk, Ievgen Konoplianchenko, Song Zhaoyang. Simplified model of wear parameters for electro-spark coatings. Proceedings of the XXXIV International Scientific and Practical Conference (August 29 – September 01, 2023). Warsaw, Poland. 2023. 169-173. ISBN 979-8-89145-197-1. (PhD participant in carrying out of experimental researches, processing of results)

18. **Xin D**, Tarellyk V., Konoplianchenko I., Zhaoyang Song. Calculation and analysis of single pulse energy for electro-spark deposition of low temperature alloy. Proceedings of the 12th International scientific and practical conference. CPN

Publishing Group. Osaka, Japan. 2023.63-67. ISBN 978-4-9783419-1-4(PhD participant in carrying out of experimental researches, processing of results)

19. Zhang Zhengchuan, Viacheslav Tarellyk, Ievgen Konoplianchenko, Liu Guanjun, **Du Xin**, Yu Hua. Research on the Characterization of Ag+Cu+B83 Composite Coatings on the Surface of Tin Bronze by Electro-spark Deposition (2021) Proceedings of the 2021 IEEE 11th International Conference on "Nanomaterials: Applications and Properties", NAP 2021, 1-8. (PhD participant in carrying out of experimental researches, processing of results)

DOI:<https://doi.org/10.1109/NAP51885.2021.9568514> (**SCOPUS**)

20. Zhang Zh., Konoplianchenko Ie.V., Tarellyk V.B., **Du X.** The future research direction of the ESD deposition technology. *Машинобудування очима молодих: прогресивні ідеї – наука – виробництво: матеріали XX Міжнародної науково-технічної конференції (м. Суми, 29 вересня – 1 жовтня 2021 року) / редкол.: В. О. Залюга, В. О. Іванов. – Суми: Сумський державний університет, 2021. 21-23. (PhD participant in carrying out of investigation, review and editing). (**SCOPUS**)*

21. V. Tarellyk, O. Gaponova, V. Martsynkovskyy, I. Konoplianchenko, V. Melnyk, V. Vlasovets, A. Sarzhanov, N. Tarellyk, **D. Xin**, Y. Semirnenko, S. Semirnenko, T. Voloshko, O. Semernya. Energy Dispersive X-Ray Microanalysis of Part Surface Layer Carburized by Electric Spark Alloying. 2020 IEEE 10th International Conference Nanomaterials: Applications & Properties (NAP), Sumy, Ukraine, 2020, pp. 01TFC13-1-01TFC13-9, (PhD participant in carrying out of experimental researches, processing of results) DOI:<https://doi.org/10.1109/NAP51477.2020.9309618>. (**SCOPUS**)

CONTENT	pages.
LIST OF SYMBOLS.....	27
INTRODUCTION.....	29
CHAPTER 1. LITERATURE REVIEW, THE PURPOSE AND THE TASKS OF RESEARCH.....	35
1.1 Problems of wear in the mechanical parts.....	35
1.2 Overview of remanufacturing engineering	38
1.3 Overview of electro-spark deposition technology	41
1.4 Features of ESD technology.....	43
1.5 The recent research progress of ESD technology	44
1.6 Optimization of the ESD process	48
1.7 The purpose and the tasks of the research.....	51
CHAPTER 2. BASIC THEORY AND METHODOLOGY OF RESEARCH.....	53
2.1 The working principle of ESD	53
2.2 Corrosion mechanism of electro-spark deposition.....	55
2.3 Pulse energy theory	60
2.4 Heat conduction.....	63
2.5 Electrospark deposition equipment	65
2.6 Experimental materials.....	67
2.7 Experiment equipment	69
2.8 Experimental method	73
2.9 Gradient deposition process	75
2.10 In situ reaction process.....	77

	26
2.11 Summary.....	78
CHAPTER 3. EXPERIMENT RESEARCH RESULTS AND ANALYSIS.....	80
3.1 The characterization of graphite coatings	80
3.2 The characterization of SKH51 coatings	92
3.3 Composite coating process.....	116
3.4 Deposition process of low-temperature super-soft materials.....	143
3.5 GO gel composite coating.....	152
3.6 Summary	164
CHAPTER 4. INDUSTRIAL APPLICATIONS OF COMPOSITE COATINGS	167
4.1 Industrial background.....	167
4.2 Problem description.....	168
4.3 Analysis of Experimental Causes	171
4.4 Design of the replacement battery box.....	172
4.5 Coating solutions of the pin shaft.....	176
4.6 Abrasion resistance test	179
4.7 Technical suggestions.....	182
4.8 Summary	183
CONCLUSIONS.....	184
REFERENCES	184
APPENDICES	215

LIST OF SYMBOLS

GO - Graphene Oxide

WC- Worfrom Carbide(tungsten carbide)

RC-Resisance Capacitance

ESD - Electro-Spark Deposition

SEM - Scanning Electron Microscopy

EDS - Energy Dispersion Spectrum

XRD - X-Ray Diffractometer

S_e -surface shape of the melted layer

S_0 -discharge layer surface shape

D -current heat function

α - value determined by the solution of the Stefan's problem

W_c - energy transferred by the heat source

a - the coefficient of temperature transfer

W_0 - energy density at the centre of the heat source.

V -the volume of the small pit

I_m -the instantaneous action current

j_m -the instantaneous action current density

b - the radius of the contact area.

U - power supply voltage

L -inductance

I -current

W -individual pulse energy

γ -mass of material thrown by electric spark

E -the energy per unit pulse

n -the pulse frequency

K -the proportionality constant

τ -the time required to charge the capacitor

R - the resistance value of the circuit

u_c -capacitor voltage

U - supply voltage

Q - heat of melting of the metal

m - mass of the metal

C - specific heat capacity (J/g)

Δt -temperature variation interval

$q(r)$ - heat flow density at r from the center of the discharge

q_m - peak heat flow density

k - energy concentration coefficient

$R(t)$ - radius of heat source at time.

V_w -wear volume of the sample

L -length of abrasion

L_{AH} -depth of abrasion

L_{BC} -width of abrasion

R_0 -radius of the friction ball,

θ - angle made by the electrode with the machining surface

h - thickness of the coating deposition

INTRODUCTION

Justification of the choice of research topic

Every year, the global economy loses more than 100 billion dollars due to friction and wear of machine parts. Friction and wear occur on the contacting surfaces of dynamic equipment parts. When using a special technology, it is possible to reduce the surface wear of metal materials, which will have a positive effect on saving energy consumption, reduce material losses, extend the service life of mechanical equipment, and increase the operation reliability. Under conditions of sustainable economic development, human beings face a strategic challenge of preserving resources. In order to extend the service life of machines and equipment, they need carry out remanufacturing of parts which of service life is expiring.

The problems of wear and increasing the wear resistance of parts have always been the most important areas of research. At the same time, the research and development of new composite materials and new technologies have always been in the focus of wear research.

Remanufactured parts can be classified into restored parts, and upgraded parts that can increase technological capabilities. Remanufacturing is closely related to surface repair. In recent years, the theory of composite coatings has been constantly developing. The theory of nanostructured coating and the theory of in-situ coating are in focus. A composite coating can implement several coating functions. High strength and wear resistance of the coating are achieved thanks to the use of multilayer combinations. An anti-friction material is used to reduce friction on the surface of the coating. Surface repair technology attracts the main

attention of remanufacturing engineering and is associated with a large number of technical problems that need to be solved. Surface repair processes include laser coating, deposition technology, electric bushplating technology, electro-spark deposition (ESD) and conventional mechanical surface treatment. Compared with other methods, ESD technology has a lower cost of use, simple and convenient equipment, accompanied by a reduction in material waste and less environmental pollution.

Researching the application of surface coating technologies and surface modification has become one of the most active areas of tribological research, and it has achieved rather fruitful results. Thus, the task of many machine-building enterprises remains the improvement of technologies for repairing mechanical parts and equipment and further increasing their tribological characteristics in order to improve protection against wear.

The electro-spark deposition (ESD) technology is important in surface strengthening. The surfaces of mechanical parts are strengthened to improve friction reduction, corrosion resistance, wear resistance, and other properties. The ESD can extend the service life on the surface of parts. The ESD repair process is environmentally friendly, has the least pollution to the surrounding environment. It is low in cost and easy to operate.

Relationship with academic programs, plans, themes.

The dissertation is a fragment of scientific programs of research work of the Ministry of Education and Science of Ukraine "Scientific methodology of parts

working surfaces maintenance properties providing by energy-efficient environmentally friendly methods" (№ 0116U002756).

The purpose of the work is to improve the quality of the surface layers at manufacturing and remanufacturing the pin shaft of the locking mechanism for the lifting device of an electric car battery by forming the composite multilayer coatings of the SKH51+WC+B83 composition on its wear surfaces with the use of the method of electro-spark deposition.

For the purpose were assigned the following tasks:

1. To conduct an analysis of the existing modern methods and technologies for repairing component parts for branch mechanical engineering in accordance with the ESD characteristics.

2. To conduct an analysis of modern materials for electrode – tools to provide for a comprehensive assessment of the properties of the surface coatings applied to improve the overall technical characteristics of the surface.

3. To conduct a research on the formation of wear-resistant composite coatings and compare various surface properties.

4. To conduct a research of the defects of low-temperature soft metal deposition and improve the existing repair technology.

5. To investigate the effect of the ESD coating repair technology on the accuracy of the surface obtained.

6. Introduce the research results into the engineering practice of enterprise remanufacturing.

Object of research is a technological process for forming functional coatings on the pin shaft surface of the locking mechanism for the lifting device.

Subject of research is the regularities of the technological process for forming a surface with specified performance properties, which ensure the necessary quality (durability, wear resistance, workability) of the pin shaft surface of the locking mechanism.

Research methods - The method of experiment analysis made it possible to improve surface performance and service life of the important mechanical parts through surface strengthening method by the ESD process. Because the surface of metal parts was insufficient surface properties of the material, it often occurred adhesive wear. This resulted in greater surface roughness and increased friction, which reduced the life of the parts and leads to damage. ESD method can effectively repair and enhance surface properties.

The experiments were based on the wear mechanism of the failed part surface. It has improved wear resistance and friction reduction properties through the ESD coating process method, which can improve the surface properties of parts and meet the service life requirements of parts. The experiment continued to improve the surface properties of parts through the use of electric spark carbonization processes, composite coating processes and other methods. Moreover, it was established a mathematical evaluation model of the transition coating by the normalization method and the weighting factor method. It can improve the deposited surface quality of friction-reducing materials by pneumatic deposition process method.

There is a need for complex research aimed at definition the quality parameters of the formed surface layers (morphology, composition, roughness,

micro-hardness, tribology properties). For the analysis of the wear resistance mechanism, Bruker x-ray qualitative equipment was used to analyze the wear resistance constituents. The surface distribution of the wear-resistant components was analyzed with Hitachi Regulus8220 and Bruker X-ray energy spectrometer. Three-dimensional morphology was observed and measured with a Leica DVM6 super depth of field microscope.

Scientific novelty of the obtained results.

1. For the first time, high-speed steel SKH51 was studied as a transitional coating. High-speed steel SKH51 has both wear resistance and impact toughness. During the deposition process, there are almost no microcracks on the surface. At the same time, it has good compatibility with WC coating and can increase the thickness of the composite coating.

2. For the first time, abrasion width method was used to research the wear resistance of ESD coatings. Due to uneven micro-textures of the ESD coating, the abrasive particles can be easily embedded in the micro-texture, which will bring large errors to measure the wear quality of the coating. The wear width is measured by the microscope, which can measure values more conveniently and accurately.

3. For the first time, the evaluation model of normalization method was used for comprehensive evaluation of ESD coating. Deposition quality, coating thickness, roughness, Vickers hardness and wear-resistant width were normalized. Corresponding weighting factors were determined and the total score of each candidate solution was obtained. The test solutions were evaluated to arrive at the optimal solution to the task.

The practical significance of the obtained results is to provide technical suggestions for remanufacturing of the core parts of the chassis swap battery box. The given coating scheme solves the technical problem of remanufacturing parts in mechanical engineering with lower cost. This technical solution is expected to save the enterprise 115 thousand hryvnia every year.

Personal contribution of PhD.

Setting goals and objectives, discussing the results, forming conclusions were carried out together with the scientific supervisor. The author analyzed the literature and patent search on the topic of dissertation.

The author personally conducted experimental studies using modern methods. Processing of the research results, conclusions and proposals for industrial implementation were developed by the author personally. The PhD's personal contribution to joint scientific publications with co-authors is specified in the list of publications.

Publications. According to the results of research, 21 scientific papers were published, including: 4 articles in professional editions of Ukraine, 11 conferences, 2 articles - in foreign editions, 4 articles in the Scopus or WOS scientific-metric publication, 1 methodical recommendation.

Structure and scope of the thesis. The dissertation is set out on 221 pages of computer text. It consists of an introduction, 4 sections, general conclusions, a list of sources used and 2 annexes. The main body of the dissertation is 152 pages of printed text. The work is illustrated with 40 tables, 70 figures. The list of references includes the name of 197 sources on 28 pages.

CHAPTER 1. LITERATURE REVIEW, THE PURPOSE AND THE TASKS OF RESEARCH

Electro-spark deposition can restore the dimensions and properties of remanufactured parts and meet the specific requirements of part surface remanufacturing. ESD technology can strengthen surface properties and repair wear surfaces.

1.1 Problems of wear in the mechanical parts

Friction consumes 30 % of the world's disposable energy, and about 80 % of machine parts fail from wear [1, 2] . In developed countries, the annual losses caused by wear account for 5% to 7% of the gross domestic product (GDP). In China, annual economic losses due to friction and wear amount to one trillion UAH [3].

Turbine generators are driven by hot steam to rotate at high speeds. The shafts are prone to wear [4, 5]. The wear of the shaft is due to the tiny metal particles and impurities in the oil supply system, which will cause abrasive wear to the shaft during long-term operation. Tiny metal particles and impurities are equivalent to abrasive particles, which cause abrasive wear on the surface of parts and accelerate the rapid damage of the surface of the shaft.

The generator rotor is a vital component of the turbine generator set. Damage defects of the journal affect the uniformity of the oil film and the vibration performance of the unit during operation. After the rotor journal was worn and strained, it affected the safe and stable operation of the unit and brings grave harm to the safety of the equipment [6].

In cement machinery, reducer devices play a vital role for major mechanical equipment. For the reducer, the gears are the main working parts for the equipment to change the speed. Due to cement production requirements, the machine can't stop [7]. Gears are in an overloaded long-term working state in a closed environment [8]. Micro-pitting and scuffing increase the wear of the gear surface, which makes more noise and accelerates wear.

Cement production equipment is larger, and the corresponding gears are larger. In the working process, if gears are damaged, cement solidification may cause the equipment to scrap. Therefore, enterprises put forward higher life requirements for gears.

In overhead cranes, the wheel components are often subject to severe wear [9-11]. When the wheels of the vehicle are moving on the track, the rim of the wheel at one end contacts the side of the track. It causes the wheel to track friction. Adhesive wear and abrasive wear occur between the wheel rim and the track. After the wheel rim is severely worn, the wheel rim will become thinner and scrap.

When the wheels had worn, the wheel components deflected and twisted at starting and braking. They made abnormal noises, and the running resistance increased. The crane suddenly derailed while travelling, which caused major equipment damage and personal casualties.

In the public transport, electric vehicles are gradually becoming the mainstream. It is gradually replacing traditional fuel vehicles. For example, the China market is developing rapidly with 160 billion UAH every year [12]. The power-changing electric vehicles are rapidly developing. The pin shaft of the

locking mechanism is an important part in the electric vehicle. It ensures the reliability of the fixing of the battery box.

When the electric vehicle battery energy storage is low, the chassis battery box is replaced. When the lifting device lifts the battery box, the pin shaft of the locking part is moved by the pull of the square push block, and the locking mechanism is pushed open. Reciprocal sliding friction occurs on the surface of the pin shaft. After long-term use, the surface of the pin shaft will wear. The friction between the pin shaft and the orifice plate caused the dimension to be out of tolerance and the assembly deterioration. The mechanism was in an open environment, and the grease loss was serious. The surface of the pin shaft accompanied with adhesive wear and corrosion wear, causing the surface roughness to increase. The locking device cannot return correctly. The battery box cannot be securely locked. It is easy to produce abnormal noise when the car is running. In extreme environments, the battery may easily fall and cause safety accidents.

Worn parts need to be repaired. The main repair methods include laser coating, spraying technology, electric brush plating technology, electro-spark deposition, etc [13]. Laser coating repair technology has higher requirements on deposited materials. The cost of powder materials is high; super-hard materials cannot be used for welding wires. Because the equipment maintenance environment requires high requirements, the repair cost is high [14]. Spraying technology is used for repair with the following characteristics: high cost of powder material, large heat-affected zone, more powder waste and high repair cost

[15]. Brush plating repair technology is more polluting to the environment and it is suitable for the repair of parts with higher surface accuracy. The ESD deposition repair technology can strengthen the surface performance [16]; Composite coating deposition can be achieved easily. It has the small machining allowance and the simple grinding process.

ESD technology has lower usage costs than other repair methods. The equipment is simple and convenient for field maintenance [17]. It enhances the wear resistance, extends the life of mechanical equipment, and improves the reliability of equipment. It has the least waste of materials and less pollution to the environment. According to the repair requirements of the pin shaft of the locking mechanism, electro-spark deposition technology is most suitable.

1.2 Overview of remanufacturing engineering

Protecting the earth's environment, building a circular economy and maintaining sustainable social development have become topics of common concern around the world [18-20]. At present, the circular economy model is strongly advocated to pursue greater economic benefits, save resource consumption and reduce social pollution.

The remanufacturing engineering is the industrialization of high-tech repair of waste mechanical and electrical products [21, 22]. The quality and performance of remanufactured products can reach or even exceed that of new products, and the cost can save energy by 60%. The negative impact on the environment is significantly reduced. Remanufacturing engineering is an important element in the

whole life cycle of products, and remanufacturing engineering runs through every stage of the whole life cycle of products [23].

Over the past 50 years, rapid advances in technology and manufacturing processes have greatly expanded the scope of remanufacturing processes for products in the automotive sector, agricultural machinery, the power sector, electromechanical equipment and more[24]. The United States uses remanufacturing engineering to repair weapons and equipment. Maintenance costs have been significantly reduced and performance greatly improved. The US department of defense has also included "new remanufacturing technologies" as a new priority for the defense industry after 2010. Remanufacturing in restoring, maintaining and even improving the technical performance of products, the means used not only include traditional mechanical processing methods, but also include surface engineering technology, disassembly technology, cleaning technology and other process technologies. Among them, surface engineering technology is also a difficult and key point in remanufacturing engineering [25, 26].

Laser coating: In 1976 the D.S Gnamuthu used a laser to melt a layer of metal belonging to another layer of the metal matrix of the cladding method. Laser coating uses a high-energy laser beam to radiate on the metal surface, which will wire or metal powder, for rapid melting, expansion and rapid solidification, with less thermal impact, it is a fine solidification organization [27]. A layer of material with special physical, chemical or mechanical properties is fused to the surface of the base. It has a surface coating that is heat resistant, corrosion resistant, wear resistant, oxidation resistant and fatigue resistant[28]. Laser cladding is produced

automatically, the equipment is not portable and has advantages in the repair of large shafts and other rotary parts.

Spraying technology: the gas, liquid fuel or electric arc, plasma and other energy sources was used, so that metal, alloy, metal ceramics, oxide, carbide, plastic and other metal powder can be sprayed, their composite materials such as spraying materials were heated to a molten or non-molten state, through high-speed airflow to make it atomized, and were sprayed. They were deposited to the surface of the pretreated workpiece so as to form a firmly attachment [29]. Supersonic cold spraying is a fast developing technology that compressed gas through a scaled lava tube can produce a supersonic air stream that impacts the surface of the substrate in a completely solid state [30]. It has advantages in aluminum alloy products, but the repair workshop has a lot of dust [31].

Electric Brush Plating Technology: Electric brush plating technology is a new development in electroplating technology[32, 33]. It uses special DC power supply equipment, the positive terminal of the power supply is connected to the plating pen as the anode for brush plating, and the negative terminal of the power supply is connected to the workpiece [34]. As the cathode of brush plating, the plating pen is in contact with the surface of the workpiece and the metal ions in the plating solution are transferred to the metal surface and deposited and crystallized to form the plating layer under the action of electric field forces. The equipment is easy to carry commonly used for on-site maintenance, and is good for repairing smooth surfaces. The brush plating process has certain requirements for the surface

quality of the brush plating in the early stage and certain requirements for the plating solution. It will produce waste liquid.

Electro-spark deposition(ESD): ESD technology can use argon or nitrogen as the protective gas, and Utilizes the high-density energy of spark discharge between electrode(connected to the positive end of the pulse power supply) and substrate(a work piece to be repaired or strengthened , which is connected to the negative end of the pulse power supply)[35]. The discharge between the electrode and the substrate coats and infiltrates a conductive material onto the surface of the substrate to form an alloyed surface layer, which has the effect of surface repair or strengthen [36-38]. ESD equipment is easy to carry, easy to use, and has minimal environmental pollution. However, the process parameters are numerous and the deposition process is rather complex [39].

In a comprehensive comparison, ESD technology has lower operating costs than other methods, simple and convenient equipment, minimal material waste, and low environmental pollution [40-42]. Under the current perspective of environmental protection and sustainable development [43], it is worth renewed attention in the industry.

1.3 Overview of electro-spark deposition technology

The electro-spark deposition (ESD) technology is widely used in the preparation of surface coating of parts, remanufacturing and repairing thereof. It has been used widely in many industrial areas. The surfaces of mechanical parts are strengthened to improve properties by ESD technology.

The electro-spark deposition technology is important in surface strengthening. It is frequently used in the field of surface engineering and remanufacturing engineering. The ESD technology can improve the performance of the surfaces of metal materials [44]. It has been reasonably used in navigation, chemical industry, metallurgy, machinery, medicine, water conservancy and other industries. The surfaces of mechanical parts are strengthened to improve friction reduction, provide corrosion resistance, wear resistant, and other properties. The ESD can extend the service life of the surface of parts. The material is deposited in multiple layers and processed in a special way to achieve a state that can satisfy the dimensional requirements of the parts on the surface defective areas of mechanical parts [45]. The ESD technology can perform micro-arc welding on different kinds of materials of metal surfaces.

In 1943, Soviet scientists Mr. Lazarenko and Mrs. Lazarenko[46] proposed the theory of the ESD strengthening process. In 1950, the URI series of ESD surface strengthening machines were developed at the Central Institute of Electrical Sciences, and electro-spark machines entered the industrial application stage. Starting in the 1990s, engineers in TechnoCoat Co. Ltd. changed from vibrating electrodes to rotating electrodes [47].

The power of the equipment was increased to enable the overlay welding process. ESD is based on its application characteristics. It is also known as electro-spark alloying (ESA) [48], pulse arc deposition (PAD) [49], pulse electrode surfacing (PES) [50], electro-spark hardening (ESH) [51] and electro-discharge deposition [52]. Through the effect of spark discharge, the conductive material of

the electrode is fused and infiltrated into the surface of the metal substrate or part. It forms an alloyed surface layer which results in the improvement of surface properties.

1.4 Features of ESD technology

ESD technology can effectively improve the physical properties, chemical properties, mechanical properties and tribological properties in the surface of mechanical parts for dynamic equipment. It can also improve their hardness, wear-resistance and corrosion resistance. It has the following outstanding advantages.

(1) Simple process and light equipment quality. The process is simple. ESD requires only a simple grinding and cleaning of the substrate surface. ESD is carried out on the surface at a uniform speed subsequently. The ESD equipment consists of two parts: vibrating power supply and operating handle, sometimes the process needs protective gas. Because the equipment is simple, it is easy to carry on-site operation.

(2) Extremely fast solidification and small thermal deformation. It is small in the heat deformation area of the substrate. The quality of the molten metal droplets is very small. The droplets cool in a very short time, the heat of the molten droplets is rapidly diffused, the heat will not be concentrated in the processing part of the workpiece, which does not change the microstructure and various properties of the substrate material of the parts, and the impact of thermal deformation on the workpiece is limited.

(3) Wide range of applications. ESD technology is not limited by the shape and size of the component substrate. It can be deposited on the large surface and complex surface, but also can be applied to parts of local small area of deposition treatment. It is suitable for all conductive, fusible metals and metal alloy materials.

(4) Low cost for maintenance and environmental protection. ESD technology consumes less energy, and the processing does not produce material splash or harmful gas, which fact prolongs the overall life of the machinery.

1.5 The recent research progress of ESD technology

ESD technology is widely used in various fields as a very promising surface engineering technology. With the development of modern technology, people have a deeper understanding of the strengthening mechanism of the ESD technology, and the ESD technology has been further developed. The Researchers have done a lot of work in the development of the ESD coatings. Based on the conventional alloy coatings, the specialists dealing with tribology issues have further researched and prepared new coating materials with better performance, improved surface quality and optimized the process for coating. Discoveries and new theories in materials provide greater scope for exploration in ESD research.

1.5.1 Electro-spark deposition of metal ceramic layer

The ESD coatings of metal ceramic layer have the advantages of high hardness, high strength, wear resistance, corrosion resistance, oxidation resistance, and low expansion coefficient. It is widely used in cutting tools, gauges, metal molds, extractive tools, etc. The ESD can rapidly deposit carbide materials on the

metal surface and form metal ceramic alloys and ultrafine crystalline alloys to improve surface properties.

Jianzheng Wang deposited WC-4Co ceramic carbide on cast steel material and used the surface wettability theory which combined with the microstructure of the surface[53]. It was found that the surface generated tiny particles of Fe_2C , Si_2W , $\text{Fe}_3\text{W}_3\text{C}$, $\text{Co}_3\text{W}_3\text{C}$, and deposited into a thickness of $20\mu\text{m}$. Professor Tarellyk V. B. used EG-4 graphite electrode to deposit on the surface of steel R6M5, and he found in situ reaction phenomena[54]. You Tao used graphite electrode to deposit on the substrate surface of titanium alloy and generate in situ TiC coating [55]. Its Vickers hardness was 5 times that of the substrate and reached $16\ 700\text{MPa HV}_{0.05}$. Ping Zhang used TC4 as the electrode and 45 steel as the substrate[56]. The deposition layer of TiN was generated by in situ reaction at a high temperature when nitrogen was used as the protective gas. The surface nano-hardness was 4 times higher than the nanohardness of the substrate.

1.5.2 Electro-spark deposition of composite coatings

ESD technology has high discharge temperature and fast cooling, but it also has its shortcomings, such as the limited thickness of the deposited layer, the low surface quality of the deposited layer. In order to overcome these shortcomings, the method of multi-layer metal deposition is usually used to achieve the effect of improving the surface properties[57-59]. Alternatively, several materials are compounded into electrodes and deposited to improve the deposition efficiency.

Maryam Kazemi used HA/TiN dual-layer deposited on Ti-6Al-4V material to utilize the corrosion behavior and biocompatibility in dental and orthopedic

implants [60]. Bing Chen deposited two kinds of materials [61], Ti-6Al-4V and YG10, as electrode materials on the surface of H13 steel alternatively, and the microhardness and thickness of each deposited layer were significantly increased compared to the substrate. Jingming Tang deposited Ti and B₄C powder on 40Cr steel substrate by ESD to generate TiC-TiB₂ composite coating [62]. The coating has better tribological properties, which of wear resistance is five times that of the substrate.

1.5.3 Electro-spark deposition of high entropy alloys

High entropy alloys are new alloy systems with five or more primary elements. A simple solid solution is formed in each principal element, and its lattice distortion leads to strong solid solution strengthening, which results in high strength, high hardness, and high corrosion resistance [63, 64]. The ESD preparation of high entropy alloy coatings play with the high mixed entropy effect of multiple primary elements. Due to the fast solidification characteristics of ESD, it is easier to form simple face-centered cubic (FCC) or body-centered cubic (BCC) solid solution phases [65]. In this case, a fine-grained structural organization is formed. It plays the role of solid solution strengthening and fine grained strengthening, which is the benefit to obtain excellent performance coatings.

Li [66] prepared a multi-element high entropy alloy coating AlCoCrFeNi on AISI 1045 carbon steel substrate using ESD technique, and the substrate obtained has a simple BCC structure, the microhardness of the coating is 2 times higher than that of the substrate material. The corrosion resistance of the coating is better than that of the substrate. Sigrun N. Karlsdottir [67] used CoCrFeNiMo high entropy

alloys electrode to generate the coating on the surface of the steel substrate. The surface of Vickers hardness is 593HV, and it had relatively high wear and corrosion resistance. Yanfang Wang [68] prepared the deposited layer of FeCoCrNiCu high-entropy alloys electrode on the surface of 45Mn2 alloy steel. The deposited layer had good corrosion resistance.

1.5.4 Electro-spark deposition of nanostructured coatings

The liquid metal is rapidly cooled above the crystallization temperature to below the crystallization temperature, which forms the amorphous alloy tissues. Some of the tissues reach ultrafine nano-crystals. Due to the significant increase in the number of grain boundaries, it emerges that some excellent new tissues and structures with good mechanical properties.

E.I. Zamulaeva [69] utilized WC (8% Co) nanopowder deposited on Armco iron surface. The upper layer of coatings deposited with nanostructured material, which exhibit a uniform amorphous structure, higher wear resistance and reduced friction coefficient. Yuxin Gao [70] utilized Ni-Cr alloy electrode to deposit on 3Cr2Mo (P20) steel substrate. The nano-crystalline structure in the upper part of the coating was found, and it increased the substrate wear resistance and corrosion resistance. Xiang Wei [71] used coarse-grained Fe₂B electrode to generate nanocrystalline Fe₂B coating on the surface of the substrate of AISI 1045 steel. The toughness of the coating was increased. Yi Zhang [72] utilized Chromium carbide cermet (Cr₃C₂20%Ni5%Cr) powder alloy electrode deposited on Cr12MoV steel. In the nanocrystalline microstructure, the coating surface was strengthened.

1.5.5 Electro-spark deposition of biological coatings

The ESD has used materials with good biocompatibility and corrosion resistance for medical applications, such as titanium alloy and stainless steel. It is required that environmental protection, non-toxic and non-allergic reactions in blood and tissue fluids. It has high strength and hardness. It is commonly used in healing bone defects and injuries. Currently, titanium alloys and ceramic materials based on calcium phosphate compounds are used in medicine, such as hydroxyapatite (HA).

Tao Jiang [73] used silicon as an electrode material to prepare an intermediate layer in TA2 material, which prevented oxidation of titanium plates and ensured the bond strength of cast titanium porcelain. NV Boshitskaya [74] deposited $TiAl_3$ or $TiN-3AlN$ layer on VT-6 titanium alloy. Then, laser fusion of a subsequent hydroxyapatite layer was used to create biocoating, which had high corrosion resistance and biocompatibility. Salih Durdu [75] utilized Ti6Al4V material deposited on the surface of St35 steel and then after MAO treatment to generate hydroxyapatite (HA). HA-based bioceramic coatings were formed. Afsaneh Esmaili [76] utilized $Fe_{37}Cr_{15}Mo_2B_{26}C_7Nb_3Si_3Al_{16}Mn_1$. It was used as the electrode, which deposited bioceramic coatings on the surface of 316 stainless steel by ESD technology. The biocompatibility of the coatings was analyzed.

1.6 Optimization of the ESD process

Researchers optimized the machining process to improve the surface quality of ESD, reduce micro-cracking and improve surface wear resistance. In particular, many researches have been conducted on the ESD voltage, pulse frequency,

discharge capacitance, deposition time, duty cycle, protective gas flow and metal surface wetting angle. At present, the research hotspots are in the ESD of the subsequent treatment process and the study of the composite process. These studies provide new ideas for ESD automation processing to obtain better surface quality.

1.6.1 Composite coating of laser processing

The ESD deposition produces such a problem as surface micro cracking. It is useful that Laser processing improved other properties such as tribological properties of ESD coatings. Norbert Radek, et al. [77] used the WC-Co-Al₂O₃ electrode which was made of nanostructured powder and deposited on the surface of C45 carbon steel. Then, laser surface melting was performed. There could be obtained a better surface quality. The micro-cracks or pores of the laser-modified outer layer could not be observed. The surface micro-hardness increased from 784 HV_{0.04} to 843 HV_{0.04}, the critical force adhesion of the coating increased from 6.33 N to 8.94 N.

Gao [78] used an alloy powder of a nickel-based alloy to deposit it on the surface of P20(3Cr2Mo) steel substrate, and the surface was melted by a JHM-1GY-300D type pulsed laser welding machine to obtain a uniform distribution of ultrafine grains. The surface quality and surface hardness were improved, and the wear resistance had been nearly doubled. The surface wear was analyzed mainly as an abrasive wear process.

1.6.2 Composite processing in view of ultrasonic machining and ESD machining

The ESD coupled with ultrasound can yield a better surface quality of the coating. The discharge gap was effectively improved, so the coating grain size was refined, cracks in the coating, and bubbles inside the coating were reduced.

According to [79], the electrode was incorporated into ultrasonic device. Chen used die steel 718 as the electrode to deposit on the surface of H13 substrate. The effect of processing process parameters on the surface deposition thickness was studied.

Hang Zhao [80] used copper-based NiCrBSi powder electrodes to generate coatings on ASTM 1045 steel, which has good continuity and few defects. The coating also has a good continuity and few defects, and the introduction of ultrasound makes the metal powder to uniformly disperse and melt, which results in better coating quality. The ultrasonic technology puts forward strict requirements for the size and material of electrode. Although remanufacturing of the surface of the mold is more restricted, it has good performance in surface fine-machining.

Electro-spark deposition technology has been developed for more than 70 years and has received a lot of attention from researchers and scholars because of its small investment, easy operation, and remarkable effect. The technology has made great progress, but there is still a need to solve the problems, such as the limited thickness of deposited layer, large surface roughness, relatively low

productivity, unstable strengthening process, reliability needs to be improved, etc. These problems has limited the promotion and application of the technology.

ESD is one of the hot spots in remanufacturing engineering, which has a great prospect of development and application. To reduce the problems of ESD technology and further improve the performance of deposited coatings, its future development may be carried out in the following aspects: (1) Strengthening the research on the mechanism of ESD deposition; (2) Researching the process to improve the thickness and surface finishing of ESD deposition; (3) Researching the process to improve coating performance and developing multifunctional coatings for various purposes; (4) Exploring more application areas of ESD.

1.7 The purpose and the tasks of the research

The purpose of the work is to improve the quality of the surface layers at manufacturing and remanufacturing the pin shaft of the locking mechanism for the lifting device of an electric car battery by forming the composite multilayer coatings.

To achieve this goal, it is necessary to solve the following **tasks**:

1. To conduct an analysis of the existing modern methods and technologies for repairing component parts for branch mechanical engineering in accordance with the ESD characteristics.

2. To conduct an analysis of modern materials for electrode – tools to provide for a comprehensive assessment of the properties of the surface coatings applied to improve the overall technical characteristics of the surface.

3. To conduct a research on the formation of wear-resistant composite coatings and compare various surface properties.
4. To conduct a research of the defects of low-temperature soft metal deposition and improve the existing repair technology.
5. To investigate the effect of the ESD coating repair technology on the accuracy of the surface obtained.
6. Introduce the research results into the engineering practice of enterprise remanufacturing.

CHAPTER 2. BASIC THEORY AND METHODOLOGY OF RESEARCH

2.1 The working principle of ESD

At a certain distance between the electrode and the substrate, the electric field strength produces electric sparks. When the electrode and the substrate reach a certain distance, the electric field strength generates electric sparks [81, 82]. The electrode discharges instantaneously to the substrate in the form of a micro-arc, they form a discharge loop. While the discharge is highly concentrated in time and space, the arc generates high surface temperatures in the tiny area of the contact point, causing localized material melting or vaporization in the area. Liquid molten droplets are formed and deposited excessively at the contact point. The pressure generated during the discharge causes parts of the materials to be thrown away from the contact area and sputtered around to form long sparks. In short durations, pulsed currents deposit electrode material onto the surface of some base metal or alloy in the area. One of the main advantages of the ESD process is that it uses very low heat transfer into the base metal[83]. The coating is applied to the metal surface in a metallurgical bond by bringing the electrode into contact with it and melting it at close to ambient temperature. ESD is completed in a very short period of time, and it consists of three processes. (1) Physicochemical process at high temperature and pressure. (2) High temperature diffusion process. (3) Rapid phase change process.

When the positive side of the power supply is connected to the substrate, the melting of the substrate is stronger than that of the electrode [84]. It causes the removal of the substrate material. When the cathode of the power supply is

connected to the substrate, it causes the electrode material to be deposited on the surface of the substrate. The electrode material is melting on the metal surface and tends to adhere to the surface. In order to avoid electrode material sticking and Improve deposition efficiency, electrodes with different vibration sources were invented successively, as shown in Fig. 2.1: (1)Vibrating electrode: 0~100 times per second vibration frequency; (2)Rotating electrode: no more than 2000r/min; (3) Ultrasonic vibration electrode: 20,000~30,000 times per minute.

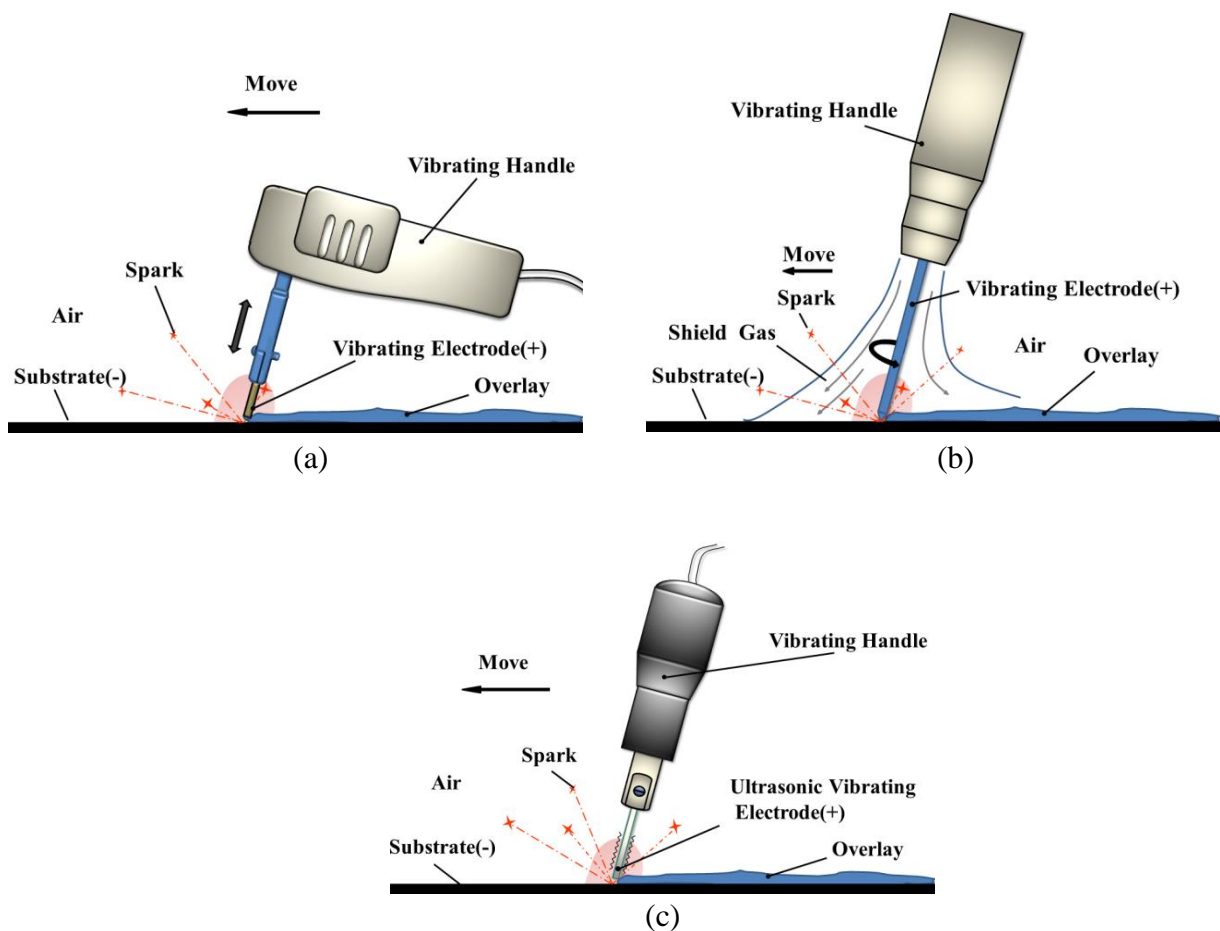


Fig.2.1 – Process diagram of electro-spark deposition: a- Vibrating electrode; b- Rotating electrode; c-Ultrasonic vibration electrode.

2.2 Corrosion mechanism of electro-spark deposition

Electrical corrosion can be broadly classified into two main categories, that is, the doctrine of thermal action and the doctrine of non-thermal action. The mechanism of corrosion by electro-spark deposition is mainly based on the theory of thermal action, which is agreed by most scholars. The thermal processes in ESD can be divided into two types: volumetric heat sources and surface heat sources.

A current passed through the discharge channel and the electrode. It heats the electrode by generating Joule-flute heat. Due to the uneven current density within the electrode, the heating and temperature distribution within the electrode is also uneven. The current is highest in the surface part of the electrode. The further inside the electrode, the more the current spreads out, the current density decreases, and the temperature also decreases greatly. Joule-flute heat is an internal heat source for the electrode, and this heat source is released within the electrode volume, so it is called volumetric heat source. In addition to Joule-flute heat, the electrode also obtains heat from the discharge channel, the current through the discharge channel also emits a large amount of heat, the temperature inside the channel is very high, through the contact surface, the heat of the discharge channel is transferred to the electrode, and spreads inside the electrode due to heat conduction. For the electrode, this heat source is external and surface, so it is called surface heat source. These two sources of heat to the electrode heating law and effect is not the same.

(1) Volumetric heat source theory (С.В.ЈебедеВ)

This theory was put forward by C.B. ЖебедеВ in 1950, who believed that the thermal process of galvanic corrosion was mainly due to the action of the Joule-flute volumetric heat source. When the discharge current passes through the channel, a high current density was formed on the contact surface with the electrode, which heated up and melts the electrode material. It was assumed that at the beginning the current density on the contact surface was sufficiently high that the effect of heat conduction can be neglected due to Joule-flute heat.

Instantaneous high-temperature Joule-flute heat made this small part of the metal melt and explodes, leaving a corrosion trace, and then the tiny channel moved to another place along the electrode contact surface, leaving another corrosion trace, and in this way, during the whole pulse discharge time, the tiny channel kept moving, melting and exploding many times. The area of the small pit was composed of many unit corrosion traces.

Calculation of the melting volume: To find the melting volume V , it is necessary to know the surface shape S_e with respect to the discharge characteristic $S_0(t)$. As the ratio of the current density to the surface shape S_e/S_0 increases, then S_e becomes deeper. V becomes closer to a hemisphere. V can be expressed as follows

$$V = \frac{1}{3\sqrt{2\pi}} \left(\frac{S_e}{S_0} \right) \left(\frac{D}{A+B} \right)^{\frac{3}{4}} \quad (2.1)$$

In Equation (2.1), S_e -Surface shape of the melted layer; S_0 -Discharge layer surface shape; D -Current heat function, $D = \int_0^t I^2(t) dt$.

(2) The surface heat source theory (Б.Н.Золотых)

The theory was first formally proposed by Б.Н.Золотых in 1953 and supported by А.С.Зингерман and others. Due to thermal conduction, heat is transferred from the discharge channels to the electrodes through their contact surfaces. Therefore, the length of the discharge channel is small in comparison with its diameter, so the heat source can be regarded as a plane equal to the area of the contact surfaces, so it was also called a planar heat source. The electrical processes on the electrodes and contact surfaces in the gap can be described as a plane transient heat source of finite size. The unstable propagation of heat from these heat sources constrained the process of evaporation (gasification) and melting of a portion of the metal confined to one place during the pulse. From the mathematical-physical point of view, the studied case was typical of unsteady processes. The thermophysical constants were determined by the temperature, since the action of the heat source was transient. The solution of this problem encountered practically insurmountable difficulties. However, using certain reasonable assumptions and studying two problems: the temperature field and the transfer of the phase transition boundary (melting). All deductions can be made to solve the linear heat conduction equation. This expression of the problem and its solution are undoubtedly approximate, but they still offer the possibility of drawing valuable conclusions.

Heat flow in a heat source was described by a Gaussian distribution. Temperature field equation (2.2) is:

$$T(r, z, t) = \frac{8g_{s\phi}\alpha k}{C\rho(4\pi\alpha)^{3/2}} \int_0^u \frac{1}{\sqrt{t}\sqrt{(4\alpha kt+1)}} e^{-\left(\frac{kr^2}{4\alpha kt+1} + \frac{z^2}{4\alpha t}\right)} dt \quad (2.2)$$

The expression for the depth of a small pit was obtained for this problem:

$$h_{\pi} = \alpha \sqrt{t_u}$$

Using the solution of Stefan's problem, the approximate expression of the volume of the funnel is:

$$V_{\pi} = \frac{1}{8} \alpha^3 \sqrt{t_u} \frac{W_x}{W_0 a} \quad (2.3)$$

In Equation (2.3), α -value determined by the solution of the Stefan's problem; W_x -energy transferred by the heat source; a -the coefficient of temperature transfer; W_0 -energy density at the center of the heat source.

In summary, a mathematical description of the thermal process of galvanic corrosion based on solving the Stefan's problem is the closest to the actual situation.

(3) The theory of surface heat sources (А.С.3 ингерман)

А.С.3 ингерман and others supported the doctrine of thermal action. They carried out experimental studies of volumetric and surface heat sources. It was concluded that surface heat sources played the main role in thermal processes. Volumetric heat source melted the metal with high electrical resistance only in short pulses and within 4% of the time of the pulse discharge. However, the volume of the melted metal was only 1 to 2 percent of the volume of the funnel, and gasification of the metal is difficult to achieve. It should also be noted that it was difficult to explain the polarity effect by the volumetric heat source theory, according to which the cathodic and anodic corrosion should be equal, which was not consistent with the experiment.

The expansion of the discharge channel was due to hydrodynamic reasons. Therefore, the diameter of the heat source increased rapidly. The increase in the diameter of the funnel was due to heat conduction and was a slower process. Therefore, the diameter of the pit was not larger than the diameter of the heat source. This conclusion has been proved by experiments. The theoretical calculations and the experimental results are in good agreement and further show that irrespective of the size of the thermal conductivity of the metal, irrespective of the pulse width and energy, the melting of the metal is the result of heat entering the electrode from the discharge channel and propagating due to heat conduction.

Electrode corrosion volume:

$$V = \frac{\pi}{12} \left(\sqrt{\frac{I_m^2}{\pi^2 j_m^2} + 4b^4} + 2b^2 \right) \sqrt{\frac{1}{\pi j_m} - 4b^2} \quad (2.4)$$

In Equation (2.4), V -the volume of the small funnel; I_m -the instantaneous action current; j_m -the instantaneous action current density; b -the radius of the contact area.

Since the heat generated from the electrical corrosion of heat source, whether it is Joule-Lenz heat or the heat generated by the discharge channel, indicates that the current density is uneven and the temperature distribution is uneven, it results in uneven energy on the electrode surface. The corroded area is formed by the accumulation of cell corrosion of multiple pulses. This explains the main reason for the inhomogeneous deposition on the surface. Therefore, the analysis of electro-spark energy, corrosion volume and energy diffusion by heat source is relatively complicated. The accurate real values cannot be obtained.

Corrosion mechanism of electro-spark deposition can be explained the mechanism of electric spark discharge. However, it is still not possible to quantitatively study all materials. The single pulse discharge energy cannot be collected during work, and the measurement of corrosion is still in the hypothetical setting of the experiment.

2.3 Pulse energy theory

(1) Pulse energy

The pulse discharge waveform and parameters have a great influence on the electrical corrosion process of the material, which determines the size of the discharge trace formed by each discharge, and then affects the processing technology index. The main parameter determining the size of the discharge trace is the individual pulse energy. Individual pulse energy is a function of discharge voltage, discharge current and pulse time width. According to different energy storage elements[85]:

a. If the spark is caused by a capacitor, then as Equation (2.5):

$$W = P_c t = \frac{1}{2} C U^2 \quad (2.5)$$

In Equation (2.5): C -capacitance; U -power supply voltage.

b. If the electro-spark is caused by an electromagnetic accumulator with inductance L and current I , then as Equation (2.6)

$$W = P_c t = \frac{1}{2} L I^2 \quad (2.6)$$

c. When the discharge circuit is more complex, it depends on the physical constants of the electrode material and the composition of the medium, as Equation (2.7):

$$W = \int_0^t P_c dt = P_c t = \int_0^t u(t)i(t)dt \quad (2.7)$$

d. The group of sparks passing through successively over a constant time T , when $T \gg t$, determines the average value of energy, as Equation (2.8):

$$P_m = Wf = W / T = P_c t / T \quad (2.8)$$

When P_m is constant, due to $T \gg t$, the pulsed power P_c can generate several kilowatts per unit of pulsed impact to achieve an increase in energy. It is the key point of the ESD theory.

(2) Discharge parameters

a. ESD sputtering amount

The amount of metal thrown by the electro-spark pulse can be obtained from the following relationship:

$$\gamma = KE n \quad (2.9)$$

In Equation (2.9), γ -the metal thrown mass of electric spark; K -the proportionality constant; E -the energy per unit pulse; n -the pulse frequency

b. Discharge mark size

According to the theory of discharge thermology, the volume of the discharge funnel is determined by the amount of heat accumulated in the discharge funnel. That is, it is determined by the difference between the heat transferred to the discharge funnel and the heat lost to the electrode body due to heat conduction.

The volume of the discharge funnel is:

$$V = \frac{Q}{g} = \frac{S(\phi - \phi')}{g} \quad (2.10)$$

In Equation (2.10), Q -the heat accumulated in the pulse discharge area on the electrode; g - the total heat of phase change per unit volume; ϕ -the unit heat flow into the electrode surface, $\phi = f(\lambda, r_K, W_0)$; ϕ' - the heat flow lost by the unit surface in the electrode body due to heat conduction, $\phi' = f(\lambda, \tau_K)$; S -the surface area of the discharge trace; λ -Thermal Conductivity; W_0 -Single pulse discharge energy.

c. The time constant of the RC circuit

Charging time refers to the time required to store the charge in the capacitor as a certain amount of electricity. In actual production, it is often necessary to use this parameter to calculate the time for charging or discharging the capacitor[86, 87]. The calculation method of the capacitor charging time depends on the capacitance value in the circuit and the resistance value of the circuit, and can be calculated using the following formula:

$$\tau = RC \quad (2.11)$$

In Equation (2.11), τ is the time required to charge the capacitor; R is the resistance value of the circuit; C is the capacitance value of the capacitor.

The equation is derived from the basic laws that capacitor charging follows. In a DC circuit, a capacitor will start charging when it is connected to a power source. The rate of charging depends on the resistance and capacitance values in the circuit because charging a capacitor consumes the potential difference that exists between the capacitor and the circuit. And the resistance of the circuit will limit the rate of flow of charge. Therefore, by adjusting the resistance values of the

capacitor and the circuit, it can be controlled that the charging rate and charging time of the capacitor. This formula is only applicable under ideal conditions, and the influence of other factors needs to be considered in practical applications, such as the internal resistance of the power supply and the internal resistance of the capacitor.

$$u_c = U - Ue^{-\frac{t}{\tau}} = U(1 - e^{-\frac{t}{\tau}}) \quad (2.12)$$

In Equation (2.12), u_c -Capacitor voltage; U - Supply voltage, when $t = \tau$, the capacitor voltage u_c can reach 63.2% of the charging voltage U ; when $t=3\tau$, the capacitor voltage u_c can reach 95% of the charging voltage U ; when $t=5\tau$, the capacitor voltage u_c can reach 99.3% of the charging voltage U . To ensure that according to the capacitor charging and discharging, the RC circuit time constant is reasonably designed.

d. Calculation model for heat of melting of metals:

$$Q = C_0 \cdot m \cdot \Delta t \quad (2.13)$$

In the formula (2.13), Q - the heat of melting of the metal (J); m - the mass of the metal (g); and C_0 -the specific heat capacity (J/g), Δt -temperature variation interval.

2.4 Heat conduction

(1) Transient heat transfer equation

The ESD deposition was considered as a transient nonlinear temperature field. It was a dynamic heat conduction process, and the temperature field changed sharply with time. According to the classical theory of heat conduction to establish

the transient heat conduction equation under the right-angle coordinate system, as Equation (2.14):

$$c\rho \frac{\partial T}{\partial t} - \frac{\partial}{\partial x} \left(k \frac{\partial T}{\partial x} \right) - \frac{\partial}{\partial y} \left(k \frac{\partial T}{\partial y} \right) - \frac{\partial}{\partial z} \left(k \frac{\partial T}{\partial z} \right) = f(x, y, z, t) \quad (2.14)$$

(2) Heat source distribution function

Gaussian heat source model mainly contains two elements: heat source distribution of energy in the action space, the radius of the action of the heat source, that is, the radius of the discharge channel. The mathematical function of Gaussian heat source distribution is:

$$q(r) = q_m \exp\left(-k \frac{r^2}{R^2(t)}\right) \quad (2.15)$$

In Equation (2.15): $q(r)$ - heat flow density at r from the center of the discharge; q_m - peak heat flow density; k - energy concentration coefficient; $R(t)$ - radius of heat source at time.

Due to the extremely short discharge time and concentrated heat source, the influence of Gaussian heat source at infinity is close to zero. Therefore, it is assumed that when $q(r) < 0.05q_m$, the influence of Gaussian heat source is not considered. This leads to the Equation (2.16):

$$q[R(t)] = 0.05q_m \quad (2.16)$$

Then the energy concentration factor k is:

$$k = \ln 0.05$$

Carried forward into eq. (2.15):

$$q(r) = q_m \exp\left(-3 \frac{r^2}{R^2(t)}\right) = q_m \exp(-3) \quad (2.17)$$

2.5 Electro-spark deposition equipment

ESD equipment has evolved from the earliest analog circuit to the current digital control circuit, and the power is getting bigger and bigger. The power of the early ESD equipment was 100W~300W in Fig. 2.2, and the power of the later development ESD equipment gradually increased, generally 500W~1500W in Fig. 2.3. The improvement of pulse power supply performance and the expansion of functions have not only significantly improved a number of performance indicators of ESD, as shown in Table 2.1. Large power electro-spark deposition equipment was also used in Fig. 2.4. But even the traditional processing technology was changed some applications, and the processing of some new materials had been achieved.

Table 2.1 – Parameters of ESD equipment

Model	Power	Voltage (V)	Capacitance (μF)	Frequency (Hz)
HL-D9110A	100W	35	---	50
HL-D9130A	300W	70	---	50
Stanley-720	153W	---	---	50
Elitron22A	500W	15-70	360	---
Elitron52A	3500W	35-210	120-2040	---
Depo50	200W	50/100/150	52.2	60-1400
Depo150	500W	50/100/150	152.2	60-1400
SparkDepo500	2500W	50/100/150	502.2	60-2000
Zhongxiang	3000W	120/130/165	30-150	50-500
SZ-Jy2800	2800W	130/260	100	50-2100
TLB—III	2100W	75-170	20-100	50-700
SZ-HMT9500	1200W	20-100	---	50-500
SZ08	1500W	20-100	---	50-500
HS-BDS07	3800W	20-100	---	50-500
DZ-4000III	4000W	20-200	30-420	1300-6000



(a)



(b)



(c)



(d)

Fig. 2.2 – Small electro-spark deposition equipments: a-HL-D9110A; b-HL-D9130A; c- Stanley-720; d-Depo50.



(a)



(b)



(c)



(d)



(e)

Fig. 2.3 – Medium electro-spark deposition equipment: a- SZ-HMT9500; b- SZ08; c- Elitron22A; d- Zhongxiang; e-TLB—III.



(a)



(b)



(c)

Fig. 2.4 – Large power electro-spark deposition equipment:
a- Sparkdepo500;b-DZ-4000III;c-HS-BDS07.

2.6 Experimental materials

(1) Substrate material

The substrate material is 45 steel plates with 2mm. This material is relatively common in the market, and its composition is shown in Table 2.2.

Table 2.2 – Basic properties of No. 45 steel

Steel	Density	Component Elements					Properties
		C	Si	Mn	P	S	
45	7.85g/cm ³	0.17-0.23	0.17-0.37	0.35-0.65	0.035	0.035	Other
					MAX	MAX	

(2) Electrode materials

a. Wear-resistant electrode

SKH-51 is a tungsten-molybdenum powder high-speed steel. The steel has fine and uniform carbide particles. It has the characteristics of high toughness, good thermo-plasticity, etc. It also has good toughness and wear resistance, and is used as a transition coating. The 3mm electrode made by Zhejiang Jinxin Co., Ltd.

is used in the test. It is made of SKH51 material from Japan, as shown in Table 2.3 and Table 2.4.

Table 2.3 – Basic properties of SKH51 alloy steel

Steel	Component Elements Properties								
	C	Si	Mn	P	S	Cr	Mo	V	W
SKH51	0.8-0.88	0.45	0.40	0.03	0.03	3.8	4.7	1.7	5.9
		Max	max	max	max	-4.5	-5.2	-2.1	-6.7

Table 2.4 – Grades of steel in different countries

JIS (Japan)	SAE/AISI (USA)	DIN (Germany)	GB (China)
SKH51	M2	S6-5-2 (1.3343)	W6Mo5Cr4V2

The electrode material consists of 90 percent WC carbide with 10 percent cobalt. WC is the most representative refractory material for cemented carbides. Industry attaches great importance to this type of material. It is characterized by a high melting point, high hardness and good wear resistance.

The 3mm electrodes were made of HF10 material (Sandvik Co., Ltd.) is used in the test. Its composition is shown in Table 2.5.

Table 2.5 – the Component Elements properties of HF10 Carbide Steel (Sandvik)

Name	Density	Hardness, Rockwell A	Component Elements Properties	
HF10	14.45g/cm ³	92.1HRA	WC 90%	Cobalt, Co 10%

b. Self-lubricating electrode

Graphite electrode is a high-temperature conductive material formed by sintering natural graphite as the main body and coal pitch additive as the binder[88,

89]. At normal temperature, it has a certain degree of lubricity [90, 91], and its composition is as follows (Table 2.6). At high temperatures it can form carbides with molybdenum, vanadium, titanium, zirconium and niobium, thus increasing the wear resistance of the material.

Table 2.6 – Basic properties of Graphite Electrodes

Name	Density	Compression strength	Bending Strength	Ash content	Resistivity	Thermal expansion coefficient
Graphite Electrode	1.6g/cm ³	30Mpa	13.5MPa	0.3%	9μΩ·m	2.5×10 ⁻⁶ /°C

Babbitt alloy B83 (SnSb11Cu6) contains 83% tin. It is a low temperature soft metal. It has good compliance and anti-friction characteristics, not easy to rust and good anti-corrosion function. It is suitable for low speed and heavy load. Tin-based Babbitt alloy is more widely used, often used in parts such as bearings, and its composition is shown in Table 2.7:

Table 2.7 – the basic composition of Babbitt alloy B83(wt.%)

Material	Sn	Sb	Cu	Pb	Other
SnSb11Cu6 (B83)	Balance	10.0-12.0	5.5-6.5	0.35	0.80

2.7 Experiment equipment

(1) Scanning electron microscope

Surface topographies are examined using scanning electron microscopy (SEM). SEM uses the method of photography and imaging, and uses the various physical signals excited by the finely focused electron beam to scan the surface of the sample to perform modulation imaging. The depth of field of the scanning electron microscope is much larger than that of the optical microscope, which can

analyze the morphology of the microscopic surface. Since the scanning electron microscope observes the microstructure, the sample can be directly observed without copying. Japan's Hitachi Regulus8220 has a high-resolution scanning electron microscope in Fig. 2.5. The field emission scanning electron microscope is equipped with a cold-field electron gun suitable for low-acceleration voltage and high-resolution observation with extremely small chromatic aberration. The maximum magnification has also increased from the previous 1 million times to 2 million times. The energy analysis energy spectrometer Bruker X-ray energy spectrometer EDS. QUANTAX can measure and analyze the X-ray photon energy of all elements on the sample surface. The energy spectrometer does not need to be focused, and can analyze various samples with different precision.



Fig. 2.5 – Hitachi Regulus8220 (SEM)

(2) X-ray diffraction phase analysis

X-ray qualitative analyses make use of the different atomic structures of substances and diffract specific patterns, which can be mechanically superimposed. Substances are analyzed using standard diffraction sample pdf cards. XRD equipment (Bruker D8 Advance A25, Germany) has with maximum output power ≥ 2.2 kW; current and voltage stability better than ± 0.005 %; ray dose ≤ 0.2 μ Sv/h.

Goniophotometer radius ≥ 200 mm, 2θ rotation range $-10^\circ \sim 168^\circ$, can be read in the smallest step of 0.0001° . It can be used for testing and analyzing samples such as powders, lumps and thin films in Fig. 2.6. The file generated by scanning can be compared and analyzed with XRD related software.



Fig. 2.6 – XRD equipment

(3) Vickers hardness tester

Vickers hardness test method was proposed in 1924. It is the use of the face angle of 136° diamond vertebrae as an indenter. The indenter pressed into the surface of the metal sample and held for a particular period of time under a certain static force. It is the fastest and most economical method of testing material properties.



Fig. 2.7 – Vickers hardness tester

The specimen preparation is simple. The surface is basically undamaged. However, the method requires low surface roughness and flatness, which is suitable for metal materials. When multilayer films are used, metal corrosion solutions can be used for delamination. Walter UHL's VMH-002VM has a 12-level hardness test force for all hardness of metallic materials, as shown in Fig. 2.7. The measuring objective has two stops, 10X and 50X, and it has a resolution of 0.01 μ m. It can be operated with a color display touch screen.

(4) Linear reciprocating friction wear machine

MWF-500 reciprocating friction and wear machine was manufactured by Jinan Huaxing Test Equipment Co., Ltd, as shown in Fig. 2.8. The size of the test force is controlled by the servo system and force sensor, and the pressurized strength is within the range of 5-500N. The servo drive mechanism drives the friction vice to carry out reciprocating motion, and the friction force and its friction coefficient of friction are determined through the test measurement and control system during the friction test. Reciprocating test stroke: 1~20 mm, friction force measurement range: 1~100 N, measurement accuracy: 1%, maximum reciprocating speed: 1~300 times/min.



Fig. 2.8 – Linear reciprocating friction wear machine

(5) Ultra-depth-of-field microscopy

Leica DVM6 Super Depth of Field Microscope can measure and quantitatively characterize the 2D surface morphology and 3D height value of coatings, as shown in Fig. 2.9. It has a maximum working distance of 60mm, a motorized focusing range of 60mm, and a focusing accuracy of 0.25 μ m, a large field of view of 43.75mm², and a highly dynamic color resolution with a maximum physical pixel count of 3664 X 2778dpi. Using LAS X software, 2D images can be reconstructed in 3D to obtain 2D super depth of field images and 3D surface morphology. The 2D and 3D morphology of wear can be effectively measured.



Fig. 2.9 – Super depth of field microscope

2.8 Experimental method

(1) Pre-treatment of coating surface

The substrate material was selected according to the research object. Using wire or laser cutting equipment, the specimen was made into 25*30mm size. The surface of the specimen was ground with sandpaper, 240, 400, 800, 1000 sandpaper was selected for grinding. Then ultrasonic cleaning was carried out for 10 minutes. The surface was blown dry by hairdryer. With anhydrous ethanol, the

specimen surface was wiped to remove oil and water stains. When the anhydrous ethanol surface evaporated, it was weighed using a balance. Thus, the experimental specimens were prepared.

(2) Coating preparation method

Drying oven was utilized to dry the electrodes at 100 °C for 30 minutes. The ESD deposition equipment was selected according to the process requirements. Pre-experimentation was carried out to rationally select and adopt frequency, voltage, duty cycle, electrode steering and rotational speed as processing parameter intervals. The electrodes were required to move in small circles or zigzag lines on the surface of the substrate. Depending on the temperature of the electrode head, a certain speed of movement is carried out. The electrode was maintained at a certain electric spark discharge distance from the metal surface. Excessive pressure makes the discharge distance smaller, the discharge energy of the arc becomes smaller, and the head of the electrode is easy to become bent after heating, which can not ensure normal processing. During processing, the electrode should be kept about 45 ° from the substrate to reduce the frictional resistance during processing. In order to ensure the quality of the deposited layer, argon is usually selected as the protective gas, and 10-15 L/min flow rate is selected for processing.

(3) Post-coating treatment

After the coating is completed, the surface is cooled waiting for room temperature. By a brush the surface metal dust is wiped. Using 130W ultrasonic cleaning machine, it was cleaned in anhydrous ethanol for 10min. Then, it was weighed and recorded by using a balance. The surface was then tested for

morphological observation, tissue composition and friction and wear properties. The specimens were cut using a low speed cutter. The metal coating was inlaid using an inlay machine. The specimens were graded for grinding using a grinder, 400, 800, 1200, 1500 grit sandpaper was selected and grinding was carried out under aqueous environment. Polishing paste of W3.5 was selected and polished using polishing machine. Then 3% nitric acid was selected as the etching solution to etch the test surface. From there, the delamination of the substrate and coating was observed. Using a Vickers hardness tester, the load was applied by selecting the appropriate range according to the thickness and hardness of the coating, and the indentation was measured using software.

2.9 Gradient deposition process

In 1987, the concept of gradient structure was first proposed by Japanese scholars Masyuhi NINO, Shuhei MAED, and Ryuzo WATANBE, and was subsequently valued by researchers in many countries[92]. Today it is still valued by industry and researchers, and combined with various processing techniques[93, 94]. It can form functional coatings that meet special requirements. The gradient structure refers to the material whose elements that make up the material change continuously along a certain dimension, so that the material properties have a corresponding gradient change in space. With the understanding of the natural gradient structure, people have also developed many new gradient structure materials. It mainly includes surface modification and overall layered structure. Surface modification is mainly to form a single-layer, multi-layer or continuous gradient structure on the metal substrate through physical or chemical methods to

improve the performance of the material. The overall layered structure mainly distributes two or more materials layer by layer, so that the new structure has a variety of material properties. Surface modification is divided into chemical and physical principles[95]. Chemical modification is to introduce new elements on the metal surface, such as carburizing, nitriding[96], sulfurizing[97], nitrocarburisation [98], etc.; Physical modification is to use the method of coating to form a single-layer or multi-layer structure on the surface of the metal material to achieve various properties of the material.

The traditional ESD process deposits mainly a single material on the substrate. If the hardness difference between the electrode material and the base material is too large, the coating has poor impact resistance. The ESD deposition is used on the metal substrate to form a multi-layer gradient structure to achieve hardness continuity[99], avoid excessive hardness difference, improve coating toughness and reduce coating brittleness and the surface quality is improved. The SKH51 material itself has less thermal cracking, and the iron matrix has good compatibility with WC and cobalt. The SKH51 material was first coated on the substrate of No. 45 steel material, and then the WC coating was deposited. It achieved a hardness gradient, reduced the maximum crack width on the surface, and increased deposit thickness. Since WC alloys will undergo corrosion and wear in the course of practical application, once corrosion occurs, the surface will deteriorate rapidly, resulting in a decrease in the mechanical properties of the alloy. The element cobalt in WC Cemented Carbide is a binder, and it is also a corrosion-prone metal. In order to avoid the corrosion of the WC coating in a wet

environment, the B83 material is deposited on the surface of the WC coating to reduce corrosion, reduce the coefficient of friction, and reduce friction. Thus, the anti-friction coating is formed. This technology was applied to the battery box of electric vehicles to ensure that the pin shaft can enter the slot smoothly. For the supporting gasket, it was remanufactured and carburized by electric spark to remove the oxidized corrosion layer on the surface, reduce surface corrosion and improve surface hardness. Graphite powder on the surface can reduce the friction between the spring and the washer, reduce the contact surface, and reduce the corrosion of the spring to the washer.

2.10 In situ reaction process

The wear resistance of the surface layer is enhanced by synthesizing hard particles on the surface[100-102]. According to the source of reinforcing particles, the method of preparing the kind of composite strengthening layer can be divided into adding particle method and in-situ synthesis method[103]. The process of in situ synthesis refers to the method in which reinforcing materials are generated or grown by themselves in the matrix during the material manufacturing process. The basic principle of in situ synthesis technology is to generate one or several ceramic or intermetallic compounds with high hardness and high elastic modulus in situ in the matrix as the reinforcing phase to strengthen the matrix properties through the chemical reaction between elements or between elements and compounds under certain conditions. Elements that have a strong affinity with carbon, such as titanium, zirconium, niobium, etc., can form carbides in situ with graphite in the ESD process. These strong carbide-forming elements are an important part of

improving the wear resistance of metal surfaces. The carburizing process is used. The surface hardness of titanium, zirconium, niobium and other coatings is enhanced by electrospark carburizing process. The surface-cured graphite powder can also reduce friction.

2.11 Summary

(1) An analysis of equipment for performing the electric spark deposition by vibrating electrodes with different design features of the operation has been carried out.

(2) Based on the theoretical studies of galvanic corrosion, a theoretical calculation of three types of corrosion parameters has been obtained.

(3) It has been proposed to introduce the concept of the theoretical value of pulse energy. The energy of an individual pulse was determined for ESD pulses of various formations. The scattering magnitude and ESD discharge parameters were obtained. The time constant of the RC circuit and an empirical calculation model for the heat of metal melting were determined, which makes it possible to establish the energy necessary for melting the electrode material.

(4) Based on the analytical dependence of the distribution of the heat source thermal conductivity, the amount of heat, which provides deposition, has been determined.

(5) A classification of ESD equipment according to discharge power has been proposed. Depending on the specified quality parameters of the surface layer of the part, the criteria for choosing equipment were formulated.

(6) The substrate materials and alloying electrode materials were selected to form a multilayer coating: steel 45+graphite+steel CX51+WC+B83.

(7) There has been analyzed modern equipment and justified the choice thereof to determine the structure, geometric parameters of the surface, analysis of the elemental composition, phase analysis, mechanical and tribological properties of the formed coatings.

CHAPTER 3. EXPERIMENT RESEARCH RESULTS AND ANALYSIS

3.1 The characterization of graphite coatings

The electro-spark deposition is used as a traditional surface enhancement method. Viacheslav investigated the carbonating process through discharge energy and graphite powder [104]. Karavaev studied surface wear resistance with the current and the number of machining cycles in ESD [105]. Shevchenko analyzed the ultrasound method in the carburizing process [106].

The 45 steel had low cost and good overall mechanical properties but had poor wear resistance [107]. The carburizing process was carried out by adding carbon to the surface layer of the metal, which formed a high-strength carbide[108]. The carburizing furnace was used by adding gas, liquid, or solid in the traditional carburizing process[109]. The metal was heated to a certain temperature, maintained a particular time to achieve, and carburized[110]. For large mechanical parts, carburizing required special large equipment and high costs. For some specific structures, it was even hard to be carburized. Carburizing process of ESD can be carried out on the surface of large machinery and equipment outdoors without the special carburizing furnace. The carburizing process was studied using graphite electrodes to improve the wear resistance of No. 45 steel [111-113]. It is particularly advantageous for agricultural machinery, pumps and mechanical tools. These machines are often made from 45 steel, which has cost performance and is used as the base material.

3.1.1 Material Process and Deposition Parameters



Fig. 3.1 – The high-speed ESD repair machine (HMT9500)

Table 3.1 – The ESD carburizing process parameters

No.	Efficiency(%)	Voltage(V)	current frequency (Hz)	Time (s)
	A	B	C	D
1	20(1)	25(1)	100(1)	120(1)
2	30(2)	35(2)	180(2)	240(2)
3	40(3)	45(3)	260(3)	360(3)
4	50(4)	55(4)	340(4)	480(4)

()-Level values in brackets

First, there was prepared a sample made of No. 45 steel with a size of 25*30mm and 2mm thick. Then, the surface was sanded separately using 600-grit sandpaper to remove the oxidized layer and impurities. The surface was cleaned with 99% ethanol. Finally, a high-speed ESD repair machine (Fig. 3.1, Huimite HMT9500, China) was used for carburizing on the 45 steel surface. The 3mm diameter graphite rod was used as an electrode, and argon was used as the shielding gas. A 4-factor and 4-level tests were carried out by a Taguchi OA factorial design [114]. The process parameters were shown in Table 3.1.

3.1.2 Materials testing methods

Graphite powder was wiped from the machined surface with a brush. The composition of the deposited surface was analyzed by the X-ray diffraction (XRD) method (Bruker D8, Germany). The experiments were carried out with a linear

reciprocating friction wear machine (Huaxin MWF-500, China). The sample was fixed through a special fixture. A 6mm diameter friction ball (ZrO₂, G10 accuracy) was used for the surface abrasion test, as shown in Fig. 3.2. The motor rotated at 100r/min, and the reciprocating distance was 6mm. Thus, the motor performed two times movements per 1 cycle. The experimental time was 15 minutes for the reciprocal dry friction experiment. The temperature of the experimental environment was 25 °C, and the humidity was 53%. Abrasion debris was produced on the surface of the friction samples. A brush removed the surface powder. The surface was scratched with alcohol and dried naturally. Then, the samples were weighed on a balance (Sartorius BSA224S-CW, China). Finally, the abrasions were measured with the microscope (Leica DVM6, Germany).

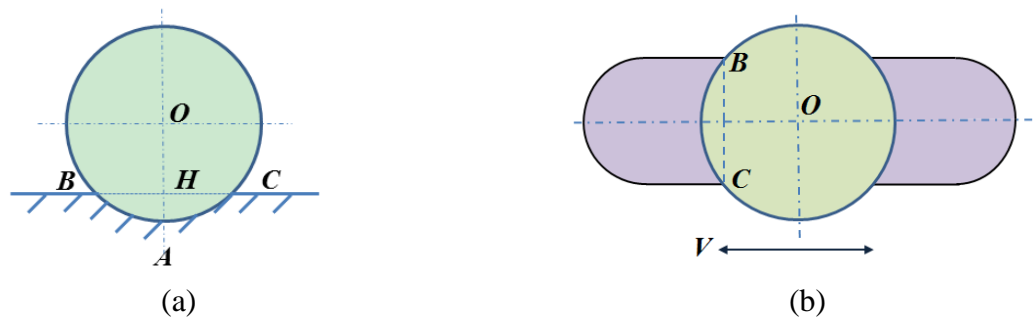


Fig. 3.2 – Schematic diagram of the friction ball: a-parameter diagram of abrasion marks; b-movement diagram of the friction ball

$$V_W \approx L \times (2L_{AH} * L_{BC}/3 + 8L_{AH}^3/15L_{BC}) \quad (3.1)$$

$$L_{AH} = R_0 - \sqrt{R_0^2 - (L_{BC}/2)^2} \quad (3.2)$$

In Equation (3.1): V_W -Wear volume of the sample, mm^3 . L -Length of abrasion, mm . L_{AH} -Depth of abrasion, mm . L_{BC} -Width of abrasion, mm . In Equation (3.2): R_0 -Radius of the friction ball, mm . Three abrasion mark experiments were carried out, and the relevant parameters were measured.

3.1.3 Abrasion morphology of the carbonized and non-carbonized experimental specimens.

Carburization deposition of No. 45 surfaces was carried out according to the experimental parameters in Table 3.1. Analysis of wear resistance can be done depending on the deposition quality. [115, 116]. Because the carburized surface had graphite powder, this study did not use abrasion mass but abrasion marks for the analysis [117].

The wear resistance was tested by the linear reciprocal friction and wear machine on the metal surfaces. There were free-form graphite powder and sintered-form graphite powder on the carburized surface. Then, free-form graphite powder on the surface was gently scrubbed with a soft brush. The machine adopted ZrO_2 rubbing ball as counter-abrasive material on a steady pressure of 15N. Each friction test was conducted three times. The width of the middle part of the abrasion was measured five times. The maximum value, minimum value, and middle values were measured (Fig. 3.3). At the edges of the abrasions, there were clear spalled areas of the material which were not smooth (Fig. 3.3a). The distinctive scratches appeared at the upper edge of the abrasion mark. When carbide powder with hard phases on the underside was broken off by the force of the friction ball, it moved toward the outside of the scratch. The abrasions gradually grew in size under the reciprocal rubbing process. The apparent oxidized sheet appeared at the bottom of the abrasion, which indicated that the friction force increased during the sliding process. These led to increase surface roughness and plastic deformation of the micro-protrusions. It caused an increase in local

temperature and accelerated oxidation of the surface. There were tiny scratches at the bottom of the abrasion, hard spot burnishing on the bottom, and craters on the surface. Through the experimental comparison group, it was found that the abrasion width was smaller than that of the sample without carbonization (Fig. 3.3b). Because of the generation of hard particles on the worn surface, increased surface friction resulted in the formation of an oxidized layer. It can be seen from Fig. 3.3 that the wear mechanisms are mainly adhesive wear and abrasive wear. There is also a small amount of oxide layer on the surface due to adhesive wear.

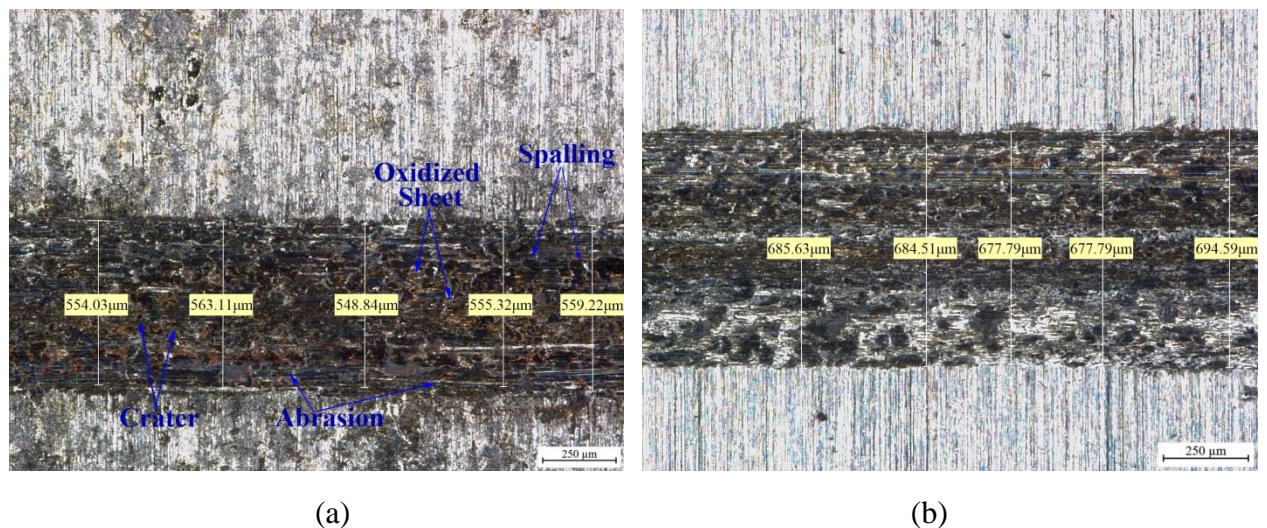


Fig. 3.3 – The 500X morphology of abrasion: a-Abrasion in carbonized materials; b-Abrasion in non-carbonized materials.

3.1.4 Results of orthogonal carbonization experiments

The deposition experiments were carried out by 4 levels and 4 factors factorial design. Four factors included efficiency (duty cycle), discharge voltage, current frequency and time[118]. Moreover, the average values and the average variances of the abrasion width were plotted, respectively. The samples without surface carbonization were also analyzed for comparison. It can be seen from Table

3.2 that the average value of sample 6 was the smallest, and the abrasion width of samples 3, 7, and 15 were smaller (Fig. 3.4). In the three samples, the variance of sample 15 was better than that of sample 3 and sample 7 (Fig. 3.5). In contrast, sample 9 had the widest wear masks. Corresponding parameters such as efficiency (duty cycle), discharge voltage, current frequency and time were all small. The carburizing effect was not good, and the wear resistance was poor.

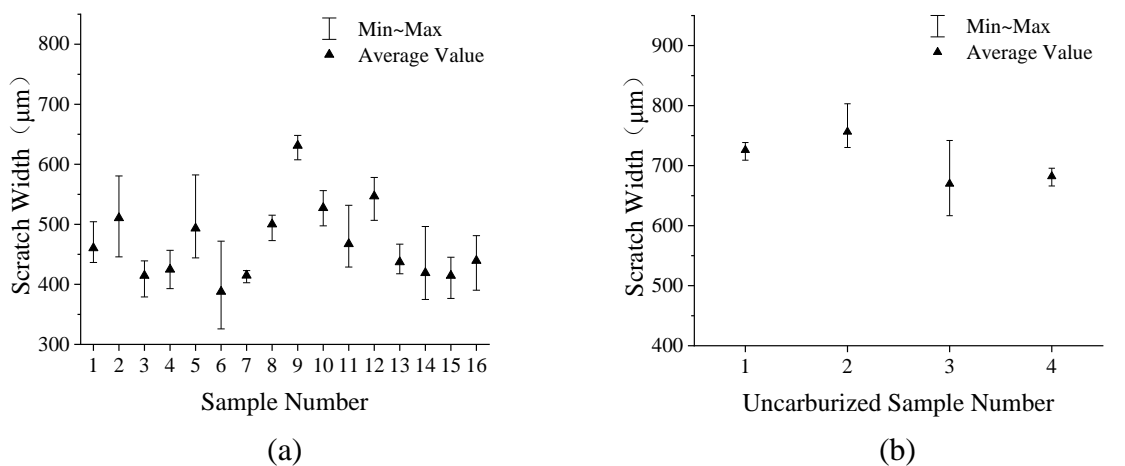


Fig. 3.4 – The Average Value of Abrasion Width: a-Experimental groups of Taguchi OA; b-Uncarbonized experimental groups

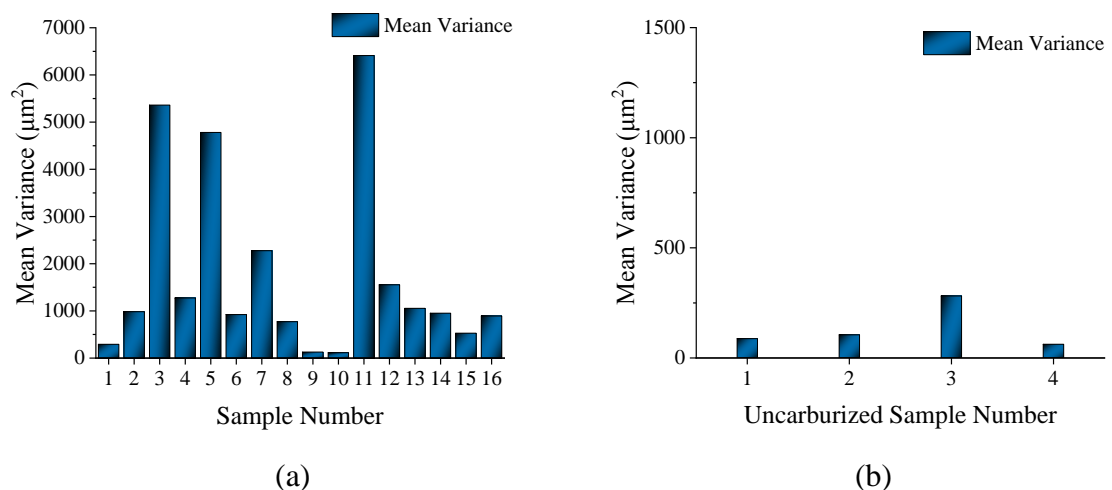


Fig. 3.5 – The Variance of Abrasion Width: a- Experimental groups of Taguchi OA; b- Uncarbonized experimental groups

Table 3.2 – The ESD carburizing process parameters

No.	Factor1	Factor2	Factor3	Factor4	Abrasion width	
	A	B	C	D	Average value, (μm)	Average variance, (μm^2)
	Efficiency, (%)	Volt, (V)	Current frequency, (Hz)	Time, (s)		
1	20	45	260	360	460.38	290.58
2	30	25	180	360	510.61	982.07
3	40	55	180	120	414.52	5360.59
4	40	35	340	360	424.84	1272.93
5	50	55	100	360	493.33	4780.89
6	20	55	340	480	387.93	921.12
7	50	35	260	120	414.88	2273.91
8	30	35	100	480	500.09	769.31
9	20	25	100	120	631.11	126.59
10	20	35	180	240	527.41	113.30
11	50	45	180	480	467.29	6410.23
12	30	55	260	240	546.79	1552.33
13	40	25	260	480	437.15	1053.56
14	50	25	340	240	419.06	949.52
15	30	45	340	120	414.47	526.93
16	40	45	100	240	439.39	891.23

Because of the accumulation effect of continuous current pulses, sample 11 had a significant duty cycle value and voltage value, but the electrode graphite was significantly ablated at the head of the electrode, and the surface deposited was not the highest value for wear resistance. It showed that the abrasion width was smaller, and the wear resistance was better. The variance was also small, indicating that the surface uniformity was good. The average values and the average variances of the abrasion width should be considered comprehensively.

According to the comparison group, it was found that non-carbonized samples had a larger width of abrasion marks than the carburized ones (Fig. 3.4b).

Their mean variances were smaller than that of the carburized group, which indicated that the material properties were close (Fig. 3.5b). However, carburized samples had been altered material properties due to the different carburizing process parameters. Because the hard phase was unevenly formed on the surface of the carburized sample, it would cause a sizeable average variance.

3.1.5 XRD analysis of carbonized surface

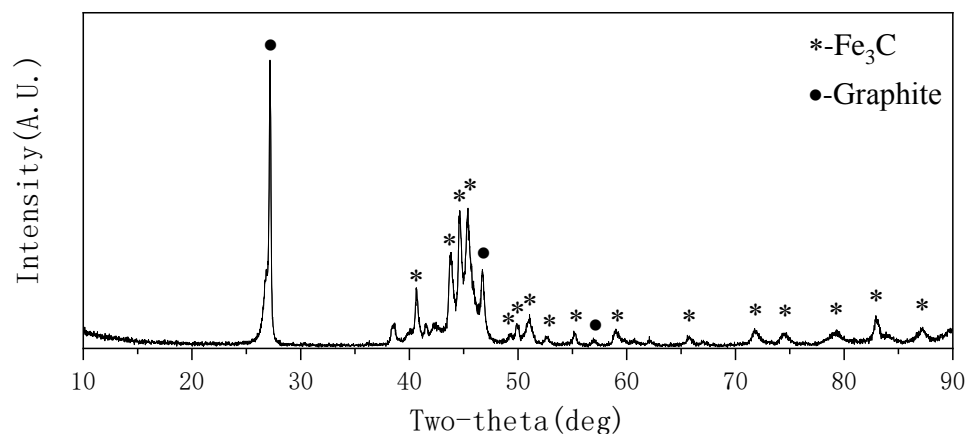


Fig. 3.6 – XRD patterns of the carbonized surface on 45 steel

XRD analyses were carried out on the deposited samples. The surface of 45 steel was found to be mainly graphite and Fe_3C . And Fe_3C generated on the surface of 45 steel [119-121] was the hard phase that increased wear resistance [122]. In the friction and wear test, the surface produced a mixture of Fe_3C hard particles and graphite, which weakened the lubrication effect of graphite in dry friction. Ferrum was not detected on the surface (Fig. 3.6), indicating that the surface was completely carbonized.

3.1.6 Data Analysis of Orthogonal Experiment

Orthogonal experimental calculation about deposition data was carried out on 4-factors and 4-levels by Taguchi theory [123-125]. As the value of the abrasion

width was smaller, the wear resistance was better [126]. It was selected that the minimum value corresponded to the four factors. It can be seen from Fig. 3.7 that a smaller extreme R meant a more significant factor. According to extreme R, the effect on wear resistance was found to be time D > efficiency A > frequency C > voltage B.

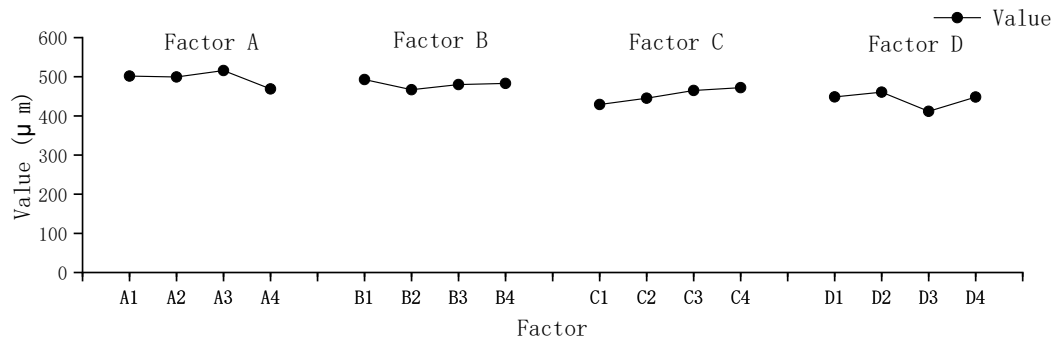


Fig. 3.7 – Variation trend of the width of the abrasion marks with process parameters

It was found that the longer time did not mean better deposition but that there were essential links in the four factors. In the experiments, the electrode temperature rose too quickly when the duty cycle, voltage, and frequency were large. The graphite ablation was serious. So the deposition process could not obtain optimal results (Fig. 3.7). Therefore, reasonable process parameters were the key to the carburizing process.

In Table 3.3, A4B2C1D3 was chosen as optimal parameters. Among the experimental samples, A1B4C1D3 (sample 6), A3B4C4D1 (sample 15), and A4B2C3D1 (sample 7) have better wear resistance and surface uniformity. They can also be used as an alternative in industrial applications.

Table 3.3 – Orthogonal experimental calculation

No.	A	B	C	D	Value
1	1	3	3	3	460.38
2	2	1	2	3	510.61

3	3	4	2	1	414.52
4	3	2	4	3	424.84
5	4	4	1	3	493.33
6	1	4	4	4	387.93
7	4	2	3	1	414.88
8	2	2	1	4	500.09
9	1	1	1	1	631.11
10	1	2	2	2	527.41
11	4	3	2	4	467.29
12	2	4	3	2	546.79
13	3	1	3	4	437.15
14	4	1	4	2	419.06
15	2	3	4	1	414.47
16	3	3	1	2	439.39
k1j	501.71	492.99	428.98	448.64	
k2j	499.48	466.81	445.38	460.64	
k3j	515.98	479.96	464.80	411.58	
k4j	468.75	483.16	472.29	448.12	
QJ	1985.92	1922.92	1811.45	1768.97	
MIN	468.75	466.81	428.98	411.58	
R(MAX-MIN)	47.24	26.19	43.32	49.07	
OPTIMAL VALUE	A4	B2	C1	D3	

3.1.7 Surface abrasion morphology and parameters of the optimal process

The optimal process parameters were selected for deposition (Table 3.4). It showed finer abrasion marks. It indicated that the material had better wear resistance. Although the solidified graphite was deposited on the surface, it had a small brown oxidized layer in the middle of the abrasion marks on the surface. The mass of wear powder was smaller, and the abrasion width was narrower. So the surface wear resistance was better. The average abrasion width of sample 2 (Fig. 3.8) was 756.441 μm . According to Equation 3.2, the depth of abrasion was 23.937 μm , which was substituted into Equation 3.1 to obtain the volume of $85.484 \times 10^{-6} \text{mm}^3$. The density of Ferrum was 7.87g/cm³, and the wear quality was calculated as $6.73 \times 10^{-4} \text{g}$.

Table 3.4 – Optimal process parameters for surface carbonization
deposition on No. 45 steel

A4 Efficiency, (%)	B2 Voltage, (V)	C1 Current frequency, (Hz)	D3 Work Time, (s)
50	35	180	360

Similarly, in the optimal process, the average value of the abrasion width was $268.206\mu\text{m}$, and the depth of abrasion was $2.999\mu\text{m}$ according to Equation 3.2, which was substituted into Equation 3.1 to give a volume of $3.217 \times 10^{-6}\text{cm}^3$. Because the density of Fe_3C was 7.694 g/cm^3 [127], the abrasion mass was $2.47 \times 10^{-5}\text{g}$. The balance is difficult to guarantee the measurement accuracy of the surface quality. Due to the rough texture of the abrasive surface (Fig. 3.8) [117], the actual wear quality should be smaller than the theoretical calculation. The wear resistance was compared by the abrasion width, and the width of the wear scar has excellent accuracy compared to the quality on the carburized surface of No. 45 steel. Optimization of the carburizing parameters results in better wear resistance.

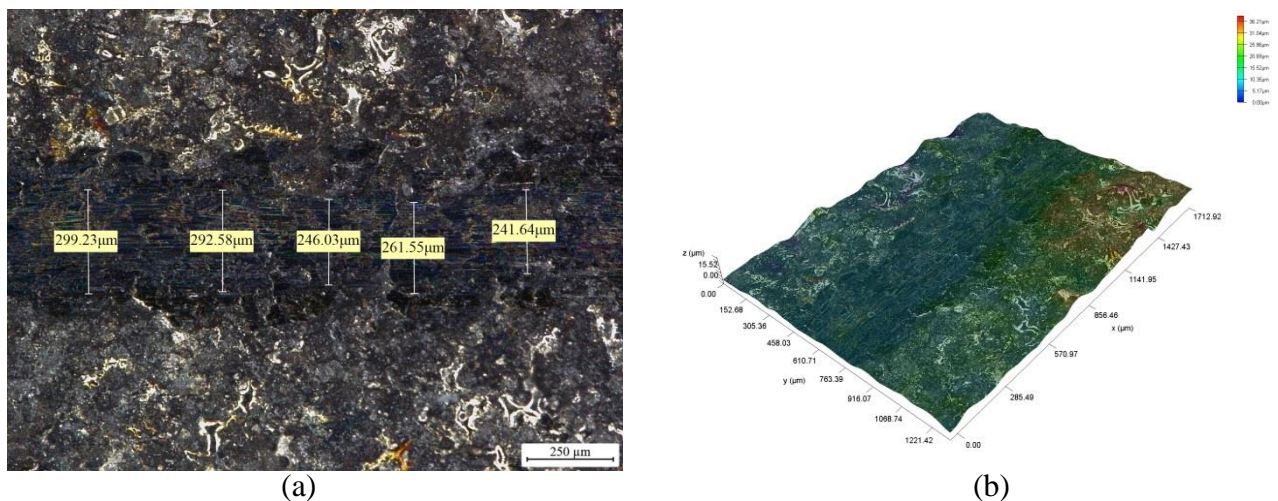


Fig. 3. 8 – Surface abrasion morphology of the optimal process: a-2D Shape;
b-3D super depth of field morphology.

3.1.8 Conclusions

Metal surfaces can be easily carbonized by the graphite electrode. On the basis of the obtained test results, ESD can increase the wear resistance of the material surface. The wear mechanisms of carburized coatings are mainly adhesive wear and abrasive wear. Process parameters are essential in electro-spark deposition.

(1) It was used to comprehensively evaluate the wear resistance with better results that average width and average variance of abrasion marks when the graphite powder and the grinding dust were small in mass.

(2) It was used Taguchi's factorial method and calculation to find out the optimal process to guide graphite deposition. The deposition parameter values were larger, but the abrasion width was not necessarily smaller, and the wear resistance was not necessarily the best. An optimal process parameter and three industrial alternatives were found by experimental design.

(3) Free graphite powder and sintered graphite powder are produced on the carbonized surface. If the wear resistance is analyzed according to the quality of the deposition, graphite powder on the surface is susceptible to treatment methods and humidity. These can then cause significant errors in the statistical results. Therefore, the abrasion marks method can accurately evaluate wear resistance. It can be used in powder composites.

(4) The graphite powder on the surface reduced friction in the early stages of friction, but it had a limited effect with the hard abrasive powder on the reduction of friction. There even was an oxidized layer on the deposition of the surface.

3.2 The characterization of SKH51 coatings

3.2.1 Introduction

(1) High Toughness and Wear Resistance Materials

Metal materials are subjected to impact loads during service. The load has a short duration of action and a certain speed of impact. The ability of the material to resist the impact load in this case is called the toughness of the material. When the coating material is brittle, it is easily dislodged by the impact. In the ESD deposition process, the coating material is more brittle and needs to increase the coating toughness. The usual solution is to refine the grain, strengthen and toughen the composite, and alloy. In the alloy method, SKH51 was selected as the electrode material. SKH51 is a tungsten-molybdenum tough high-speed steel. The carbide particles in this steel are fine and uniform. The presence of molybdenum can reduce carbide segregation. Vanadium can make the steel form a higher stability when heated. It is 2 times more wear resistant and 1.5 times tougher than high chromium high carbon steel. Therefore, it has good toughness and wear resistance, was mostly used in mould industry and cutting tool industry. Bai proposed to use gradient coatings, layered structure coatings and multi-scale structure coatings to obtain high hardness and high toughness wear-resistant coatings[93]. G. Rolland proposed that cobalt-based Stellite 6 has good toughness and hardness[128]. Liu modified the toughness of AlCrSiN coatings by increasing the nickel content[129]. SKH51 materials use the element of iron to ensure sufficient toughness, which can be well balanced for the relationship between hardness and toughness[130, 131].

(2)Wear Resistant Coating

SKH51 has fine tungsten carbide particles, which can guarantee a certain wear resistance. Metal hard compounds have higher hardness and better wear resistance. The carbide and nitride of metal elements are used to enhance the surface hardness of the coating. Hossein deposited WC/TiC/Co/Ni coating on the surface of St52 steel with a maximum hardness of 710HV[132]. Yusuf Kayali deposited WC coating on AISI 5140 to obtain better wear resistance [133]. Wang used the ESD process to deposit Ni and Mo as transition layers on the surface of H13 steel, and deposited a WC-Ni composite coating [134]. Wang deposited a WC-10%Co coating at TC11, comprehensively evaluated the coating quality and determined the process parameters for repairing coating defects[135]. Mert Onan used ESD technology to deposit two layers of WC (tungsten carbide) and WC + SS (tungsten carbide and stainless steel) coatings on the surface of CK45 die steel to change the surface properties of the die[136].

3.2.2 Experimental method

A 45 steel plate with 2mm thickness was cut into 25*30mm size samples with laser cutting. The specimen was cleaned by ultrasonic cleaner, and the surface of the specimen was blown dry by a hair dryer. Then, 240, 400, 800, and 1200 grit sandpaper was selected in turn to grind the surface to remove the oxide layer and impurities. The specimens were again cleaned using an ultrasonic cleaner and were blown dry. The surface of the specimen was wiped with 99% anhydrous ethanol and weighed using a balance (OHAUS AR1140, 0.0001g analytical balance). HMT9500 (Shengzao Co., Ltd., China) was used for ESD equipment. A SKH51 rod with 3mm diameter was used as an electrode and argon was used as the

protective gas. Electro-spark deposition was conducted on the 45-steel surface. The process parameters were shown in Table 3.5. Four factors and four levels of experiments were carried out by Taguchi OA factorial design, and the deposition time was 5 minutes, as shown in Table 3.6.

Table 3.5 – The ESD carburizing process parameters

No.	Current frequency (Hz)	Voltage(V)	Efficiency(%)	Rotate Speed (r/min)
	A	B	C	D
1	100(1)	20(1)	25(1)	150(1)
2	200(2)	28(2)	30(2)	225(1)
3	300(3)	36(3)	35(3)	300(1)
4	400(4)	44(4)	40(4)	375(1)

()-Level values in brackets

Table 3.6 – Taguchi OA experimental parameters for SKH51 deposition experiments

Sample	Current Frequency (Hz)	Voltage(V)	Efficiency(%)	Rotate Speed (r/min)
1	100	20	25	150
2	100	28	30	225
3	100	36	35	300
4	100	44	40	375
5	200	20	30	300
6	200	28	25	375
7	200	36	40	150
8	200	44	35	225
9	300	20	35	375
10	300	28	40	300
11	300	36	25	225
12	300	44	30	150
13	400	20	40	225
14	400	28	35	150
15	400	36	30	375
16	400	44	25	300

After the deposition, a brush was used to remove the metal powder and the specimens were weighed by a balance (OHAUS AR1140, 0.0001g analytical balance). A coating thickness meter (Aicevoos, AS-x6) was used to measure the coating. XRD physical examination of the surface was conducted. The surface morphology of the samples were observed by SEM. The experiment was carried out using a ball-disc friction and wear tester (MS-T300, Lanzhou Huahui Co., Ltd., China), in which the test parameters were set: load 5N, test time 10min, spindle speed 600r/min, test radius 3.5mm. The 5mm friction balls (ZrO_2 , G10 precision) were used to carry out the surface abrasion test. After the test, the powder generated on the abraded surface of the parts was removed by a brush, wiped with alcohol scratches and dried naturally. The abrasion marks were measured by a super depth of field microscope (Leica DM6, Germany).

3.2.3 Discussion of results on SKH51 coating

(1) Coating Quality

According to the experimental parameters in Table 3.6, SKH51 material was deposited on the 45 steel surfaces. Using a balance, the weight of the sample was measured 4 times before the experiment, and the average value was taken. After deposition, remove free metal shavings on the surface, wait for cooling to normal temperature, carry out weighing 4 times, and take the average value. After deposition, the free metal chips were removed from the surface and weighed four times when it was cooled to room temperature and the average value was taken. The two average values were subtracted to obtain the coating quality. The range of process parameters was first selected based on pre-testing SKH51 on the 45 steel

plates. According to Table 3.7 of the orthogonal experiment of coating deposition quality, it was found that the sequence of deposition factors is: Current Frequency>Rotate Speed>Voltage>Efficiency. Under the selected range of process parameters, Current Frequency had a greater impact on deposition quality than other parameters, while efficiency had little impact on deposition quality. Under the condition that the three process parameters of Efficiency, Voltage, and Current Frequency were fixed, a small rotation speed can improve the deposition quality. Excessive rotation speed does not bring about the improvement of deposition quality. Due to the rapid increase in temperature, the metal contact points melt, the spark sputtering is increased and the deposition is deteriorated. Higher speeds have a greater impact on the quality of the deposited surface. In the machining process, the electrode speed is too large resulting in the electrode temperature raises too quickly, the handle temperature results in the inability to machine. In the machining process, the electrode speed is too large resulting in the electrode temperature rise too quickly, the handle rises, resulting in the inability to machine. Duty cycle and voltage have the following effect on ESD. It is found from the data that the process parameter data presents nonlinear changes. Sample 15 has the largest deposition mass. Sample 1 deposition quality is minimum. When the parameters of current frequency, voltage and rotate speed increase, the deposition quality tends to increase. Among them, Samples 4, 8, 10, 12, 14, 15, and 16 are all alternative feasible solutions in Table 3.7.

Table 3.7 – Taguchi OA Experiments on Coating Quality

Sample	A	B	C	D	Coating Quality (μg)
--------	---	---	---	---	-----------------------------------

1	1	1	1	1	5.53
2	1	2	2	2	12.6
3	1	3	3	3	36.27
4	1	4	4	4	64.05
5	2	1	2	3	10.6
6	2	2	1	4	17.95
7	2	3	4	1	35.67
8	2	4	3	2	57.53
9	3	1	3	4	23.53
10	3	2	4	3	100.57
11	3	3	1	2	32.55
12	3	4	2	1	66.93
13	4	1	4	2	47.92
14	4	2	3	1	80.58
15	4	3	2	4	124.38
16	4	4	1	3	77.4
K1j	29.6125	30.4375	55.895	82.57	
K2j	21.895	52.925	57.2175	66.4775	
K3j	33.3575	53.6275	49.4775	62.0525	
K4j	47.1775	37.65	56.21	57.4775	
R	25.2825	23.19	7.74	25.0925	

(2) Coating Thickness

The thickness of the deposited surface was measured. To eliminate measurement errors, the surface was measured at five different places and the average value was taken. According to the orthogonal experiment Table 3.8, it was found to be basically consistent with mass deposition. The extreme value R in the orthogonal Table 3.8 was discovered that in a certain energy range, the deposition factors role is: Rotate Speed > Current Frequency > Voltage > Efficiency, which is basically consistent with the quality of the deposition. Rotate Speed process parameter has a greater effect on the thickness of the deposited layer, and Efficiency has a lesser effect on the deposited thickness. The greater the deposition quality is, the greater the thickness of the deposited coating is. However, the

surface deposition process becomes less uniform due to the high electrode rotate speed. In Fig. 3.9, samples 10, 12, 14, 15 and 16 are alternative feasible solutions.

Table 3.8 – Taguchi OA Experiments on Coating Thickness

Samples	A	B	C	D	Coating Thickness(μm)
1	1	1	1	1	11.1
2	1	2	2	2	12.4
3	1	3	3	3	16.6
4	1	4	4	4	24.1
5	2	1	2	3	10
6	2	2	1	4	15.6
7	2	3	4	1	20.9
8	2	4	3	2	20.2
9	3	1	3	4	18.7
10	3	2	4	3	36.9
11	3	3	1	2	17.2
12	3	4	2	1	34.1
13	4	1	4	2	26.7
14	4	2	3	1	40.6
15	4	3	2	4	45.9
16	4	4	1	3	40.3
K1j	16.05	16.675	26.725	38.375	
K2j	16.625	26.375	25.15	29.675	
K3j	21.05	25.6	24.025	27.15	
K4j	26.675	19.125	25.95	26.075	
R	10.625	9.7	2.7	12.3	

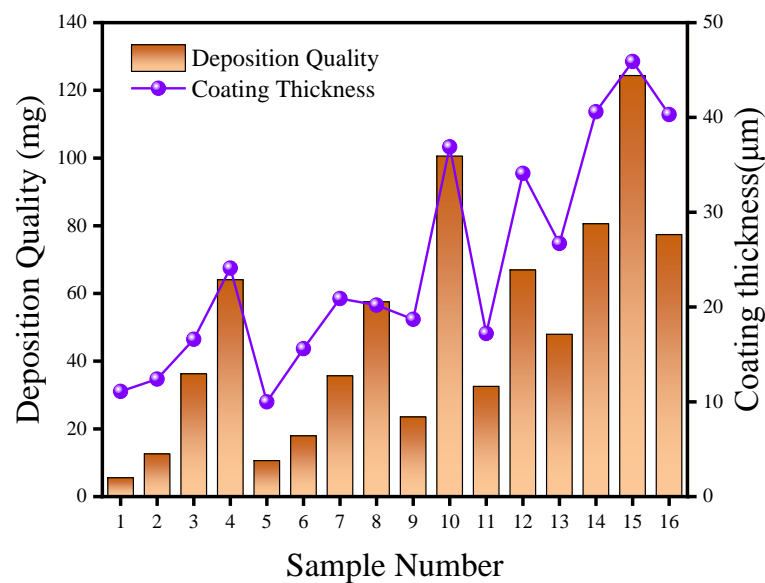


Fig. 3.9 – Deposition quality and coating thickness of SKH51 coating

(3) Coating roughness

The ESD surface was measured by Mitutoyo SJ-210 roughness meter. The ISO 1997 standard was selected to measure the surface over a length of 3mm, and the standards selected were shown in Table 3.9. The roughness measurements were carried out on the ESD surfaces, three measurements were carried out on the surface of each specimen, and the mean and standard deviation of the Ra of the samples were counted and calculated in Fig. 3.10. The results were analyzed through orthogonal experiments. According to the extreme value of R in the orthogonal Table 3.10, it was found that rotate speed has a significant effect on the surface roughness than other process parameters in terms of roughness averages. At the certain energy, too much and too little rotate speed will cause an increase in the surface roughness. When the energy is greater, the three process parameters of current frequency, voltage and efficiency are increased; when the energy is increased, the coating quality and thickness are increased, and the surface roughness value is increased. The three process parameters also affect the uniformity of the surface roughness values, which can be seen from the extreme deviation of the standard deviation in the orthogonal table. This is not favourable for the deposition of other materials on the transition layer. For example, samples 14, 15 and 16 have large roughness as shown in Table 3.10. There is a tendency for the surface roughness to decrease as the deposition thickness decreases, as shown in Fig. 3.11. Smaller thicknesses have better roughness and are not conducive to the deposition of the transition layer. Specimens 4, 12, 10 are suitable solutions.

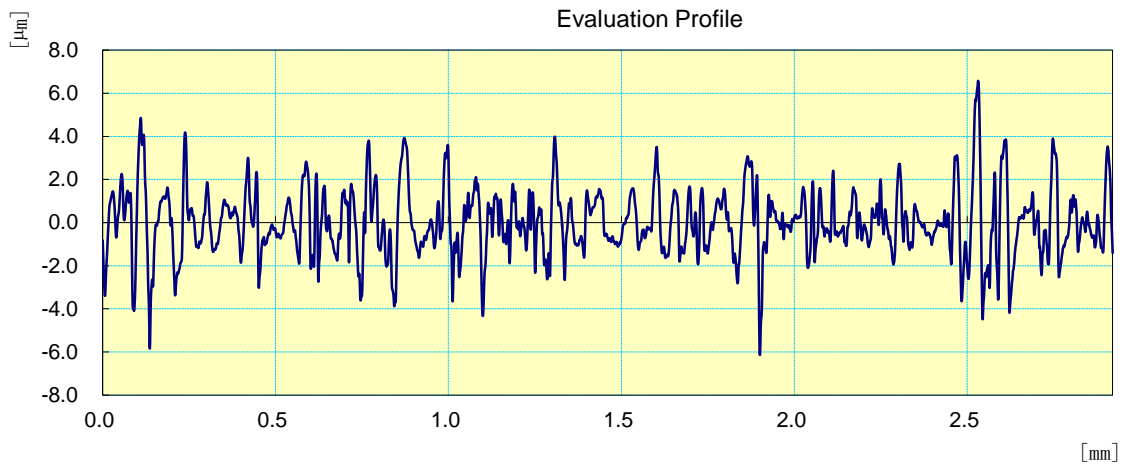


Fig. 3.10 – Surface roughness measurement

Table 3.9 – Mitutoyo SJ-210 roughness setting parameters

Standard	Profile	λ_s	Evaluation Length	Cut-Off	Filter
ISO 1997	R	2.5 μm	2.92mm	0.08mm	GAUSS

Table 3.10 – Taguchi OA Experiments for mean values of coating roughness

Sample	A	B	C	D	Mean Values of Coating Roughness (μm)	Standard Deviation of Coating Roughness σ
1	1	1	1	1	1.108	0.0786
2	1	2	2	2	1.016	0.0724
3	1	3	3	3	0.922	0.1897
4	1	4	4	4	0.917	0.0474
5	2	1	2	3	0.939	0.1265
6	2	2	1	4	1.04	0.2397
7	2	3	4	1	0.825	0.2147
8	2	4	3	2	0.871	0.1306
9	3	1	3	4	0.845	0.0897
10	3	2	4	3	1.162	0.1449
11	3	3	1	2	1.103	0.1775
12	3	4	2	1	0.962	0.1079
13	4	1	4	2	1.222	0.0363
14	4	2	3	1	1.347	0.2455
15	4	3	2	4	1.457	0.221
16	4	4	1	3	1.127	0.1438

K1j	0.99075	0.91875	1.018	1.28825
K2j	1.0285	1.14125	1.07675	0.96925
K3j	1.0945	1.0935	0.99625	1.0315
K4j	1.0605	1.053	1.0375	1.06475
R	0.10375	0.2225	0.0805	0.319
R_σ	0.0789	0.073675	0.070725	0.054225

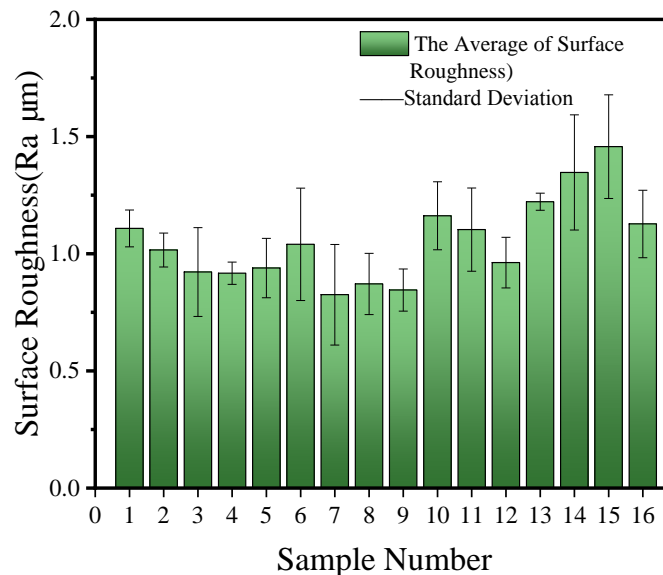


Fig. 3.11 – Mean and Standard Deviation of Roughness

(4) The XRD analysis of SKH51 coating

The XRD was analyzed on the deposited surfaces. It was found that the SKH51 coating surface was mainly composed of Fe、 Fe_3C_7 and $(\text{Cr,Fe,W,Mo})_{23}\text{Fe}$ $(\text{W,Mo})_2\text{C}_{12}$ [137, 138]. The main element of SKH51 coating is Fe, which has good toughness. It contains a certain amount of other metal carbides, so that the surface has a certain wear resistance. Its performance is better than that of No.45 steel. As SKH51 can be better compatible with the composition of 45 steel, it is easy to form an excessive layer. The main peak of Fe is high in the XRD diagram, so that the carbides such as Cr, Mo, V, W, etc. are not observed, as shown in Fig. 3.12.

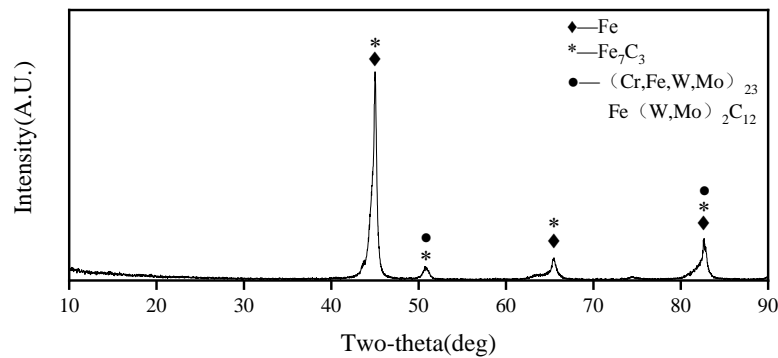


Fig. 3.12 – the XRD diagram of SKH51 coating

(5) The SEM analysis of SKH51 coating

The surface morphology of the specimen was observed by SEM, as shown in Fig. 3.13[139, 140]. The surface was relatively flat, with many small irregular droplet points of fusion. No obvious microcracks were found, indicating that SKH51 material can be well deposited on the 45 steel. The two material organisations don't create a large number of cracks compared to high hardness carbide materials. During the rapid heating and cooling of the spark discharge process, the residual thermal stress in the SKH51 coating will not cause large deformation and cracks. There are many small holes on the surface of the coating, which can effectively release the thermal stress, reduce the expansion of cracks, and have a better surface morphology. In Fig. 3.13, the deposited surface has small protrusions due to the hardness of the material. The deposition sites between the small protrusions have large pores, reducing the expansion caused by thermal stress. At the same time, during the deposition process, the electrode sputtering droplets can be well bonded to the surface of such protrusions, and the surface is constantly thickened.

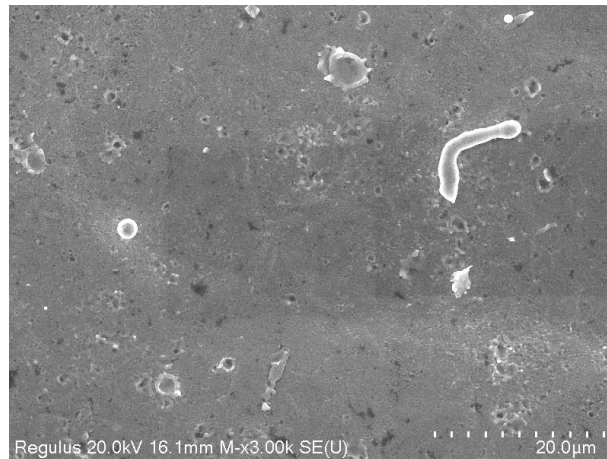


Fig. 3.13 – SEM image of SKH51 coating

Through the energy spectrum analysis (EDS), it was found that the electrode material was able to deposit uniformly onto the surface of the substrate in the distribution of elements deposited on the surface, as shown in Fig. 3.14[141, 142]. For some elements that could not be observed by XRD, their distribution on the surface could easily be observed by EDS, as shown in Fig. 3.14 and Table 3.11. As shown in Fig. 3.15, it was found that W, Cr, Mo and V were able to be deposited uniformly on the surface of the coating. There are high content of carbon elements on the surface. During the deposition process, the content of W, Cr, Mo and V declined during the deposition process, which led to a reduction in the surface hardness. High carbon ensured the stability of the surface content of carbides such as W and Cr during the deposition process. The carbide material in the electrode can ensure the hardness and the wear resistance.

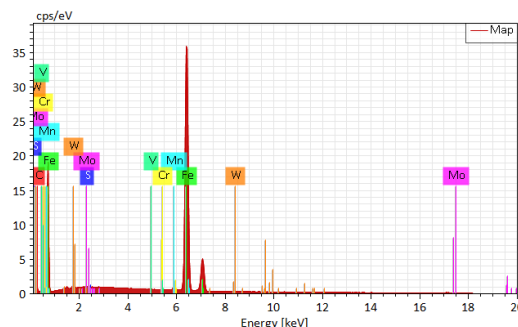


Fig. 3.14 – EDS elemental analysis diagrams of SKH51 coatings

Table 3.11 – Element content on SKH51 coating surface

Element	Fe	C	W	Mo	Cr	Mn	V	S
Atomic Number	26	6	74	42	24	25	23	16
wt.%	91.86	4.28	1.21	0.96	0.80	0.55	0.26	0.08
at.%	80.21	17.38	0.32	0.49	0.75	0.49	0.25	0.12

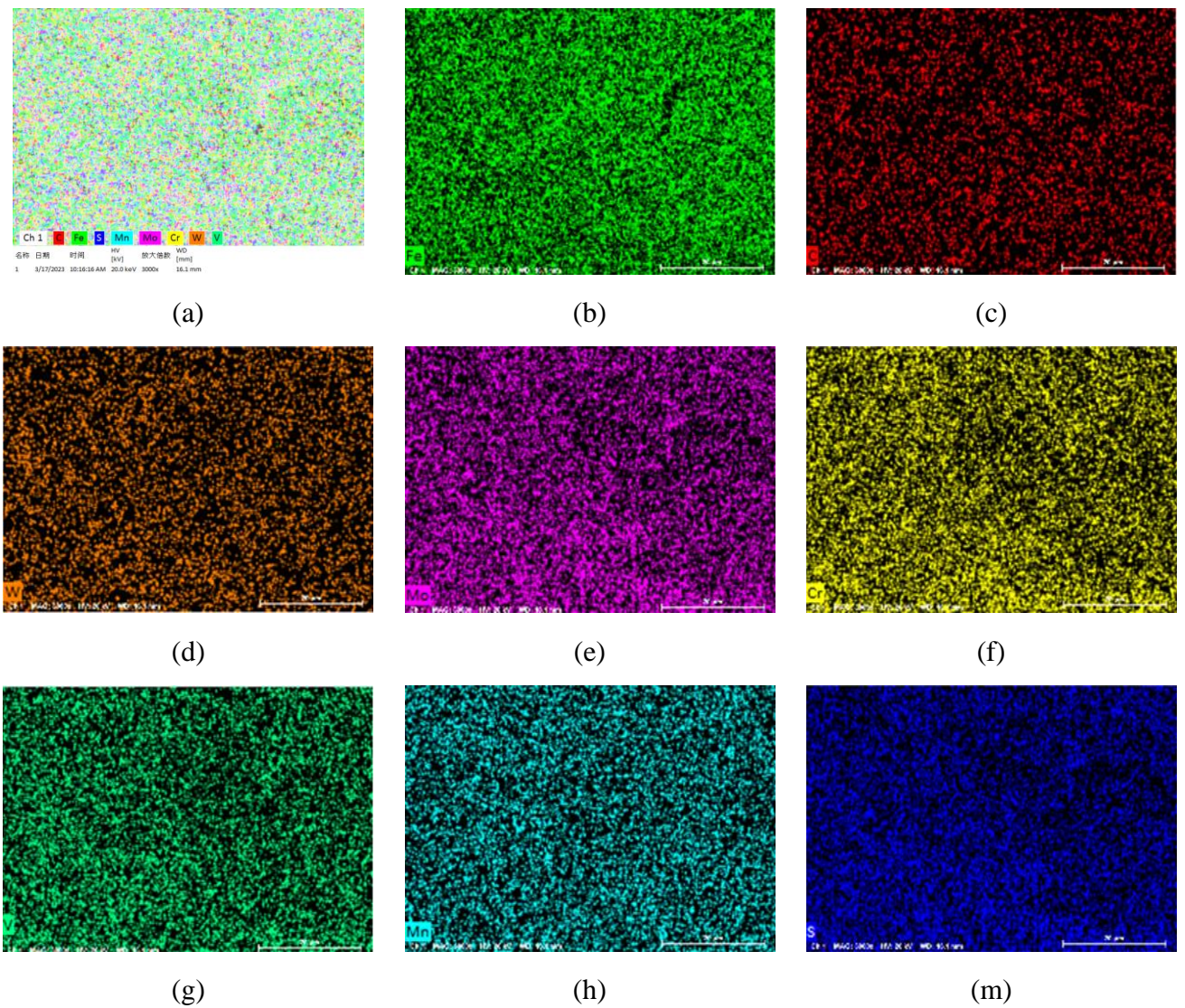


Fig. 3.15 – Elements Distribution on the Coating Surface: a-distribution of elements; b-Fe; c-C; d-W; e-Mo; f-Cr; g-V; h-Mn; i-S.

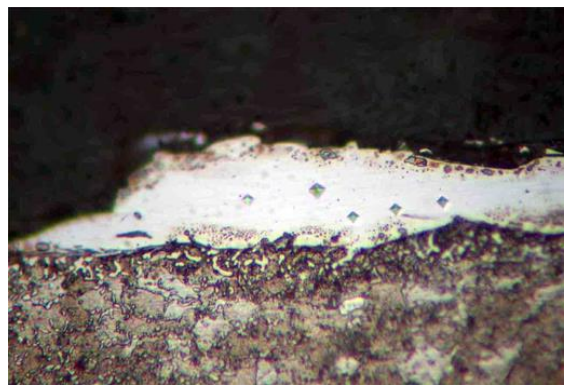
(6) The Vickers hardness of SKH51 coating

Specimens were cut by a low speed cutter. During the cutting process, the samples were cooled by a water bath, which prevented the coating from undergoing organizational changes because of excessive heat during cutting. Then the specimens were set with 22mm hot setting machine (XQ-2B, Weiyi Co., Ltd). Experimental specimens were carried out by mechanical grinding, and the particle sizes P400, P600, P800, and P1200 were respectively selected for grinding in sequence. In order to avoid coating shedding, the coating direction was consistent with the tangential direction of the rotation of the grinding disc, and each rotation was 180 degrees for grinding. W2.5 diamond abrasive paste was selected for polishing. When the surface was smooth, the specimens were blown dry by a hairdryer. The surface was wiped with anhydrous alcohol to remove polishing paste and water stains. Since there was no clear boundary between 45 steel and SKH51 coating, the metallurgical surface was etched by 3% dilute nitric acid. After 10~15 seconds, a corrosion layer appeared on the surface of 45 steel, which need be quickly rinsed with water. Because of the good corrosion resistance of SKH51 material, the coating gloss was not affected. It can clearly distinguish the boundary between the coating and the substrate, as shown in Fig. 3.16a. A 10 g force was used to test the coating cross-section by a Vickers hardness tester, as shown in Fig. 3.16b. Four experiments for each coating were perform, the mean and standard deviation were taken. The data were statistically presented as shown in Fig. 3.17. It was found that the Vickers hardness of sample 10 was maximum, followed by samples 11, 5, 4 and 14 of Vickers hardness values were larger. The thicker the coating, the less uniform the quality of the coating deposition. The

thermal influence of processing heat was smaller on the coating. The surface hardness of the coating was closer to the electrode material. Considering SKH51 as a transition layer, the surface hardness did not need too high.



(a)



(b)

Fig. 3.16 – The cross section morphology of SKH51 coating: a-Cross-sectional corrosion morphology of SKH51 coating; b- Vickers hardness morphology of SKH51 coating section

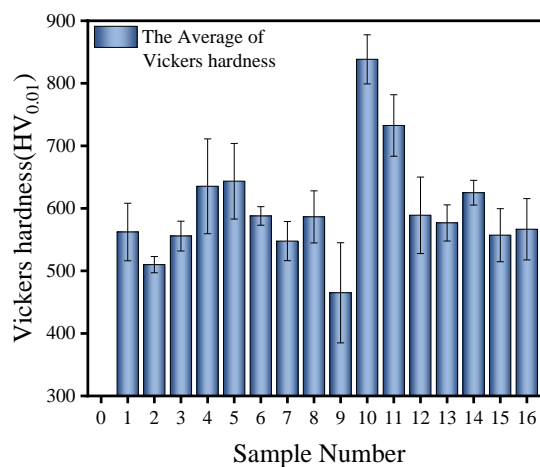


Fig. 3.17 – The Vickers hardness of SKH51 coating

(7) Abrasion resistance tests of SKH51 coating

The abrasion resistance of metal surfaces was tested by a rotary friction wear machine (MS-T300 ,Lanzhou Huahui Instrument Technology Co., Ltd., China) with a load of 5N, as shown in Fig. 3.18a. The maximum width of the wear scar was measured by ultra-depth-of-field microscope in Fig. 3.18b. The maximum width of the wear scar was measured by ultra-depth of field microscope. Due to the influence of the surface roughness of the coating, the wear scar was uneven, and its friction force and friction coefficient cannot truly reflect the degree of wear resistance.

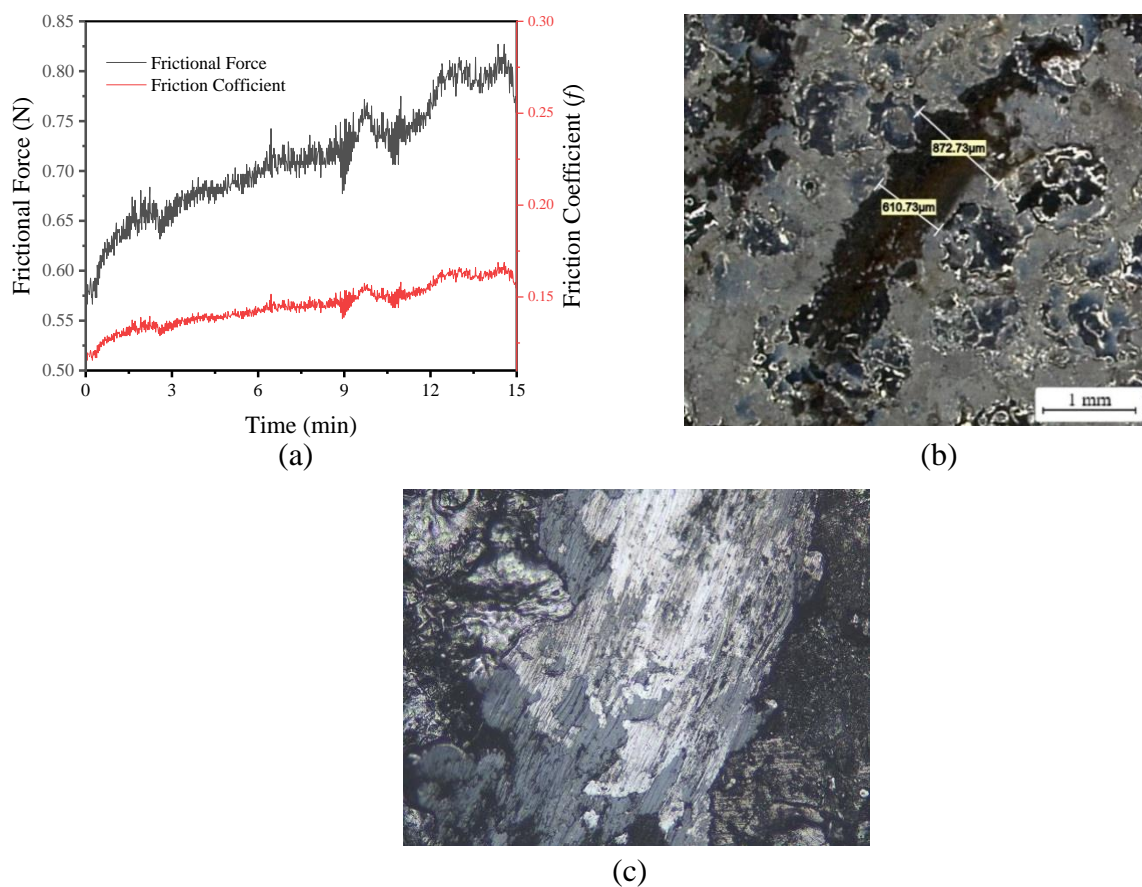


Fig. 3.18 – Experimental results of friction and wear of SKH51 coating: a- Coefficient of friction and friction of SKH51 coating; b- Friction wear morphology of SKH51 coating; c-500X surface wear morphology

The maximum width of the wear scar was used to eliminate the influence of surface roughness and surface topography. The experimental environment temperature was 25°C, and humidity was 53%. Three experiments were conducted

for each sample. The maximum width values were measured separately and the average values were taken for analysis. According to the orthogonal experiment, it was hoped that the maximum abrasion width was as small as possible. Current frequency and efficiency had a greater influence relative to other ESD parameters. In Fig. 3.18c, there were obvious scratches on the wear surface. The wear mechanism of SKH51 coating was mainly abrasive wear.

From Table 3.12 and Fig. 3.19, sample 15 had the largest width which means the worst abrasion resistance. Samples 15, 8, 4, 3, 7 and 10 had larger width of abrasion marks and poorer abrasion resistance. Due to the effect of surface morphology and roughness, the surface wear resistance of the coating was not completely consistent with the Vickers hardness. However, in SKH51 coatings, the higher the Vickers hardness value was, the better the wear resistance was, such as samples 10, 11 and 5.

Table 3.12 – Taguchi OA Tests for mean values of the maximum abrasion width

Sample	A	B	C	D	Mean values of abrasion width
1	1	1	1	1	543.67
2	1	2	2	2	713.91
3	1	3	3	3	810.84
4	1	4	4	4	839.41
5	2	1	2	3	600.24
6	2	2	1	4	613.44
7	2	3	4	1	783.42
8	2	4	3	2	925.23
9	3	1	3	4	712.45
10	3	2	4	3	783.23
11	3	3	1	2	645.15
12	3	4	2	1	693.47
13	4	1	4	2	606.75

14	4	2	3	1	590.41
15	4	3	2	4	956.54
16	4	4	1	3	713.58
K1j	726.9575	730.5825	708.575	716.82	
K2j	615.7775	675.2475	798.9875	792.9225	
K3j	628.96	741.04	759.7325	753.2025	
K4j	652.7425	722.76	726.9725	780.46	
R	111.18	65.7925	90.4125	76.1025	

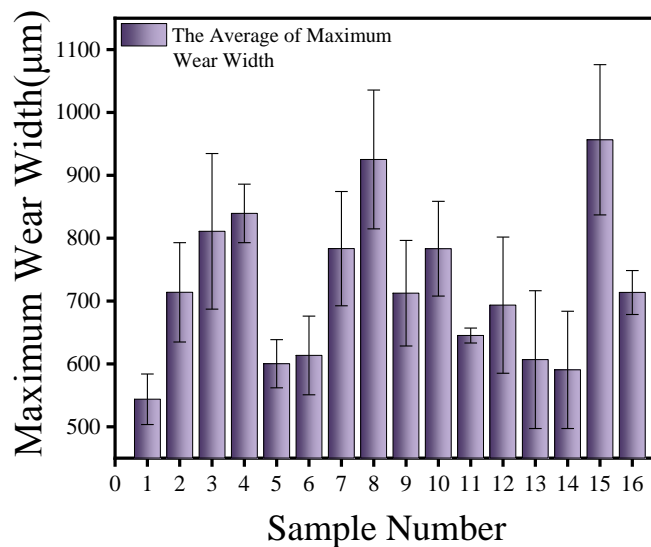


Fig. 3.19 – The maximum abrasion width of SKH51 coating

(8) Comprehensive performance evaluation model

The transitional coatings can be comprehensively evaluated according to deposition quality, coating thickness, roughness, Vickers hardness and abrasion width. Coatings should be favoured in terms of coating thickness and roughness to ensure the transition coatings. In the optimization design, the problem that requires two or more design indicators to be optimal at the same time is called a multi-objective optimization design problem. It is difficult to make comparisons if there is no unified measurement standard among the various sub-goals among the goals. The function error of each sub-objective function value increases during the minimization process. In 1772 Franklin proposed the multi-objective problem. By

now multi-objective optimization problems have a variety of well-established optimization theories and have been used in optimal engineering design. This model used the weighted factor method and the normalization method to transform multiple evaluation factors into a single objective method. The numerical intervals were determined for each factor from the best to the worst; different efficacy coefficient functions were selected according to the physical significance of the numerical magnitude of the factors. Thereby, the effect of different units of each factor was eliminated by the normalization method[143, 144]. The normalised values in each factor were multiplied by the corresponding weight factors[145, 146]. The total score of each candidate scheme was obtained as Equation (3.1). The experimental schemes were evaluated to reach the optimal scheme.

Weighting factor objective function, as Equation (3.1):

$$f(X) = \sum_{j=1}^n a_j f_j(X) \quad \left(\sum_{j=1}^n a_j = 1, a_i \geq 0 \right) \quad (3.1)$$

The factors were normalized due to the different units of the factors:

(1) If the value of $f_j(\mathbf{x})$ is large, the value of d_j is also large. The efficacy coefficient function (Equation 3.2) is:

$$d_j = \begin{cases} 0 & f_j(\mathbf{x}) \leq \alpha_j \\ (f_j(\mathbf{x}) - \alpha_j) / (\beta_j - \alpha_j) & \alpha_j < f_j(\mathbf{x}) < \beta_j \\ 1 & f_j(\mathbf{x}) \geq \beta_j \end{cases} \quad (3.2)$$

(2) If the value of $f_j(\mathbf{x})$ is small, the value of d_j is large inversely. The efficacy coefficient function (Equation 3.3) is.

$$d_j = \begin{cases} 1 & f_j(\mathbf{x}) \leq \alpha_j \\ 1 - (f_j(\mathbf{x}) - \alpha_j) / (\beta_j - \alpha_j) & \alpha_j < f_j(\mathbf{x}) < \beta_j \\ 0 & f_j(\mathbf{x}) \geq \beta_j \end{cases} \quad (3.3)$$

(3) If the value of $f_j(\mathbf{x})$ increases firstly and then decreases, both d_j will change. The efficacy coefficient function (Equation 3.4) is:

$$d_j = \begin{cases} 0 & f_j(x) \leq \alpha_j, \text{ or } f_j(x) \geq \beta_j \\ (f_j(\mathbf{x}) - \alpha_j) / (f_i - \alpha_j) & \alpha_j < f_j(\mathbf{x}) < f \\ 1 - (f_j(\mathbf{x}) - f) / (\beta_j - f) & f < f_j(\mathbf{x}) < \beta_j \\ 1 & f_j(\mathbf{x}) = f \end{cases} \quad (3.4)$$

Substituting d_j into the objective function (Equation 3.1) gives:

$$f(X) = \sum_{j=1}^n a_j d_j \quad \left(\sum_{i=1}^n a_i = 1, a_i \geq 0 \right) \quad (3.5)$$

Table 3.13 – Performance parameters of SKH51 coatings

NO.	Coating quality (μg)	Coating thickness (μm)	The maximum abrasion width (μm)	Standard deviation of maximum abrasion width	Average roughness of coating	Standard deviation of coating roughness	Vickers hardness ($\text{HV}_{0.01}$)	Standard deviation of Vickers hardness
1	5.53	11.1	543.67	40.13	1.108	0.0786	562.13	45.98
2	12.60	12.4	713.91	79.04	1.016	0.0724	509.98	13.01
3	36.27	16.6	810.84	123.81	0.922	0.1897	555.65	23.85
4	64.05	24.1	839.41	46.52	0.917	0.0474	635.30	75.88
5	10.60	10.0	600.24	38.36	1.533	0.8466	643.38	60.44
6	17.95	15.6	613.44	62.62	1.040	0.2397	587.85	14.91
7	35.67	20.9	783.42	90.91	0.825	0.2147	547.65	31.38
8	57.53	20.2	925.23	110.42	0.871	0.1306	586.35	41.70
9	23.53	18.7	712.45	84.06	0.845	0.0897	464.98	80.06
10	100.57	36.9	783.23	75.31	1.162	0.1449	838.38	39.31
11	32.55	17.2	645.15	11.85	1.103	0.1775	732.53	49.18
12	66.93	34.1	693.47	108.41	0.962	0.1079	588.90	61.20
13	47.92	26.7	606.75	109.67	1.222	0.0363	576.73	28.94
14	80.58	40.6	590.41	93.35	1.347	0.2455	624.95	19.77
15	124.38	45.9	956.54	119.56	1.457	0.2210	557.13	42.43
16	77.40	40.3	713.58	34.94	1.127	0.1438	566.63	49.01

Table 3.14 – Normalized data for coating parameters

NO.	Coating quality (μg)	Coating thickness (μm)	The maximum abrasion width(μm)	Standard deviation of maximum abrasion width	Average roughness of coating	Standard deviation of coating roughness	Vickers hardness ($\text{HV}_{0.01}$)	Standard deviation of Vickers hardness
1	0.00000	0.03064	1.00000	0.74741	0.60028	0.94780	0.71952	0.50828
2	0.05949	0.06685	0.58767	0.39987	0.73023	0.95545	0.33328	1.00000
3	0.25865	0.18384	0.35290	0.00000	0.86299	0.81069	0.67153	0.83833
4	0.49239	0.39276	0.28370	0.69034	0.87006	0.98630	0.85192	0.06234
5	0.04266	0.00000	0.86298	0.76322	0.00000	0.00000	0.81802	0.29262
6	0.10450	0.15599	0.83101	0.54653	0.69633	0.74898	0.91001	0.97166
7	0.25360	0.30362	0.41931	0.29385	1.00000	0.77983	0.61228	0.72603
8	0.43753	0.28412	0.07584	0.11960	0.93503	0.88362	0.89890	0.57211
9	0.15145	0.24234	0.59120	0.35504	0.97175	0.93410	0.00000	0.00000
10	0.79966	0.74930	0.41977	0.43319	0.52401	0.86598	0.00000	0.60776
11	0.22735	0.20056	0.75421	1.00000	0.60734	0.82574	0.44404	0.46055
12	0.51662	0.67131	0.63717	0.13755	0.80650	0.91164	0.91779	0.28128
13	0.35667	0.46518	0.84722	0.12630	0.43927	1.00000	0.91779	0.76242
14	0.63147	0.85237	0.88679	0.27206	0.26271	0.74182	0.89534	0.89918
15	1.00000	1.00000	0.00000	0.03796	0.10734	0.77206	0.68249	0.56122
16	0.60471	0.84401	0.58847	0.79377	0.57345	0.86733	0.75285	0.46309

Higher values of coating quality and average coating thickness represent better performance, which is treated according to the increasing function of the coefficient of efficacy (Equation 3.2). The smaller the average width of the maximum wear scar and the average roughness and standard deviation, the better the performance. It was processed according to the decreasing function of the efficiency coefficient (Equation 3.3). The mean Vickers hardness values were

normalized according to the decreasing efficacy coefficient increasing decreasing function (Equation 3.4). The normalized data were shown in Table 3.14.

SKH51 coating was used as a transition coating and required a good surface quality to facilitate the deposition of subsequent coatings. Transitional coatings require a good surface quality to make the deposition of subsequent coatings easier. Secondly, it was considered to have a certain coating thickness and coating quality, and it has a certain wear resistance compared to the substrate requirements. Finally, it is avoided to anneal severely during the deposition process, it is required that the hardness should not be too high or too low to ensure the continuity of the hardness of the gradient coating. Therefore, the selection of parameters should take into account the characteristics of the transitional coating. Selection factors: coating roughness \geq coating thickness \geq coating quality \geq wear resistance \geq coating hardness. Because of the influence of surface topography, the standard deviation of the maximum abrasion mark width and average roughness and Vickers hardness reflect the surface unevenness. Also, the effect of standard deviation on the data was taken into account, and the weighting factor was taken as 20 per cent of this factor. Therefore, according to the above factors, the weighting factors were selected according to the table, as shown in Table 3.15.

Table 3.15 – Weighting factors of coatings performance parameters

Coating Quality	Coating Thickness	Average roughness of coating	Standard deviation of coating roughness	Average maximum abrasion width	Standard deviation of maximum abrasion width	Average Vickers hardness (HV0.01)	Standard deviation of Vickers hardness
0.15	0.2	0.28 (80%)	0.07 (20%)	0.16 (80%)	0.04 (20%)	0.08 (80%)	0.02 (20%)

Data in Table 3.14 were substituted into Equation (3.5), and the maximum value of the objective function were calculated (Equation 3.6). The result of the objective function was shown in Fig. 3.20. By comparing the values of the objective function, the objective function of sample 12 was the maximum value, which was 0.687887, and the comprehensive evaluation of the transition coating was optimal. The deposition process parameters were as follows: Current Frequency was 300Hz; Voltage was 44V; Efficiency was 30%; Rotate Speed was 150r/min, as shown in Table 3.16. In addition, samples 16 and 14 can be used as an alternative for industrial production.

$$\text{MAX } f(X) = \sum_{j=1}^n a_j d_j \quad (3.6)$$

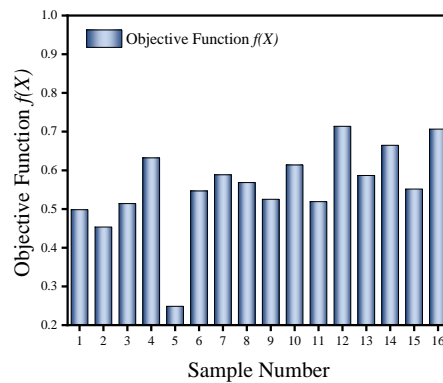


Fig. 3.20 –Objective function of SKH51 coating

Table 3.16 – Optimal deposition process parameters of SKH51 coating

Sample	Current Frequency (Hz)	Voltage(V)	Efficiency(%)	Rotate Speed (r/min)
12	300	44	30	150

3.2.4 Conclusion of SKH51 coating

Deposition experiments of SKH51 coatings on 45 steel surfaces were carried out by ESD. The orthogonal design of experiments method was used. The effects

of ESD parameters on coating quality, average coating thickness, average width of maximum abrasion marks, average roughness, and Vickers hardness were discussed separately. The coating properties as the transition layer were analysed.

(1) By means of orthogonal experiments, the ESD process parameters such as rotate speed, current frequency, voltage and efficiency were considered respectively, which affected the parameters of SKH51 coating performance parameters coating quality, average thickness of coating, average width of maximum abrasion marks, average roughness, Vickers hardness. The optimal sample process parameters and alternative process parameters were determined under a single performance parameter.

(2) By XRD and EDS devices, SKH51 surface wear-resistant components were determined and analyzed.

(3) The wear mechanism of SKH51 coating is mainly abrasive wear. By the surface corrosion method, the SKH51 coating and substrate (45 steel) were delaminated. Because the corrosion resistance of SKH51 was better, the coating cross-section can be observed and the Vickers hardness can be measured.

(4) SKH51 coating was used as a transition coating, and the weighting factor was determined according to the coating performance parameters. The objective function of the comprehensive performance parameters of the coatings was evaluated by the normalized method and weighting factor method, the optimal coating deposition process parameters were obtained. Sample 12 objective function is the maximum value, which is 0.687887. Finally, the performance of SKH51

coating is better than that of 45 carburized coating, and the wear resistance is further improved.

3.3 Composite coating process

3.3.1 Composite coating schemes

Composite coating is the deposition of different materials separately, or the same material with different processes to produce different organizational properties, deposited separately onto a metal surface. Composite coating breaks the limitation of single coating and single process, so that the coating has special functions and high service life. In the ESD process, the composite coating can break the thickness limit and increase the life and the reliability. The latest technology of composite coatings is represented by gradient coating technology and in-situ reactive coating technology. Gradient coatings are widely used in a variety of industries, including defense, aerospace, and vehicles. Due to conflicting coating properties, the researcher studied surface coatings on metal substrates. Composite coatings can improve the bond strength, micro-hardness, wear resistance, corrosion resistance and thermal cycling resistance, which became an effective way to improve the surface properties [147]. Zhang conducted research on the Ag+Cu+B83 composite coating on the surface of tin bronze, using anti-friction metals to obtain better surface quality and wear resistance of sliding bearings, but the cost needs to be evaluated [148]. Maryam deposited HA/TiN double-layer coating on the surface of Ti-6Al-4V alloy to obtain wear resistance and anti-corrosion performance, which met the requirements of biological coatings [149]. V.B. Tarelnyk performed multilayer deposition of carbon, aluminum and

T18K10 hard layers on a 15Kh6N12T steel substrate to obtain the hardness and thickness of the coating. M. Shehryar Khan deposited WC and In625 coatings on 22MnB5 steel substrate by electro-spark deposition and then coated Al-Si material by laser. Different processes are used for composite coating to obtain better mechanical properties. Wang deposited Mo/WC-Ni composite coating on H13 steel substrate to get better wear resistance. M. C. Perju deposited three coatings of Ti/W/WC on cast iron surface to improve the mechanical properties of the surface by gradient hardness[150]. Al-Quraan carried out electro-spark deposition of dual coatings of VK8 + Cu on the surface of aluminum alloy to improve the wear resistance of the surface[151]. The advantage of gradient coating in the ESD process was that it can combine a variety of functional materials[152]. The advantage of the gradient coating in the ESD process is the possibility of performing a combination of multiple functional materials[153]. In particular, super-hard materials are coated in layers to increase the thickness of the coating and the property. Soft friction-reducing materials are coated to help improve surface quality and reduce friction. Corrosion-resistant materials are coated to reduce the rate of surface corrosion and increase the service life of the part.

In the design, the high toughness and wear-resistant material SKH51 was used as the transition layer, the wear-resistant material and corrosion-resistant material, and the anti-friction material were used as the protective layer. Some schemes were designed, as shown in Table 3.17.

Table 3.17 – Composite coating schemes

Scheme	Coating composition	Coating layers
1	SKH51	1
2	SKH51+WC	2
3	SKH51+WC+B83	3
4	SKH51+Nb	2
5	SKH51+TA1+C	3
6	SKH51+TC4+C	3
7	SKH51+TC21+C	3
8	SKH51+Zr+C	3
9	SKH51+Nb+C	3
10	SKH51+BT20+C	3
11	SKH51+NbZr+C	3
12	SKH51+GO Gel	2

3.3.2 Composite coating experiments

Some of the schemes were carburized on the surface for an in-situ reaction, and carbides were formed on the surface to increase wear-resistant. Titanium, zirconium, niobium and other elements have strong corrosion resistance and can form carbides with higher hardness to improve the wear resistance of the surface. The transition coatings were applied using the optimized process parameters from the above experiments. The carburizing process was applied with the optimized process parameters. The experimental schemes were installed for deposition experiments, and the surface morphology of the samples was shown in Fig. 3.21 and Fig. 3.22.

SKH51 coating was deposited on the 45 surface and a white fish scale-like coating was formed in Fig. 3.21. No large metal cracks were found on its surface after magnification. HF10 electrode material contains 90% WC and 10% Co. Because of argon protection, no oxide layer was generated on the surface, and the brightness of coating was high. WC coating was deposited on the surface of

SKH51, and longer metal micro-cracks appeared on the surface. Through a certain deposition time, it was found that the WC coating had a tendency to reduce the cracks on the surface of SKH51 compared to No.45 steel. But when the deposition thickness increased, the cracks in the WC coating gradually increased, and the width of the cracks gradually increased because of the influence of thermal stresses [154, 155]. In the SKH51+WC+B83 scheme, because B83 is soft, it is easy to produce large droplets during the deposition process. Therefore, lower energy parameters were chosen for deposition. The deposition of large droplets on the metal surface had a great influence on the surface roughness, which was not conducive to the next step of deposition. On SKH51+Nb surfaces, internal stresses on the surface resulted in the formation of fine cracks on the surface because the element Nb had a refining effect. It was smaller than the cracks on the tungsten carbide deposited surface. On the carburized surface, because the graphite rod was at high temperature, the surface of the metal carbide coating was relatively flat and a large amount of graphite was attached, and no cracks and pores were found on its surface. The graphene oxide gel surface was flatter. The metal protrusions were encapsulated by smooth gel graphene oxide, which had the best surface flatness of the graphene oxide coating due to the opacity of the graphene oxide and the high reflectivity. They were only clearly visible from the super-field microscope (Leica DVM6) image. The graphene oxide coating had the best surface flatness, as shown in Fig. 3.23.

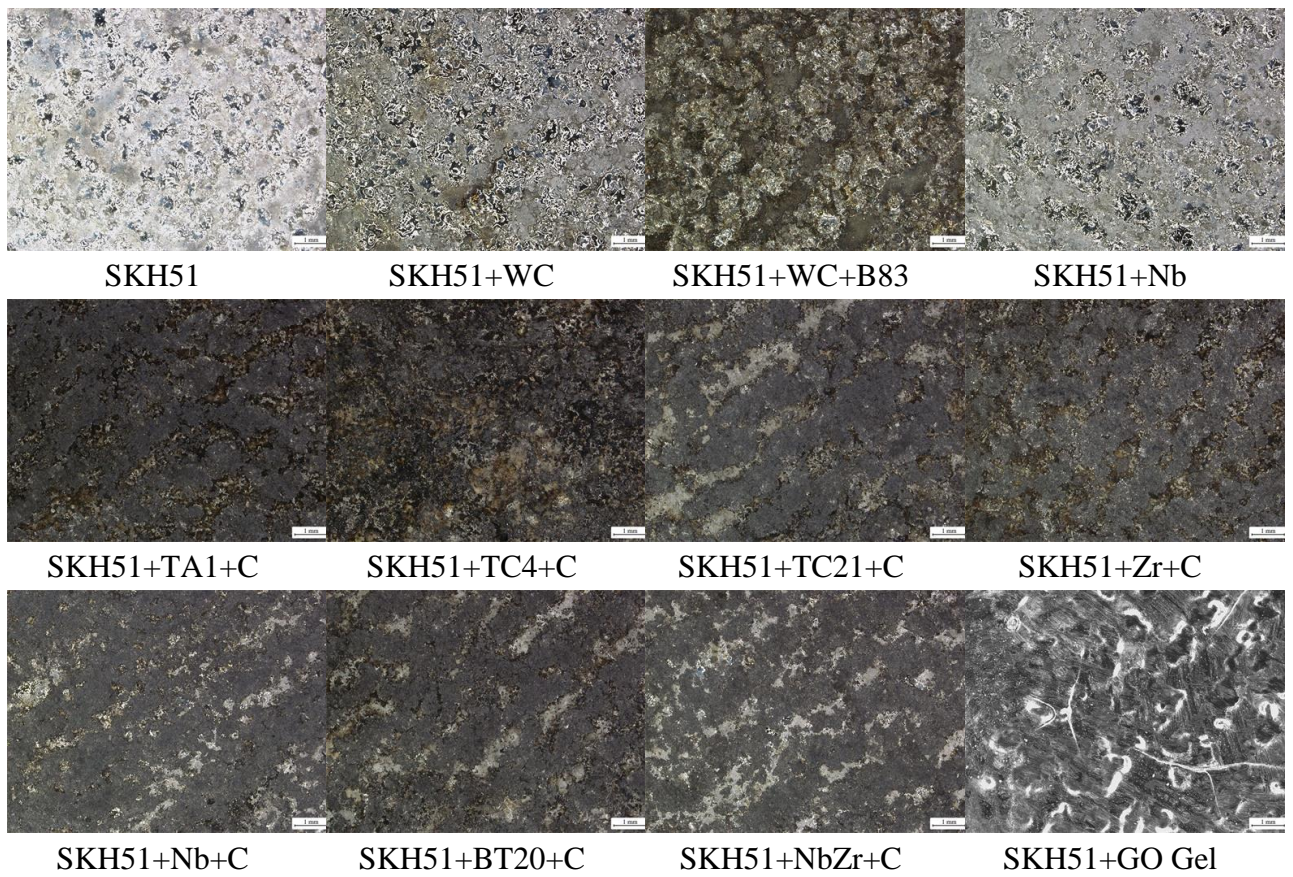


Fig. 3.21 –Coating surface topography at 100X magnification

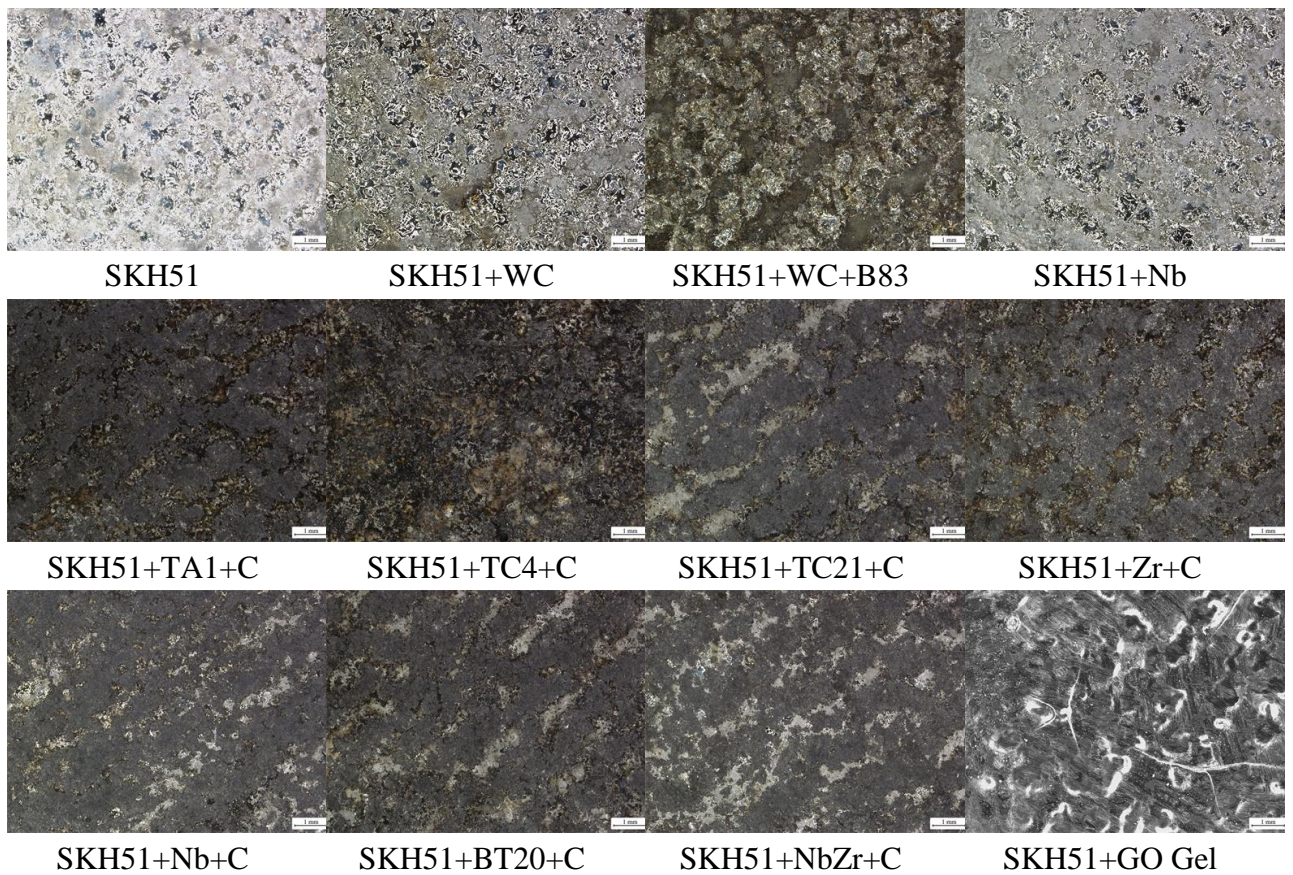


Fig. 3.22 – Coating surface topography at 500X magnification

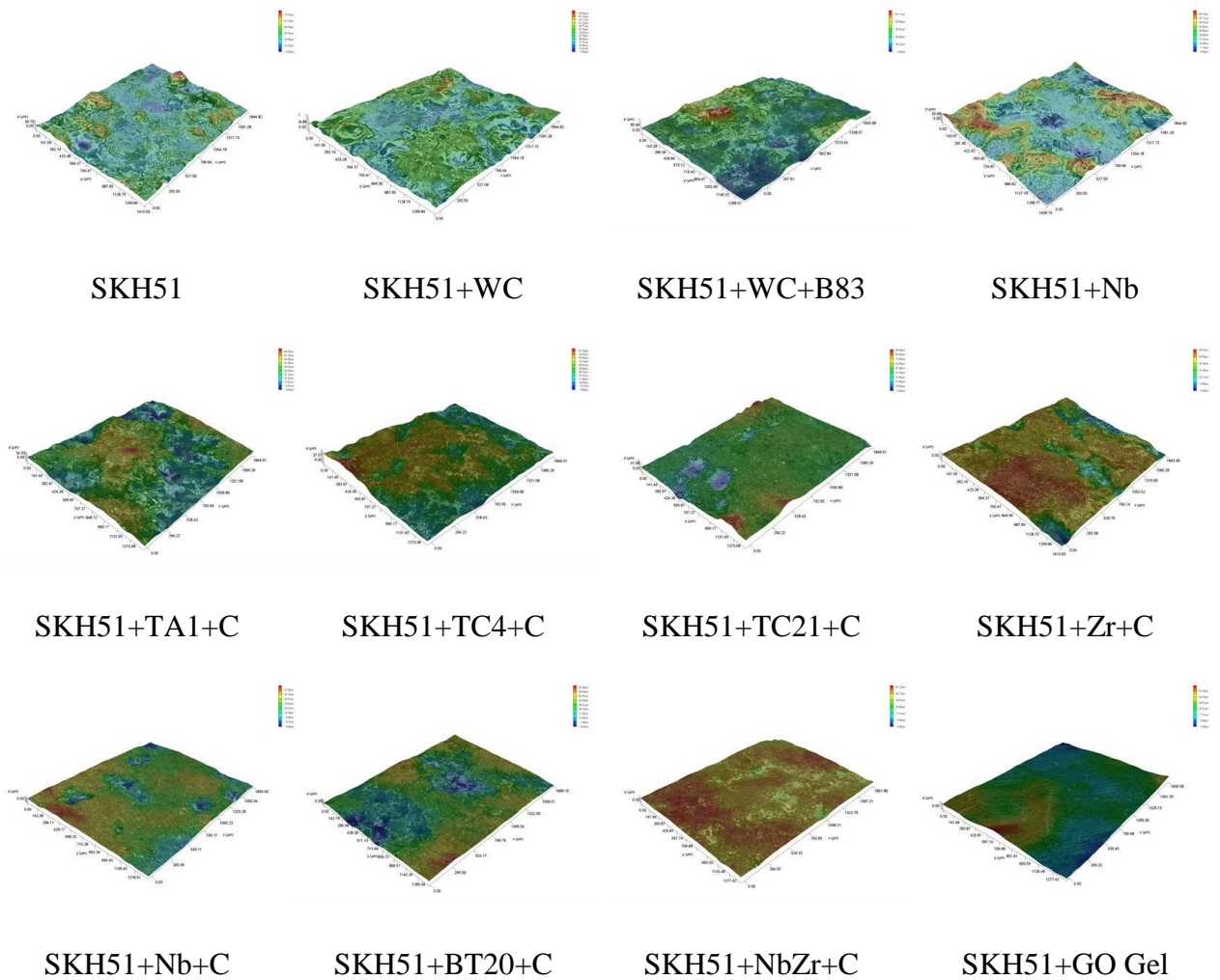


Fig. 3.23 – 3D Topography of super field microscope

The surface was wiped of metallic dust or free-form graphite powder by a brush, which was convenient for measurements of SEM and surface abrasion resistance in the later stage. The specimens were cleaned in anhydrous ethanol for 20 min with a 130W ultrasonic cleaner. Then, the specimens were placed in air and a hair dryer was used to blow away the residual alcohol on the surface. The morphology of treated surfaces was shown in Fig. 3.24. Among them, SKH51, SKH51+WC and SKH51+Nb have relatively smooth surfaces with fish-scale metal coatings. The B83 coating was soft. It was coated in the air, and black substances will appear on the surface. All other deposition processes were protected by argon gas. When the in-situ carburizing reaction was carried out, the carburizing time

was certain, the surface temperature rose, the quality of metal surface was significantly improved, and gray substances appeared. The surface gloss of SKH51+GO gel was good, and it was very obvious to improve the surface quality of the original coating. The cavities on the original metal surface had been blocked, and the height of the deposition points was effectively reduced, so that the surface roughness of the SKH51 coating was reduced the most, and the surface quality was improved better.



Fig. 3.24 – Surface topography of the treated coatings

3.3.3 Surface roughness of coatings

Surface roughness of composite coating was measured by Mitutoyo SJ-210 roughness. The ISO 1997 standard was selected and the surface was measured over a length of 3 mm, and the standard was shown in Table 3.18. The electro-spark

deposited surface was subjected to roughness measurements, and three measurements were taken on the surface of each specimen, and the mean and standard deviation of Ra on the specimens were counted and calculated, and the measured values were shown in Table 3.18[155, 156]. The graph was plotted based on the relevant data. It was found that the GO gel coating had the smallest roughness value and had a good surface quality. ESD coating surface quality was significantly improved, which reached the best surface quality relative to other metal coatings, which of surface roughness reached $0.113\mu\text{m}$. Niobium metal was deposited on SKH51 coating, which was the best surface quality on the metal surface, as shown in Table 3.19. The surface roughness value of niobium coating was $1.014\mu\text{m}$. Since niobium has a high melting point of $2648\text{ }^{\circ}\text{C}$ and titanium has a melting point of $1688\text{ }^{\circ}\text{C}$ [157], there is not much difference in the hardness of the two materials. Because niobium metal has a refining effect on the metal surface, it leads to an increase in surface roughness during deposition. Specimens 4 and 9, which form metal coatings containing niobium, had relatively small roughness values. Due to the fact that niobium has a somewhat higher melting point and can refine the metal surface material. Specimens 4 and 9, which form metal coatings containing niobium, have relatively small roughness values. Since niobium has a higher melting point, the metal surface material can be refined. As a result, niobium coatings and niobium-carbon coatings have a smaller roughness. Because there was the influence of other metal components in the more expensive titanium alloy, and there was a hard phase on the surface of the coating, which of surface roughness was also affected by the content of other alloys. It has a larger surface

roughness value than pure titanium coating (TA1). Even if the TC4 and TC21 materials with better strength were used as electrodes, the surface roughness of the formed coating was larger than that of Ta1. As shown in Fig. 3.25, it was found from sample 1, 2 and 3 that the roughness increased gradually with the increase in the number of layers. Tungsten carbide coating hardness was higher. The standard deviation of surface deposition roughness was the smallest, which was 0.080143. SKH51 and WC materials were harder. It had better high temperature performance and the surface quality was easier to control compared to soft metals Ti, Nb and Zr. In the coatings, the surface roughness value increased with the coating thickness. The B83 coating had a low melting point, melting point 240 °C[158, 159], which was easy to melt during deposition, and caused deterioration of the surface roughness. In these experiments, small capacitance and medium frequency vibration were used to control the surface roughness, and better results were obtained.

Table 3.18 – Mitutoyo SJ-210 roughness setting parameters

Standard	Profile	λ_s	Evaluation Length	Cut-Off	Filter
ISO 1997	R	2.5 μm	2.92mm	0.08mm	GAUSS

Table 3.19 – Mean and standard deviation of composite coating roughness

Scheme	Coating composition	Mean of coating roughness	standard deviation of coating roughness
1	SKH51	1.086	0.107979

2	SKH51+WC	1.142	0.017518
3	SKH51+WC+B83	1.259	0.080143
4	SKH51+Nb	1.014	0.118955
5	SKH51+TA1+C	1.189	0.120267
6	SKH51+TC4+C	1.538	0.119656
7	SKH51+TC21+C	1.514	0.303799
8	SKH51+Zr+C	1.259	0.143954
9	SKH51+Nb+C	1.041	0.014166
10	SKH51+BT20+C	1.313	0.053506
11	SKH51+NbZr+C	1.115	0.228255
12	SKH51+GO Gel	0.113	0.0445

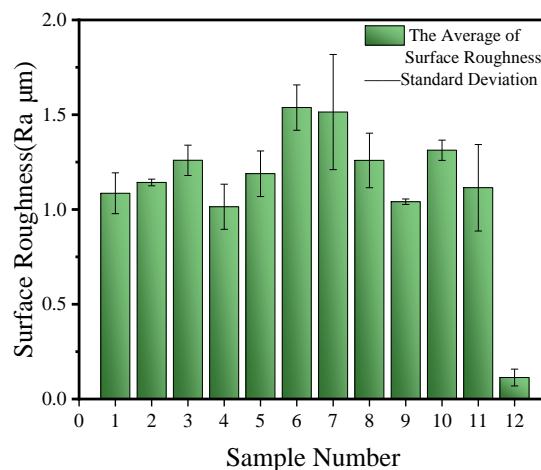


Fig. 3.25 – Mean and standard deviation of composite coating roughness

3.3.4 Analysis of Coating Abrasion Resistance

A linear reciprocating friction and abrasion machine MWF-500 was utilized for the experiments. The samples were fixed by special fixtures. A 6mm friction ball (ZrO_2 , G10 precision) was used for the surface abrasion test. Stable pressure of 30N was used; the machine motor was 100r/min; The reciprocating distance was 6mm. The surface dry friction experiments were carried out for 10 minutes. The

abrasion marks were measured by adjusting the parameters of light source scene, PL illumination and CXI illumination with Leica super depth of field microscope (Leica Co, DVM6). The experimental ambient temperature was 20 °C. For each friction test, 3 times experiments were performed. The width of the middle part of the abrasion mark was measured 6 times, including measuring out the maximum, minimum, and intermediate values. The data were statistically calculated, as shown in Table 3.20.

Table 3.20 – Mean and standard deviation of abrasion mark width for the coating

Scheme	Coating composition	Mean of abrasion mark width(μm)	Standard deviation of abrasion mark width(μm)
1	SKH51	619.22	134.48
2	SKH51+WC	586.12	212.27
3	SKH51+WC+B83	746.70	243.09
4	SKH51+Nb	1261.74	280.84
5	SKH51+TA1+C	695.85	84.91
6	SKH51+TC4+C	886.18	72.02
7	SKH51+TC21+C	1215.34	158.68
8	SKH51+Zr+C	668.04	166.43
9	SKH51+Nb+C	769.15	98.38
10	SKH51+BT20+C	834.08	136.34
11	SKH51+NbZr+C	767.80	60.45
12	SKH51+GO Gel	1377.93	149.57

As shown in Fig. 3.26, it can be seen that the WC coating had the lowest wear rate. Sample 12 the non-metallic surface coatings had higher wear. Because niobium was softer, niobium had the highest wear in metallic coatings. The amount of wear was higher. Sample 9 and sample 4 were compared, and when the surface was graphite deposited on the surface, the surface wear resistance was increased and the maximum abrasion mark width was reduced. In sample 8, graphite was

deposited on the metal zirconium coating, and zirconium carbide appeared on the surface, which increased the wear resistance of the surface. In titanium and titanium alloy coatings, it was found that titanium elements pass through graphite coatings, and after in-situ reactions occurred, titanium carbide coatings were formed on the surface, and the wear resistance increased. Partial annealing had occurred in TC21 titanium alloy, and less titanium carbides were formed on the surface, which reduced its bonding strength, and its wear resistance was not as good as the combination of pure titanium coating and graphite coating. Pure titanium coatings can be selected for in-situ reaction, which were better wear-resistant and less costly than titanium alloy coatings. Titanium, zirconium and niobium metal coatings can generate carbide coatings after graphite deposition. TiC, ZrC, NbC coatings were formed in situ, which of micro-hardness order is: $TiC > ZrC > NbC$. So TiC has better wear resistance than the other two coatings. Since the thickness of carbides formed by in-situ reaction is lower than that of WC coating, the degree of wear resistance was not as good as that of WC coating. B83 was used as an antifriction material. It was effective in resisting wear and was better than titanium and graphite combination coatings. B83 was used to cover the cracks in the surface WC coating and improve the corrosion resistance of the coating. Therefore, SKH51+WC+B83 composite coating was effective in resisting wear, and its wear resistance was better than that of the carbonized in-situ reaction coating. GO gel coating belongs to non-metallic. Non-metallic coating wear resistance is not as good as other metal coatings, which can improve the surface accuracy, there is still meaningful from the point of view of the process.

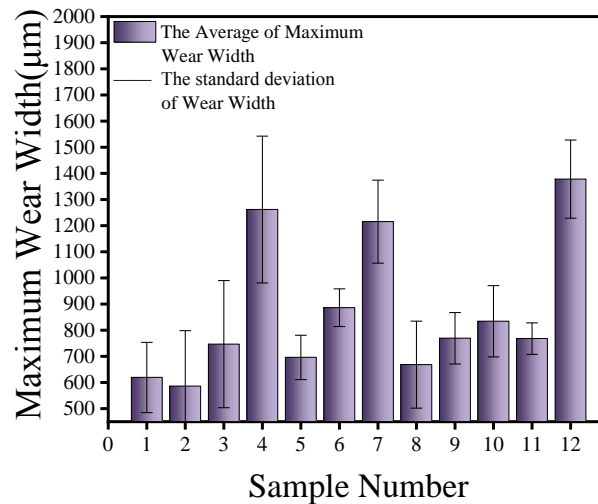


Fig. 3.26 – Mean and standard deviation of abrasion mark width for composite coatings.

According to the friction experiment, the 12 schemes were divided into 4 groups. After the friction and wear experiments on the sample, there were three schemes in one group, as shown in Fig. 3.27. The first group includes SKH51, SKH51+WC, SKH51+WC+B83. The second group included SKH51+TA1+C, SKH51+BT20+C, SKH51+TC4+C. The third group included SKH51+Zr+C, SKH51+NbZr+C, SKH51+Nb+C. The fourth group included SKH51+TC21, SKH51+GO Gel, SKH51+Nb.

In the first group, the surface roughness of SKH51 was small, and the surface had certain hardness, so that the material had a small friction coefficient of 0.07. In order to improve the wear resistance, the deposition of WC coating was carried out, which of surface friction coefficient increases to 0.23. However, after B83 material was coated, it had a lower friction coefficient because of the softness of the tin-based alloy, the friction coefficient of the coating dropped to 0.12. Since B83 was a friction-reducing material, it had a more stable friction coefficient as seen in the Fig. 3.27a.

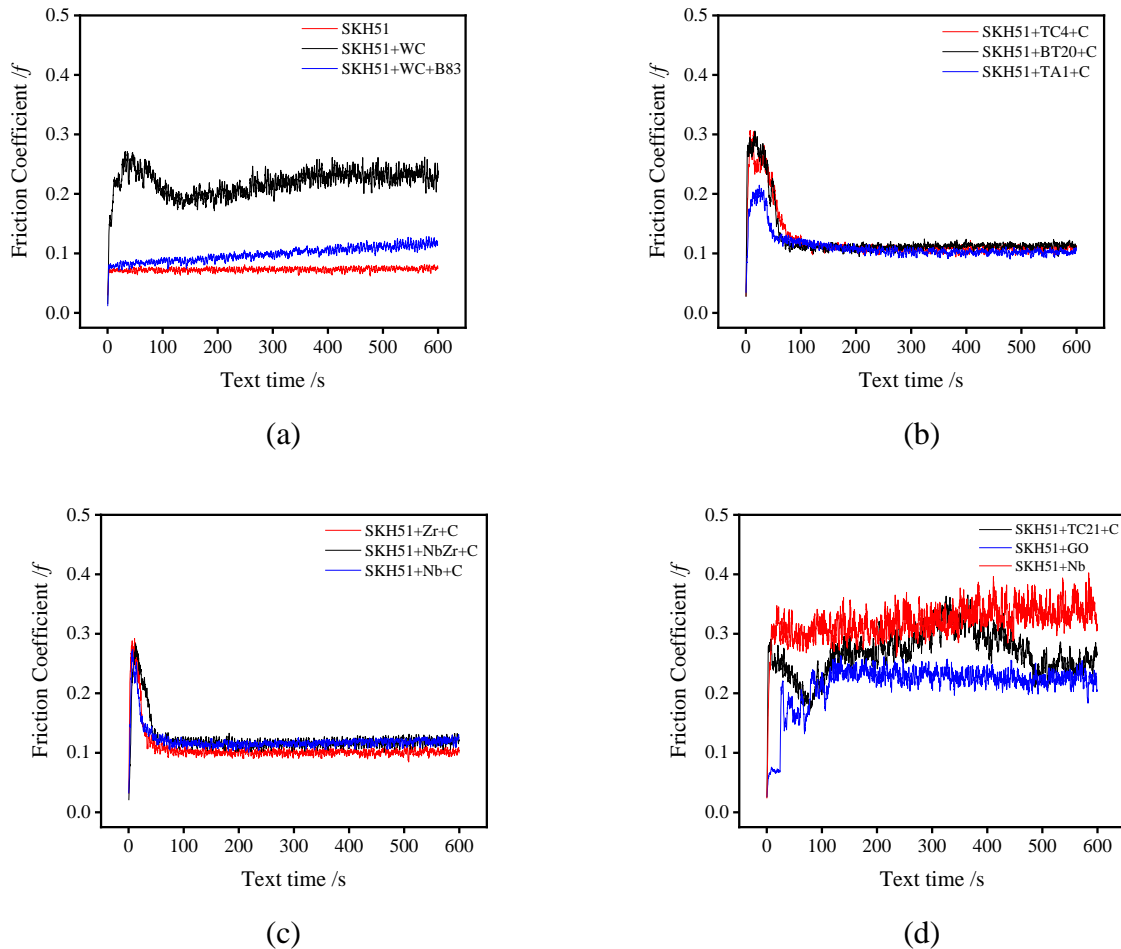


Fig. 3.27 – Friction coefficients of composite coatings: a - Group 1; b - Group 2; c - Group 3; d - Group 4.

In group 2, pure titanium (TA1) had a closer coefficient of friction to the titanium alloy coating. After the in-situ reaction, titanium carbide was produced, which increased the coefficient of friction of the coatings. In the later stages of friction, the coefficient of friction of the coating of TA1 changed more gently because the coating had the highest titanium content and the surface was more homogeneous. BT20 and TC4 didn't have the same surface content as pure titanium coatings due to the relatively low titanium content and the low level of carbide coatings generated by surface reactions. Because the in-situ coating of Ti alloys was softer and has a trace amount of cemented graphite on the surface, it has a lower coefficient of friction and can also be used as a friction-reducing material.

In addition, titanium and titanium alloys had good corrosion resistance in Fig. 3.27b.

In group 3, the graphite carbonized layers of zirconium and niobium had not much difference in the values of the coefficient of friction, which had good stability during friction. Zirconium carbide and niobium carbide formed on the surface had a lower coefficient of friction. According to the abrasion marks, the wear resistance of the three schemes was relatively close. Zirconium carbide coatings have a better surface quality. It had a relatively small coefficient of friction. Niobium-zirconium alloy was composed of niobium and zirconium. It was close to the graphite reaction layer of pure niobium or pure zirconium alloy coating after graphite in situ reaction. Among them, zirconium carbide coating has a smaller friction coefficient than titanium and titanium alloy graphite carburized layer, and its value was 0.1, as shown in 3.27c.

In group 4, SKH51+Nb coating had the highest coefficient of friction with a value of 0.32. Pure niobium which was deposited on SKH51 coating had a large surface roughness. And micro-cracks appeared on the surface of the coating, which indicated an increase in the brittleness of the surface coating. Niobium can form intermetallic compound Fe_2Nb_2 with Fe, which caused uneven surface hardness and micro-cracks. The titanium content of TC21 coating is about 84% lower than that of TC4. Because it contained Ti, Mo, Cr, Nb and other elements, it can react with carbon element to produce carbide, which made the surface hardness uneven and the coefficient of friction large. The friction coefficient of SKH51+GO Gel scheme was 0.2, which was lower than the above two metal coatings. The friction

coefficient was reduced due to the addition of graphene oxide gel, but it was larger than B83. It was also inferior to the friction coefficient of graphite coating of metals such as niobium, zirconium and titanium. However, it was better than the substrate iron. GO gel coating had a great improvement on the surface quality of the previous coating in Fig. 3.27d.

It can be seen from Fig. 3.28 that the surface friction coefficient of SKH51 is the smallest, its value is 0.07, and the friction force was also the smallest. The surface roughness of the SKH51+Nb coating was the largest, and it produces a large noise during the friction process, which had a value of 0.32. In SKH51+Nb with SKH51+WC coating, tiny cracks were found in the surface coating. In the surface coating of SKH51+Nb and SKH51+WC, tiny cracks were found. The non-metallic coating of GO gel can reduce the coefficient of friction. However, its friction coefficient was not as good as that of in-situ reaction coatings of Zr, Nb, Ti and their alloys. B83 was a good anti-friction material, which reduced the roughness of SKH51+WC coating from 0.23 to 0.12. The coating can deposit multiple layers, the thickness value increases, and there was no crack on the surface.

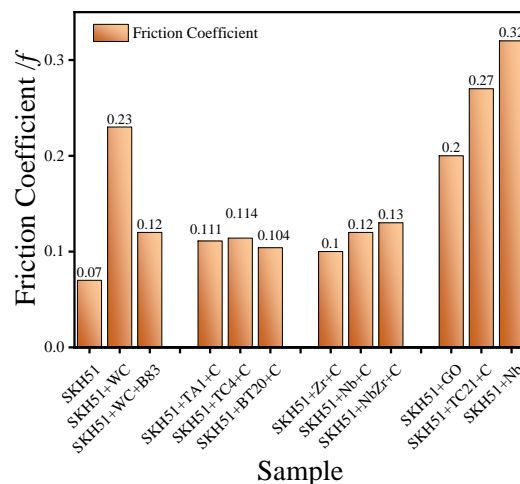
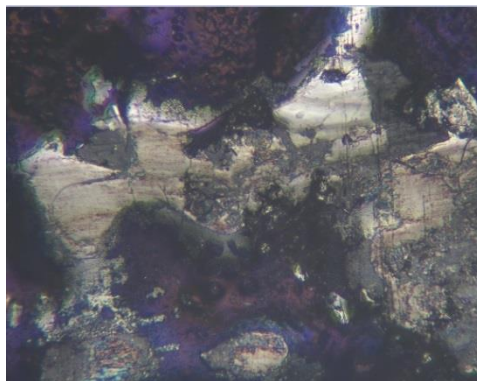


Fig. 3.28 – Coefficient of friction of coatings

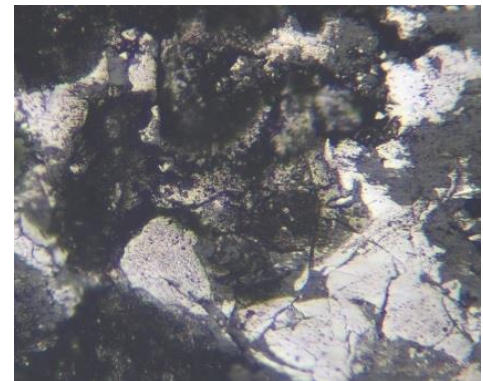
SKH51+TA1+C coating had a lower cost and the carbides on the surface give it a relatively low coefficient of friction and little friction. It increased the coating thickness and at the same time has good corrosion protection. It was not comparable to SKH51 single coating.

Therefore, after the coefficient of friction, abrasion mark width and surface roughness were compared and analyzed, Scheme SKH51+WC+B83 had the best performance of the composite gradient coating.

As shown Fig. 3.29a, the wear mechanism of SKH51+ WC composite coating was mainly abrasive wear. In Fig. 3.29b, the B83 material was the outermost layer of the SKH51+ WC+B83 composite coating, there were free of scratches and abrasions on the abrasion mark, the wear mechanism of the optimal coating was mainly plastic deformation accompanied by slight polishing.



(a)



(b)

Fig. 3.29 –Wear surface morphology: a-WC coating;b-B83 coating.

3.3.5 XRD analysis of SKH51+WC+B83 coatings

XRD analysis was performed on the deposited surface on the WC coating. The WC coating surface was found to be mainly composed of electrode materials WC, W_2C , Co, Fe_3W_3C and Fe, as shown in Fig. 3.30a[160-162]. As the main

surface components were WC and W_2C , the surface performance and wear resistance of SKH51 are further improved. Between the WC coating and SKH51 coating, a small part of Fe in the SKH51 substrate was alloyed into the carbide surface coating due to the influence of the electrode rotation process. The electrode material of HF10 contains 10% of cobalt, and Co is a preferred bonding material for WC and W_2C [163]. Since the presence of iron can also form a bonding effect, any intermetallic compound components were not detected, but the effect obtained was not as good as that of Co and Ni. Fe_3W_3C is M_6C type carbide that can increase the wear resistance of the surface.

XRD analysis was performed on the B83 deposition surface, as shown in Fig. 3.30b. On the surface of the B83 coating, there were mainly Sn, Sb, Cu, Cu_6Sn_5 , $Cu(Sn,Sb)$, SnO_2 , C and other components[163-165]. Electrode material included Sn, Sb, Cu and Cu_6Sn_5 . On the surface of WC coating, because the process was not protected by argon gas, SnO_2 and C components were generated on the b83 coating surface. The appearance of carbon was due to the loss of carbon due to oxidation of cemented carbide material WC at 500~800 °C, as shown in Equation (3.7). Oxygen in the air and tin in the coating form an oxide substance SnO_2 , and gray spots appear on the surface, as shown in Equation (3.8). The content of Sn in B83 accounts for 83%, so it shows a strong diffraction intensity, indicating that the content of Sn is relatively high for the composite coating. Sb had multiple main peaks in XRD diagram. Precipitated C was not well combined with WC coating, and it was mixed in B83 coating. Since the vibration shock process was chosen

instead of the rotating electrode process, no strong main peaks of WC and W_2C were found in the B83 coating.

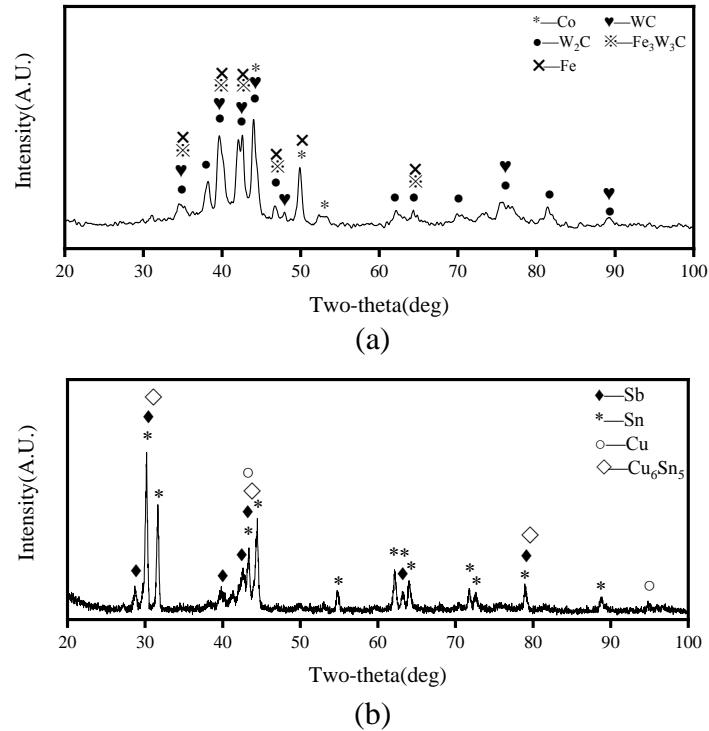


Fig. 3.30 – XRD analysis of SKH51+WC+B83 coatings: a- WC coating;b-B83 coating.



3.3.6 SEM analysis of SKH51+WC+B83 coatings

As shown in Fig. 3.31, spot deposits appeared on the b83 coating surface. Since the B83 material has a low melting point. If high-power ESD deposition equipment was used, the B83 electrode was easy to melt. And the molten droplets cause uneven surface, so that the deposition cannot be evenly coated. The new ESD process was utilized to control the electrode temperature, which prevents high temperatures from reducing the melt droplet size. It can be seen from Fig. 3.30 that

the top of the droplet deposition was relatively flat, and there were large layered pores at the bottom of the droplet. These small holes led to uneven deposition of the surface coating because the B83 material cooled too quickly. It was difficult to repair them at a later stage since the melted droplets were bulged out. On the surface of the coated surface, no cracks were found. In the metal surface coating, there were small sputtered melt drops.



Fig. 3.31 – SEM of the B83 coating

As shown in Fig. 3.32, there was a bright white layer on the surface of the WC deposited layer that was not easily abraded. The surface of WC coating was relatively flat, with many irregular small droplets melting point and less pores on the surface. However, a large number of micro-cracks appeared on the surface of the coating. When the high-hardness carbide material was rapidly heated and cooled during the spark discharge process, the residual thermal stress in the coating will cause the material itself to undergo large deformation, resulting in cracks. These cracks cannot be avoided. As the deposition thickness increases, the cracks gradually expand. Excessive cracks will lead to a decrease in the performance of the coating.

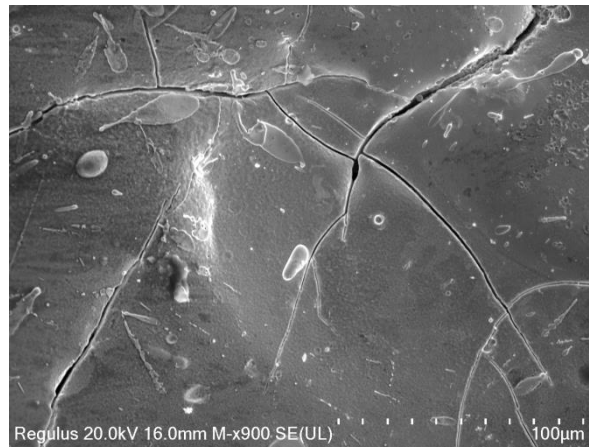


Fig. 3.32 – SEM of the WC coating

3.3.7 EDS analysis of SKH51+WC+B83 coatings

(1) EDS analysis of B83 coatings

The B83 coating was selected in surface scanning mode and its morphology was shown in Fig. 3.33. The elements contained in the B83 coating were shown in Fig. 3.34. From the B83 energy spectrum elemental statistics table (Table 3.21), the wt.% of Sn was 56.44%, the content of C was 12.09%, the content of O was 9.64%, and the content of Fe was 8.76%. In Fig. 3.35, since the main component of the B83 electrode was Sn, the content of Sn in the coating was the most. In the absence of argon protection, C was produced because of the pyrolysis of WC, which appeared in the deposition bumps. According to the distribution diagram of oxygen element, the B83 coating had the infiltration of oxygen element and existed in the form of oxide. In the layered pores, the B83 alloy coating was less. From the element distribution diagram, there was almost no distribution of Sn, Sb, and Cu in the pores. It was mainly the WC and SKH51 coating below, so the Fe content was relatively high, and it was found that W elements had gathered. The EDS measurement depth was generally 1~5 μm , and a small amount of underlying

coating elements can also be observed. According to the surface distribution map of carbon element, it was not possible to determine whether it is tungsten carbide or free graphite by EDS, which was combined with XRD to analyze the physical phase. In the distribution map of the element Fe, it can be seen that the distribution of the coating was not uniform, and the thinner parts can be seen to have a higher content of Fe at that place. In the laminated pores, the elements of the B83 material were not distributed, because the measurement distance cannot be found in the corresponding elements.

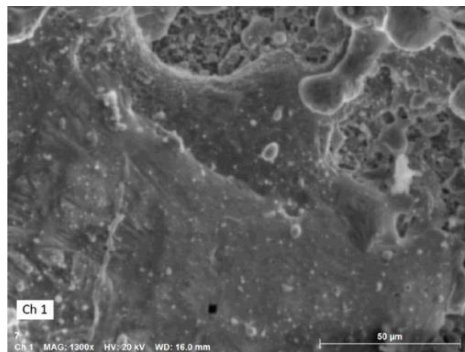


Fig. 3.33 –EDS energy spectrum analysis on B83 coating

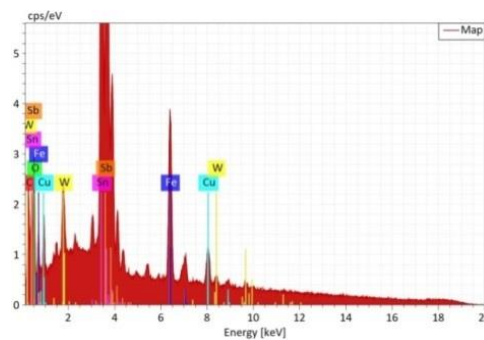
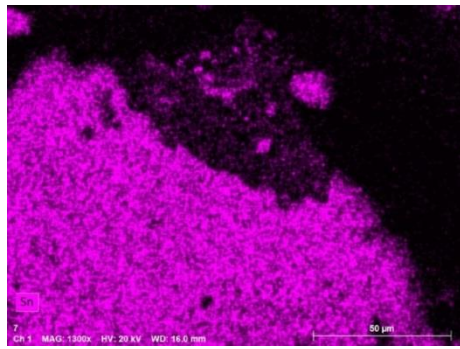


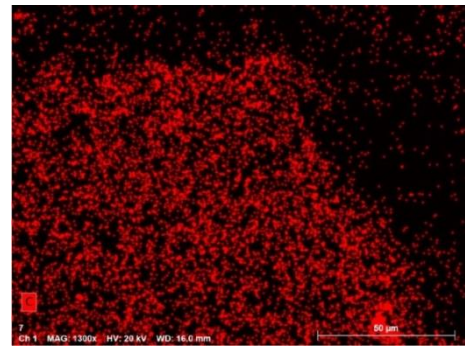
Fig. 3.34 – EDS Elemental Analysis Diagrams of B83 Coatings

Table 3.21 – Element content on B83 coating surface

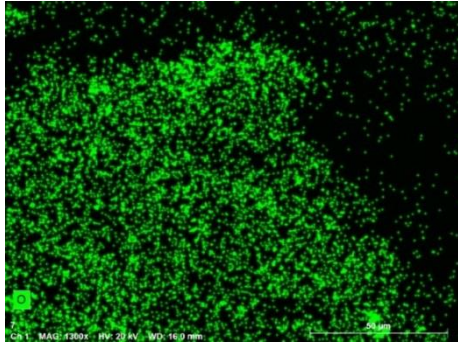
Element	Sn	C	O	Fe	Sb	Cu	W
Atomic Number	50	6	8	26	51	29	74
wt. %	56.44	12.09	9.64	8.76	8.23	2.94	1.89
at. %	20.10	42.56	25.46	6.63	2.86	1.96	0.43



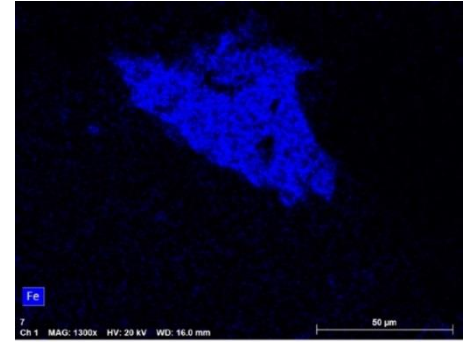
(a)



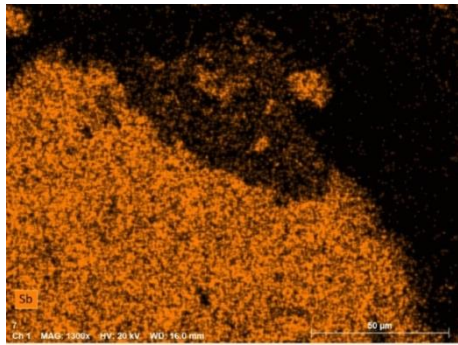
(b)



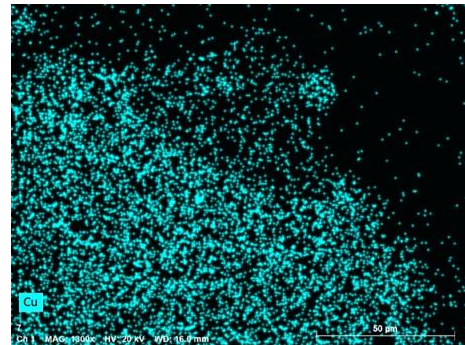
(c)



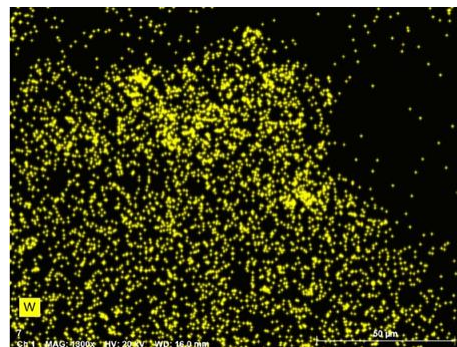
(d)



(e)



(f)



(g)

Fig. 3.35 – Element distribution of EDS energy spectrum: a-Sn; b-C; c-O; d-Fe;

e-Sb; f-Cu; g-W.

(2) EDS analysis of WC coatings

The surface scanning mode was selected for the WC coating, and its morphology was shown in Fig. 3.36. The elements contained in the WC coating were shown in Fig. 3.37. From the WC energy spectrum elemental statistics table (Table 3.22), the wt. % of Fe was 55.77%, the content of W was 29.76%, the content of C was 9.96%, and the content of Co was 4.5%. The content of Fe is the highest and the content of Co was the lowest. Fe was the main element in SKH51 coating, and Co was the material in the electrode. Among them, WC coating was thinner, and EDS can test the main element Fe in the SKH51 coating in Fig. 3.38. Because other element content is less, it is not found in the WC coating. In the case of argon gas protection, because WC can still maintain stability at 2850 °C, the W element reflects the deposition of the WC electrode. The distribution of elements Fe, W, C and Co was very similar. The distribution of Fe elements in EDS was basically the same as that of W, C and Co. It indicated that the WC coating contained some amount of SHK51 material. In the non-deposited place of the pores and cracks, owing to the depth of measurement limitations of the EDS, there should be a blind spot test. The sputtered molten droplets of metal were on the surface of the coating. According to the distribution map of tungsten elements, it was mainly W carbides.

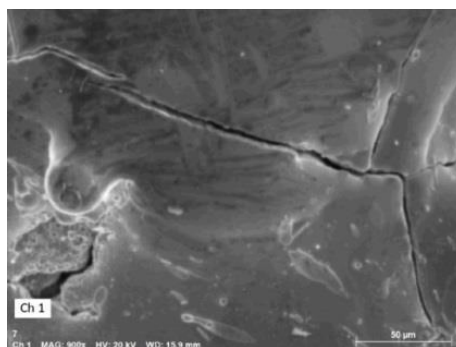


Fig. 3.36 – Surface scanning area on WC coating surface

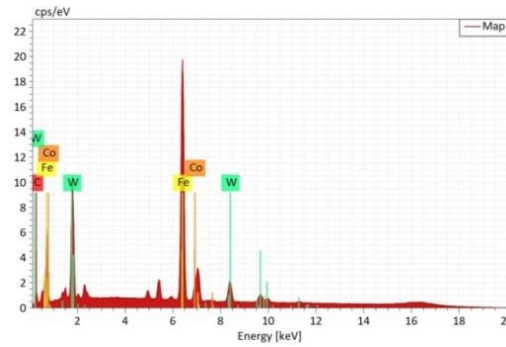
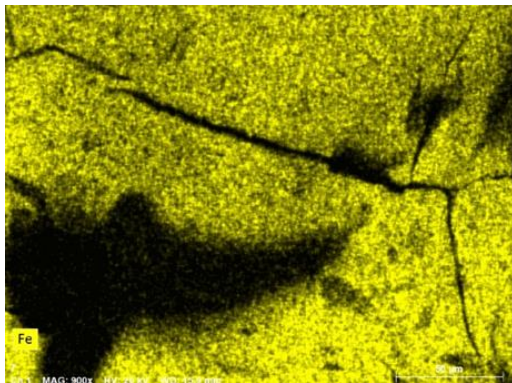


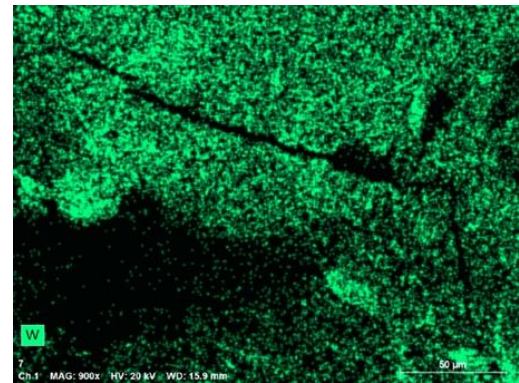
Fig. 3.37 – EDS elemental analysis diagrams of WC coating

Table 3.22 – Element content on WC coating surface

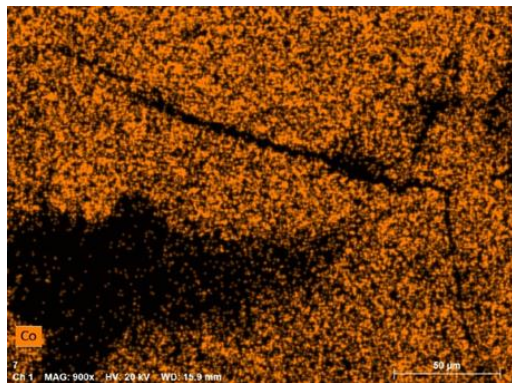
Element	Fe	W	C	Co
Atomic Number	26	74	6	27
wt. %	55.77	29.76	9.96	4.50
at. %	48.32	7.83	40.15	3.70



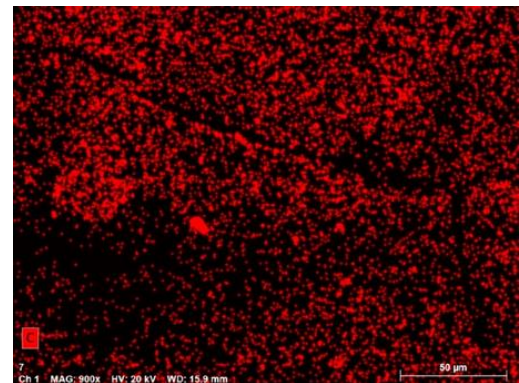
(a)



(b)



(c)



(d)

Fig. 3.38 – Element distribution of EDS energy spectrum:
a-Fe; b-W; c-Co; d-C.

3.3.8 Composite coating conclusion

The performance of optimal coating solution can be improved by composite

coating technology. Composite coating can realize multiple functions such as wear resistance, friction reduction and corrosion resistance. The optimal coating solution is SKH51+ WC+B83 composite coating. By using gradient coating SKH51+ WC, the value of the coating has gradient wear resistance, which has better morphology and lower roughness, its Ra is 1.086 μ m. The WC coating has the best wear resistance among all the schemes, and the abrasion width is 586.12 μ m. B83 coating has a very stable coefficient of friction, which is 0.12. It is 48% lower than the friction coefficient of WC coating. Ti coatings, Nb coatings and Zr coatings have very good corrosion resistance. Ti, Nb, Zr and their alloys form carbides in situ on the surface after the graphite coating was deposited, which had a low friction coefficient and can effectively reduce the surface friction of the coating. The higher the Ti, nb, Zr content, the more carbides will be formed in situ, and the friction coefficient will be reduced. After ultrasonic cleaning with anhydrous ethanol, the small amount of graphite particles were cemented on the surface, which was also effective in reducing friction.

(1) A reasonable process was used in SKH51 coating, and the surface quality of the SKH51coating was the best. Because SKH51 material has good impact toughness, it has certain wear resistance and surface hardness. Therefore, it was selected as the transition layer. There are no cracks on the surface of the SKH51 coating, which can be achieved by increasing the thickness of the SKH51 coating. If the thickness of the WC coating was reduced, thus reducing the cracks produced by the thermal stresses.

(2) The WC coating had better wear resistance and smaller friction trace width than in-situ reactive coatings deposited, on which the friction force was larger. The surface of the coating was subject to micro-cracks due to rapid deposition. The deposition thickness increased when the deposition time increases. The more the surface coating was affected by thermal stress, the more obvious the surface micro-cracks were. Excessive micro-cracks will affect the performance of WC coatings.

(3) Titanium alloys, Ti, Zr and Nb materials have good corrosion resistance. Graphite was deposited on the surface of Ti coating, Nb coating and Zr coating, and there were in-situ reaction coatings on the surface. The surface produced TiC, ZrC, and NbC with higher hardness, which effectively improved the wear resistance of the surface coating. Due to the deposition process, the amount of carbides on the surface was less than that of the WC coating, and the wear resistance was worse than that of the WC coating. However, the surface friction coefficient was low, which can reduce the friction of the coating.

(4) Since the B83 coating has a low melting point, a small capacitance need be selected, which will reduce the deposition energy and prevents excessive metal melting droplets. When the vibration frequency was reasonably chosen, the deposition surface quality was improved. Because the B83 coating was deposited directly in the air, SnO₂ was produced on the surface. In this regard, it was proposed to use Ar gas protection to improve the surface gloss of the coating.

(5) Graphene oxide (GO) has good anti-friction properties, which can reduce friction. In the electro-spark deposition, because GO material is not easy to fix, it is

not easy to combine with other coatings. The use of sodium silicide gel can effectively improve the binding force of GO material. With the sodium silicide gel, it can effectively improve the GO material bonding force, which resulted in GO gel coatings. It significantly reduces the roughness of the deposited coating, the coefficient of friction, and the friction force. The process is relatively simple and low cost.

3.4 Deposition process of low-temperature super-soft materials

3.4.1 Experimental scheme for deposition of super-soft materials

The deposition of soft low-temperature metal has always been a difficult point in the deposition process. Because the electrode of melting temperature is low, the conventional vibratory impact process or rotary electrode process make the shape of the electrode to bent, the metal droplets on the coating surface will become larger[166, 167]. The degree of bending was usually reduced by increasing the electrode diameter. Ultrasonic deposition was used to effectively solve the electrode bending problem. It illustrated that the amplitude of vibration shock was reduced, and the problem of electrode bending was effectively solved. The capacitance was rationally selected to reduce the temperature of the electrode melt drop, which reduced the problem of excessive metal droplet size. Pneumatic deposition has less impact than conventional vibratory deposition, as shown in Fig. 3.39. Therefore, this study decided to utilise gas vibration to shock the electrode. It was achieved by controlling the air pressure of the air pump and the amplitude and frequency of the electrodes, as shown in Fig. 3.40.



Fig. 3.39– Vibratory deposition process:a- conventional vibratory deposition;b- Pneumatic vibratory deposition



Fig. 3.40–Pneumatic electrode experiment

A fixing device was utilised to fix the pneumatic vibration handle. The pneumatic pressure was controlled by using pneumatic valve (SMC IR2020). The data collector (YE6232B) was used, the piezoelectric acceleration sensor (SA-AV-D100, Table 3.23) was selected, and the IEPE mode was taken for the measurement. The sensor was fixed on the bench vise, and the measurement was carried out by different distances from the sensor to the electrode and different ranges of the electrode handle.

Table 3.23 – SA-AV-D100 Sensor Parameter

Model	Unit	Value
Reference Sensitivity	mV/m·s ⁻²	10.03
Frequency range	Hz	1-10000
Max. lateral sensitivity	%	<5%

Max. permissible acceleration	m·s ⁻²	5×10 ²
Mounting thread	mm	M5
Weight	g	9
IC Operating Voltage	V	18-28
Operating Current	mA	2-10
Operating Temperature	°C	-40~120

Experimental scheme: the maximum amplitude of the vibration handle was 0.6mm. If the electrode head of the vibration handle was too short from the workpiece, the electrode cannot vibrate. When the vibration handle knob was turned to a small degree, the air pressure was small and the electrode vibration was unstable. The b83 material with a diameter of 3mm and a length of 20mm was selected as the electrode. The electrode head was flat. The distance from the electrode head to the transducer was controlled with plug gauges, which were divided into 3 distances. The experiments were carried out by selecting the vibration handle knob 60 per cent, 80 per cent and 100 per cent range. Therefore, distance and vibration grade were selected as experimental parameters, and 9 groups of experiments were carried out as shown in Table 3.24.

Table 3.24 – Pneumatic vibration experiments

Experiment No.	Vibration grade	Vibration distance	Operating air pressure
1	(60% of knob range)1	0.092mm	0.45-0.62
2	(60% of knob range)1	0.187mm	0.45-0.62
3	(60% of knob range)1	0.377mm	0.45-0.62
4	(80% of knob range)2	0.092mm	0.45-0.62
5	(80% of knob range)2	0.187mm	0.45-0.62
6	(80% of knob range)2	0.377mm	0.45-0.62
7	(100% of knob range)3	0.092mm	0.45-0.62
8	(100% of knob range)3	0.187mm	0.45-0.62
9	(100% of knob range)3	0.377mm	0.45-0.62

3.4.2 Experimental results and discussion

In the process of measuring the vibration, the vibration handle knob was switched on. Because the air pressure was initially low, a discontinuous shock was produced. When the air pressure was stable, the vibration was correspondingly stable. Vibration related parameters were measured. In Fig. 3.41, the vibration waveform were shown mainly during the vibration 4 to 5 seconds time period. The vibration parameters were counted separately. The sampling rate was 96k per second. The corresponding frequency domain was analyzed. The corresponding vibration was mainly below 5000Hz, as shown in Fig. 3.42.

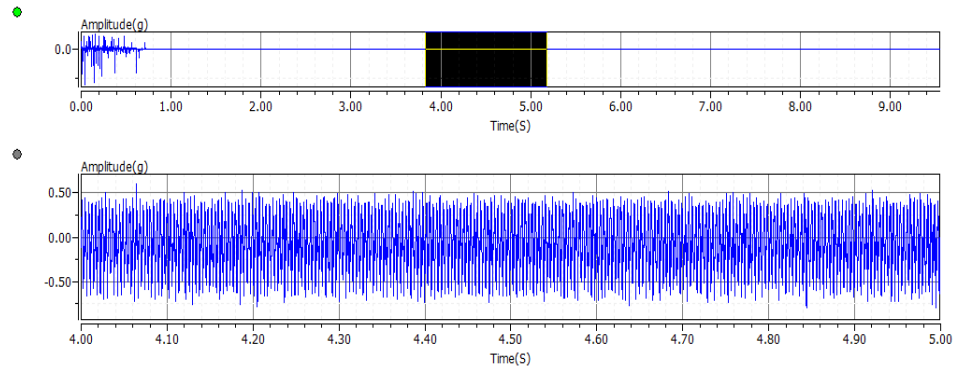


Fig. 3.41 – Vibration time-domain analysis curve during 4 to 5 seconds

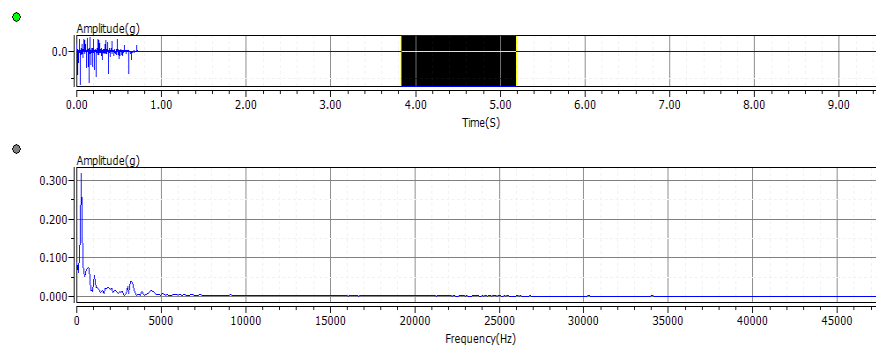


Fig. 3.42 – Spectrum analysis curve during 4 to 5 seconds

When the vibration stabilization process was in progress, three similar periods of time were taken at 4~5 second, the shock waveforms were

experimentally captured. The time-domain waveform corresponding to each test in Table 3.24 was shown in Fig. 3.43.

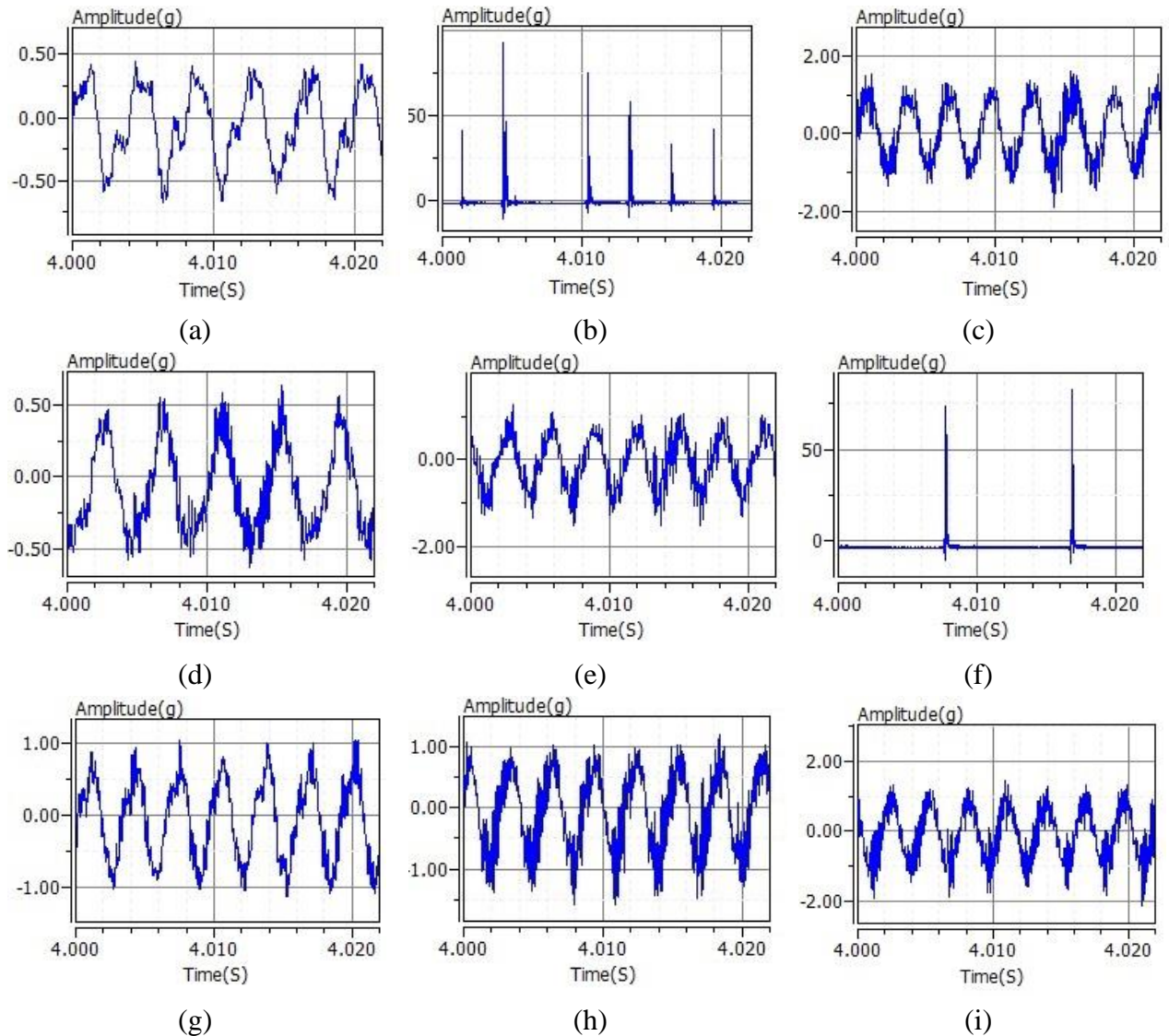


Fig. 3.43 – Vibration time domain waveforms:a- Experiment No.1;b-Experiment No.2; c- Experiment No.3;d- Experiment No.4; e- Experiment No.5; f- Experiment No.6;g- Experiment No.7;h- Experiment No.8; i- Experiment No.9.

The 20 vibration waveforms of three consecutive time periods were counted. The average vibration time was calculated. And the maximum amplitude of the three periods was taken. The average mean time of individual vibrations was obtained, as shown in Table 3.25.

Table 3.25 – Parameters of vibration characteristics on the time domain analysis

No.	Average vibration time of 20 waveforms(s)	Average single waveform of vibration time(s)	Frequency(Hz)	Maximum amplitude(g)
1	0.077147	0.003857	259	1.320983
2	0.076423	0.003821	262	105.95
3	0.05927	0.002964	337	4.1051
4	0.084693	0.004235	236	1.258913
5	0.061877	0.003094	323	3.344233
6	0.182013	0.009101	110	96.96367
7	0.063727	0.003186	314	2.3395
8	0.060283	0.003014	332	2.7933
9	0.057267	0.002863	349	3.8994

The time domain signals of the steady vibration process were processed by means of the signal processing software YE7600. Through the Fourier transform, the frequency value and the amplitude under Fourier were obtained[168]. It was found that the frequency number of the maximum value of the FFT amplitude was basically consistent with the manual sampling data, as shown in Table 3.26[169, 170]. The corresponding Fig. 3.44 was plotted. When the electrode knob was larger, the vibration was more stable. For example, the vibration frequencies of experimental samples 7, 8, and 9 were not much different, which were all at 350Hz. Amplitude increased as the electrode distance increased. When the amplitude of vibration increased, the impact force became smaller. When the handle air pressure increased with the knob, the vibration frequency increased. By comparing the experimental results of samples 7, 8, and 9, the vibration frequency of sample 9 was 11.2% higher than that of sample 7, the amplitude was 68.9% higher, and the impact force was improved. However, if the air pressure of the handle itself was unstable, the handle would generate a greater impact force, and the vibration cycle

was changed, such as sample 2 and sample 6. Therefore, it can be seen through experiments that reducing the pressure between the electrode and the deposition substrate and appropriately increasing the distance between the electrode and the substrate surface, which can obtain a stable vibration frequency and a stable impact force. Through the adjustment of the handle knob, the appropriate impact force and frequency were selected to ensure the deposition quality of the soft low melting point metal surface.

Table 3.26 – FFT analysis of time domain signals

No	Low-order frequency	FFT amplitude
1	252	0.37
2	331	1.54
3	337	0.73
4	236	0.38
5	323	0.49
6	110	1.15
7	313	0.45
8	330	0.71
9	350	0.76

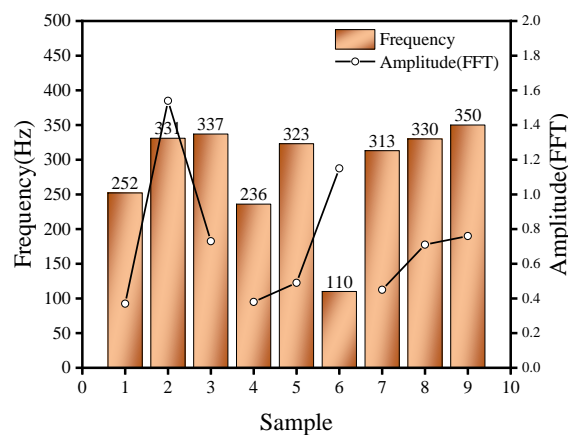


Fig. 3.44 – Frequency and amplitude of vibration of pneumatic impact electrodes

Calculation of deposition energy: RC circuits with smaller energy were selected for B83. RC circuits had higher machining accuracy and good glossy finish. It had reliable operation and simple device, and can be used for

electro-spark deposition of super-soft low-temperature metal materials. The circuit schematic was shown in Fig. 3.45:

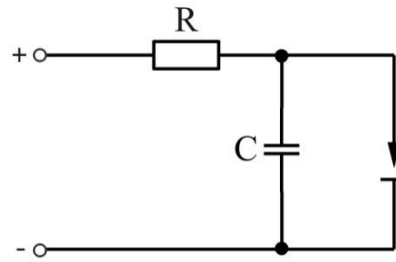


Fig. 3.45 – RC circuit schematic diagram of ESD

Charge or discharge time constant calculation as Equation (3.9):

$$t = RC = 7.5 \times 1 \times 10^{-6} = 7.5 \times 10^{-6} \text{ s} \quad (3.9)$$

According to Table 3.24, sample 9 has the highest frequency, and its average time for a single vibration was 0.002863s. When $t_m = 5t$ (Formula 3.9) $\ll 0.002863$ s, the capacitor can be fully charged not long after each discharge. Therefore, the energy of one pulse (Equation 3.10) is equal to:

$$W = P_c t = \frac{1}{2} C U^2 = \frac{1}{2} \times 1 \times 10^{-6} \times 35^2 = 6.13 \times 10^{-4} \text{ J} \quad (3.10)$$

After the losses are considered, the actual pulse energy (Equation 3.11) was:

$$W_i = \eta W = 0.7 \times 6.13 \times 10^{-4} = 4.29 \times 10^{-4} \text{ J} \quad (3.11)$$

In the formula: η - the utilization of electrical energy, which was generally 60~70%, 70% was selected for RC circuits[171].

The empirical formula for the heat of fusion of metals is:

$$Q = C_0 \cdot m \cdot \Delta t = C_0 \cdot \frac{R^2 \pi}{\cos \theta} \rho h \Delta t \text{ J} \quad (3.12)$$

In Equation (3.12), Q is the heat of melting of the metal (J); m is the mass of the metal (g); C is the specific heat capacity (J/g); R - radius of the deposition

spot(mm); θ - angle made by the electrode with the machining surface; Δt - temperature variation interval; and h - thickness of the coating deposition.

It was found by Equation (3.11) that the larger the deposition spot, the thinner the coating thickness. When the deposition spot was small, the deposition thickness increased. When the electrode temperature rose, it can be cooled by controlling the argon gas pressure; or the coating thickness can be reduced by increasing the moving speed of the coated electrode. With both of these deposition methods, the droplet size was not well controlled. The traditional ESD process required the electrode to be sufficiently cooled in air before it can be deposited, which will improve the surface quality of the coating. The temperature profile of the electrode is complex due to heat conduction, heat radiation, and frictional heat of the metal electrode, which makes it impossible to calculate accurately. Currently, it is only possible to improve the surface quality of soft cryogenic metals by reducing the discharge energy, increasing the deposition frequency and reducing the impact. Using this method, soft low-temperature metals do not need to be cooled for a period of time and can be continuously deposited.

3.4.3 Experimental conclusions of soft low temperature metals deposition

ESD of soft low-temperature metals can get better surface deposition quality by using RC discharge circuits and gas vibration processing technology [172-174]. This method avoided soft cryogenic metals to generate large molten droplets because of increased temperature, which deteriorated the deposition. A smaller discharge capacitance can be selected to reduce and control the discharge energy. The electrode did not need to be cooled for a long time, and it can be deposited

continuously. However, when the electro-spark pulse energy was less than the heat energy of melting of the metal, the electrode material cannot be melted. At this point the electrodes will not be deposited on the surface of the substrate, but will be ground on the surface of the substrate.

Since the electrodes were not deposited by rotation, the cross-section shape of the electrodes was less required. In the processing, the working air pressure was 0.45~0.62MPa, and the proper working distance of the electrode was required. When the handle knob was opened to the maximum, a stable vibration frequency of 310~350Hz can be produced, and the pneumatic impact was more stable, which can get better deposition effect. Electrode processing distance was small, or the working air pressure was low, which will make the vibration frequency decrease and the number of shocks decrease. As a result, the vibration shock was unstable and the deposition efficiency became lower. This process can also be applied to other metal coating materials, the coating surface quality can be significantly improved than the traditional deposition process.

3.5 GO gel coating

Because the electro-spark deposition method of pulse energy wasn't stably and continuously, it led to a large roughness of the deposited surface. The accuracy of electro-spark deposited surfaces was improved by machine processing. This can also be done by various surface machining methods to improve the quality of the ESD coated surfaces. These methods complicate the surface modification process which made the cost more expensive. Alexander used one or more low-energy pulses to grind deposits and improve surface accuracy[175]. Gadlov used

VOK-60 mineral ceramics for surface polishing to reduce surface roughness[176]. Kirik reduced roughness and improved the surface quality of aluminum coatings by using lower discharge energy[177]. Pablo used machine hammer peening to reduce ESD surface roughness[178]. Mykhailo proposed a brand new idea using coatings to reduce the roughness of ESD surfaces, with lower hardness but significantly improved roughness compared to metal coatings[179].

Graphene oxide(GO) is cheap and easy to obtain raw materials, and it is expected to become a high-quality filler for nanocomposite [180]. GO has low density, large specific surface area, high mechanical strength, excellent mechanical properties, wear resistance, adsorption properties, excellent electrical and thermal conductivity, non-toxic and good biocompatibility, etc.[181-185]. These comprehensive properties make GO coating materials have incomparable performance. GO has the architecture of graphene, but also has the hydrophilicity that graphene does not have, and it has better water solubility than graphite powder to avoid powder agglomeration[186]. In the experiment, stable quasi-two-dimensional graphene oxide suspension and sodium silicate gel solution were selected, as shown in Table 3.27.

Table 3.27–SP38 sodium silicate (Na_2SiO_3) liquid specifications

Index	Content
Na_2O	8.53%
SiO_2	26.98%
Density (20°C)	1.366 g/cm ³
Baumédegrees	38.5 B é
Solid content	35.5%
PH	10-13

3.5.1 Preparation method of GO gel coating

At first, the liquid sodium silicate solution, and graphene oxide solution were selected and mixed through a certain volume ratio, and then which was mechanically and physically stirred for 20 minutes. Next, the coated surface was coated with a dropper. Finally, it was placed in a drying and heating box for baking at a certain temperature, and then cooled in the oven for 30 minutes. If the number of layers and thickness of the GO gel coating were required, it can generally be repeated 2-3 times for repeated coating and baking.

3.5.2 Surface morphology of GO gel coating

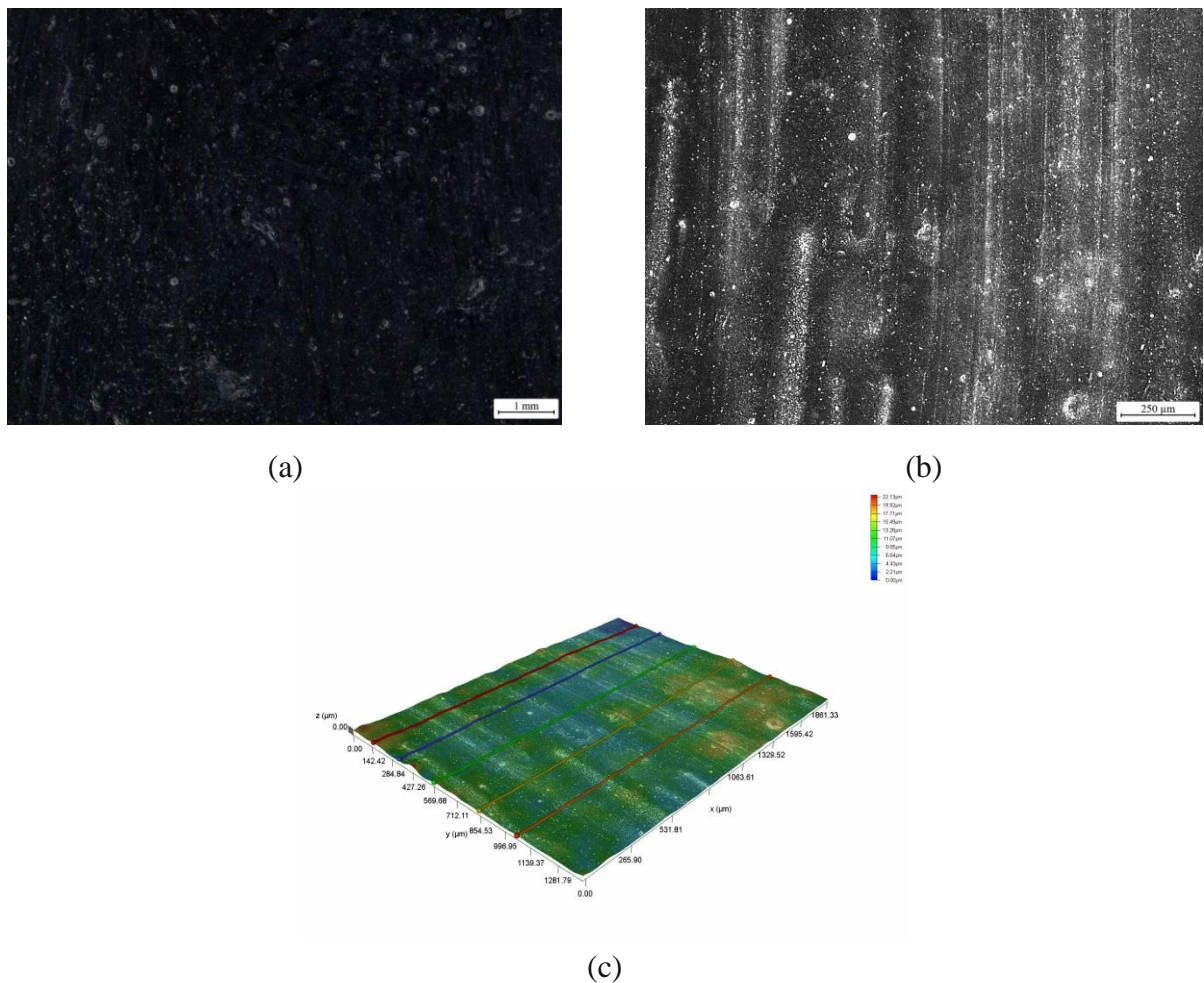


Fig. 3.46 – Surface topography of GO gel coatings: a-100X 2D morphology; b-500X 2D morphology; c- super depth field of 3D morphology

The surface morphology was observed by the Leica super depth of field microscope (Leica Co, DVM6), as shown in Fig. 3.46. In the 2D morphology, there were tiny bubbles on the surface. When the microscope was enlarged, the graphene oxide particles could be seen on the surface. Through the 3D morphology synthesized by the depth of field, it was found that the surface of the GO gel coating was relatively flat. Its surface roughness was 0.16 μ m.

3.5.3 Composition analysis of GO gel coating

(1) XRD analysis of GO gel coating

XRD equipment (Bruker D8 Advance A25, Germany) was used to measure separately the GO gel coatings and the pure cel (Na_2SiO_3) coatings without graphene oxide. In the XRD diagram (Fig. 3.47), a small bump at 10.7° and a valley at 27.5° indicate the possible presence of graphene oxide. The GO content in the coating was low due to dilution by Na_2SiO_3 gel. Therefore, the peaks were not obvious[187-190]. The graphene oxide composition could not be clearly determined based on the characteristic peaks.

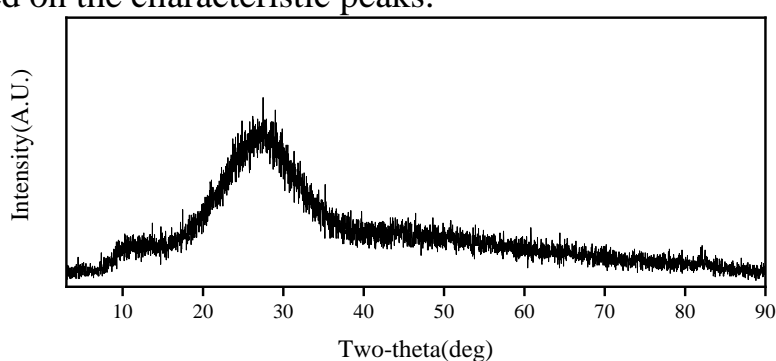


Figure 3.47 – XRD of GO gel coatings

Na_2SiO_3 gel was deposited directly on the substrate surface. From the XRD plot (Figure 3.48), the valley peak appeared at 27.9° and there was no small bump

at 10° . It was different from GO cel, which indicated that the two types of amorphous materials have different surface compositions.

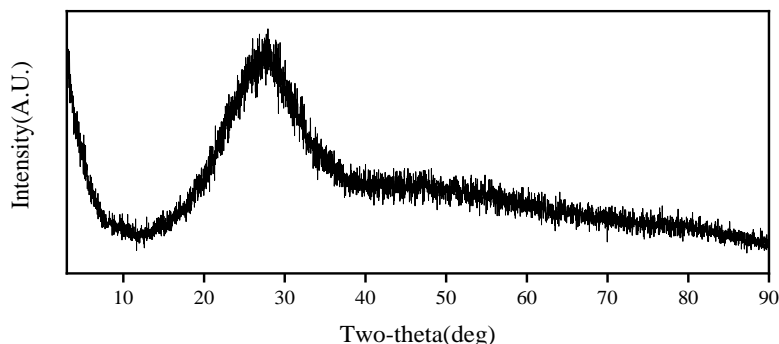


Fig. 3.48 –XRD of gel coating (Na_2SiO_3)

(2) Raman analysis of GO gel coating

Laser Raman spectroscopy can analyze ions, molecular species and the structure of substances. The instrument (DXR2xi, Thermo Fisher Scientific Inc.) was used for this experiment. Laser Raman was commonly used in the analysis of graphene oxide and graphene materials. This type of material had unique characteristics that were easily recognizable [191, 192].

From the measured Raman spectrum (Fig. 3.49), it can be observed that there were two characteristic peaks at 1359.23 cm^{-1} and 1592.57 cm^{-1} [193]. In the research process of Nano carbon materials, general carbon materials contain two significant Raman peaks. Among them, the peak around 1359.23 cm^{-1} was considered to be the A_{1g} vibrational mode of the diamond-like carbon sp_3 electronic structure. The peak at around 1592.57 cm^{-1} was considered to be the E_{2g} vibrational mode of the sp_2 electronic structure of graphitic carbon.

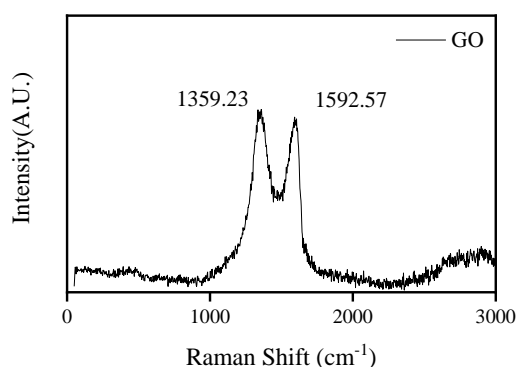


Fig. 3.49 –Raman diagram of GO gel coating.

In Fig. 3.50, the GO-free coating (Na_2SiO_3) was shown. There were no peaks of the two features evident in its Raman diagram. Therefore, there were different compositions contained in the matrix and the GO gel coating. As can be seen in Fig. 3.47, graphene oxide was clearly present in this coating.

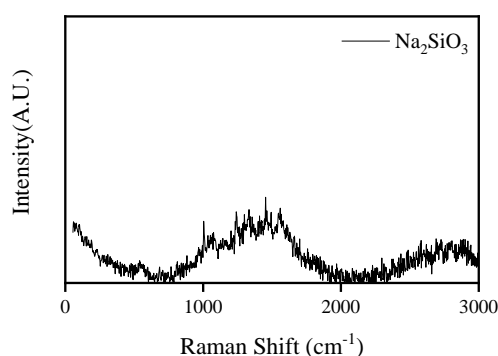


Fig. 3.50 – Raman diagram of gel coatings (Na_2SiO_3)

3.5.4 Abrasion resistance analysis of GO gel coating

(1) Coefficient of friction

The comparison of the wear resistance of GO gel coating, gel coating (Na_2SiO_3), SKH51+GO coating, and gel graphite coating was carried out. The deposition process of GO gel coating was to mix graphene oxide suspension and Na_2SiO_3 gel, which was coated on 25*30mm size 45 steel sheet and sintered at 80 °C. The deposition process of gel graphite coating was to mix graphite powder

and Na_2SiO_3 gel at a mass ratio of 1:1, which was also coated on 25*30mm size 45 steel sheet and sinter it at 80 °C. In the same way, the gel coating was to paint Na_2SiO_3 gel on a 25*30mm size 45 steel sheet and sintered at 80 °C. As for SKH51+GO coating, SKH51 material was first coated on the surface of 45 steel by ESD process, and the GO gel coating was allowed to be applied afterwards.

The abrasion resistance of the coated surfaces was performed with the linear reciprocating friction wear machine MWF-500. The sample surface was gently rubbed by anhydrous ethanol. The friction machine used 6 mm size ZrO_2 friction balls with a surface accuracy of G10 as a counter grinding material, and used a stable pressure of 30N. The motor speed of the equipment was 100r/min, the reciprocating distance was 6mm, and the motor performed 2 movements per revolution. The experiment time was 10 minutes, and the surface dry friction experiment was carried out. Dry friction experiments were carried out on GO gel coating, gel coating (Na_2SiO_3), SKH51+GO coating, and gel graphite coating respectively, and the results are shown in Fig. 3.51. The gel-graphite coating was found to have the lowest coefficient of friction, followed by the GO gel-coat. Due to the roughness of the surface of SKH51, the coefficient of friction of SKH51+GO composite coating was slightly larger than that of GO gel coating. The gel coatings have the highest coefficient of friction. It showed that GO material played the role of reducing the coefficient of friction and friction force.

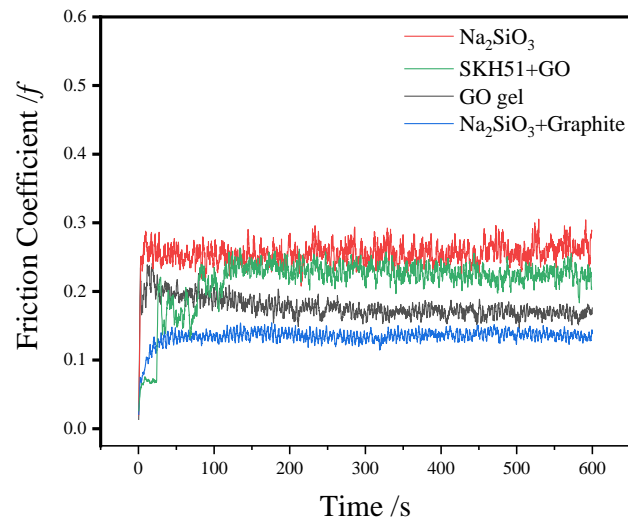


Fig. 3.51 –Friction coefficients of four composite coatings

(2) Abrasion mark width

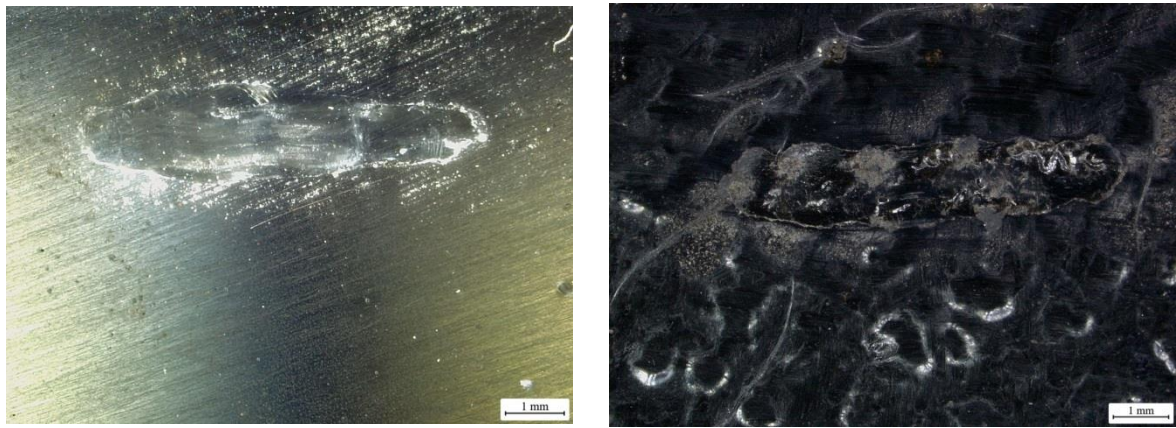
The maximum width of the abrasion marks was measured by using a super depth-of-field microscope (Leica Co., DVM6), as shown in Fig. 3.52. Because of the roughness of the coating surface, the abrasion marks were not uniform, and whose friction force and coefficient of friction cannot truly reflect the degree of abrasion resistance. The maximum width and standard deviation of the abrasion marks were used to reflect the wear resistance of the material. For each sample, experiments were carried out to separately measure the average value of equidistant abrasion marks and to calculate the standard deviation.



(a)



(b)



(c)

(d)

Fig. 3.52 – Coating abrasion morphology: a- $\text{Na}_2\text{SiO}_3+\text{C}$; b- $\text{Na}_2\text{SiO}_3+\text{GO}$;
c- Na_2SiO_3 ; d-SKH51+GO.

Measurement of the maximum width of the abrasion mark was performed with a super depth-of-field microscope. The appropriate light mode was selected. When the abrasion marks were shown most clearly, the measurement was carried out. Six sets of data from the middle section of the scratches were taken separately, averages were calculated and standard deviations were obtained. It can be seen from Fig. 3.53 that the graphene oxide coating deposited on the substrate No. 45 steel had the smallest wear scar, with an average width of $1283\mu\text{m}$ and a standard deviation of $43\mu\text{m}$. The GO gel coating on the surface of SKH51, and the wear scar of the coating was second, with an average width of $1378\mu\text{m}$ and a standard deviation of $150\mu\text{m}$. The gel coating deposited (Na_2SiO_3) on the substrate No. 45 steel had an average wear scar width of $1416\mu\text{m}$ and a variance of $234\mu\text{m}$. Adding graphite powder to Na_2SiO_3 gel, the graphite gel coating had the widest wear scar of the coating.

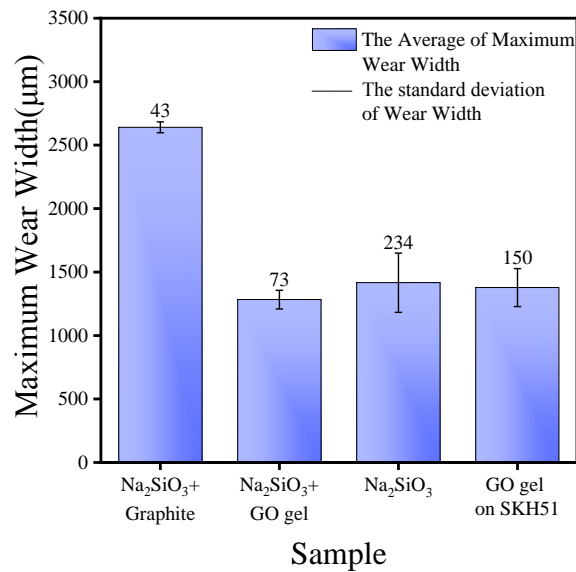


Fig. 3.53 – Average wear scar and standard deviation of coating

Although graphite had certain lubricity, the coating had poor wear resistance. It showed that the smaller graphene oxide particle coating had the smallest wear scar width, which can improve the performance of gel coating and improve its wear resistance. Even if the surface roughness of the substrate material was large, it can reduce friction and improve wear resistance.

3.5.5 Scratch bonding force of GO gel coating

In order to investigate the bonding of GO coating and substrate, scratch tests (RSX, Anton Paar) were performed [194-196]. A 200μm ball diamond indenter was selected, and 3 sets of experiments were performed on the coated surface in the 0~50N test interval. From the test results of friction test results and acoustic emission signals, it can be judged that the bonding force was 17.11 N, as shown in Fig. 3.54. The results of the three tests showed that the coating bonding strength was 16.57~20.35N, and the average value was 18.01N, as shown in Table 3.28. As shown in Fig. 3.55, it can be seen from the morphology diagram that the launch of

the coating will peel off after 3 mm from the initial point of the scratch, which corresponded to Table 3.28. This binding force can ensure the normal combination of the coating and the base material in the friction and wear test. In the industry, the bonding force was used to reflect the quality of the coating bonding. If it was based on Young's modulus, Poisson's ratio, and bonding force, the coating contact stress can be calculated. The calculated contact stress results had large errors. Therefore, the binding force is based on the actual applied force of the indenter.

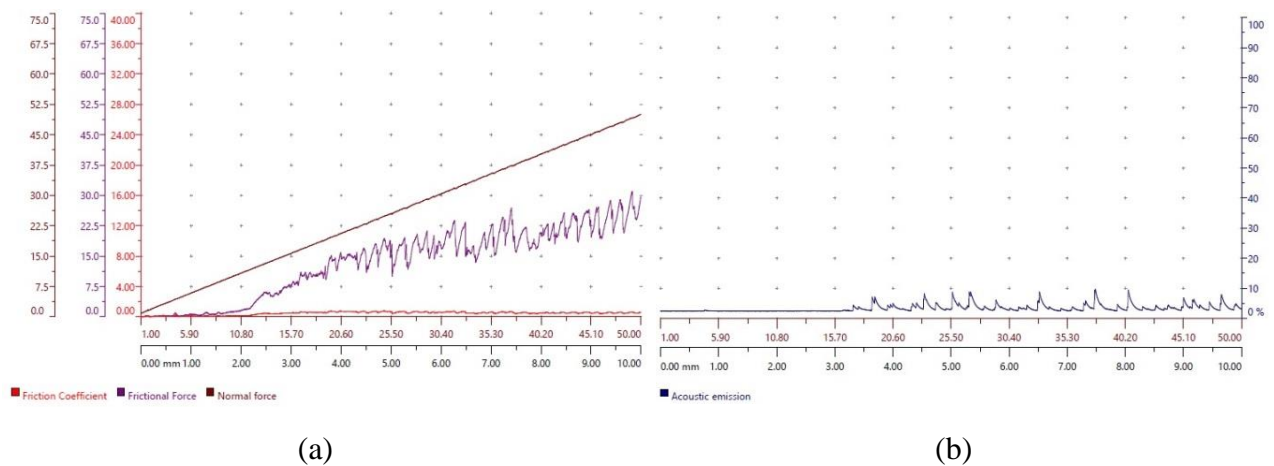


Fig. 3.54 –GO coating scratch experiment: a-Friction force and friction coefficient;b-Acoustic emission

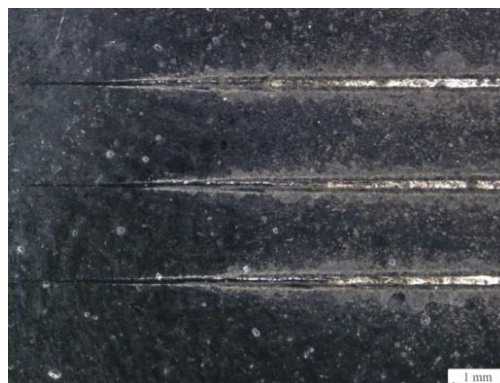


Fig. 3.55 – Scratch morphology of GO gel coating

Table 3.28 – Scratch bonding force of GO gel coating

1	2	3	Average value
17.11 N	16.57 N	20.35 N	18.01 N

3.5.6 GO gel coating conclusion

Graphene oxide gel coating can effectively improve the surface quality of the coating and has a small roughness. In the ESD process, the surface quality was not high due to the unstable electric energy. How to improve the surface quality of ESD had become an industry challenge in the ESD process. Traditionally, it was processed with a grinding machine. Its production efficiency was low, the coating thickness was not easy to control, and the product performance was not uniform. The use of ultrasonic processing was also a research hotspot. The surface quality of ultrasonic deposition was not high, and many ultrasonic equipment processing parameters need to be adjusted. And, when some coatings were relatively hard and the surface hardness is uneven, the surface defects after processing were relatively large. At present, this research is still in the laboratory, and the industry has not yet used it. The use of nanomaterials is a brand new research, which can modify the surface of ESD. It is low in cost, very effective in improving surface quality, and easily recognized by the industry. Through the research on the performance of GO gel coating, it was found that the friction coefficient was 0.17, the grinding width was 1283.02 μm , the surface quality was the lowest, and the bonding force was 16.57~20.35N.

3.6 Summary

This chapter is centered on increasing surface wear resistance coatings gradually. Tests were carried out which utilized respectively carbide, HSS, composite coating and other coating processes. A new deposition process to enhance surface quality was improved for low temperature soft metals. Continuous deposition can be carried out with pneumatic impact deposition and RC low-energy circuit. Considering graphite powder for lubrication, it was easy to fall off. so self-lubrication coating was utilized. Due to graphite and sodium silicate composite coating, wear resistance was poor. A nano self-lubricating coating was proposed, which was graphene oxide gel coating.

(1) The metal surface was easily carbonized by the graphite electrode, which can improve the wear resistance of the material surface. The high-speed ESD repair machine (HMT9500) was selected for the deposition. According to the Abrasion width, the Taguchi orthogonal method was used to find the best process for graphite deposition. Optimal process parameters for surface carbonization deposit were that efficiency 50%, voltage 35v, current frequency 180Hz and work time 360s. As a result, the average value of the abrasion width was 268.206 μm , and the depth of abrasion was 2.999 μm . It was 59.96% less wide than 45 steel. It had good wear resistance.

(2) The deposition experiment of SKH51 coating on the surface of 45 steel was carried out by electric spark. Orthogonal experimental design was used to discuss the effect of the deposition parameters on coating quality, average coating thickness, average width of maximum abrasion marks, average roughness, and

Vickers hardness according to respectively. Coating properties were analyzed from the transition layer. The weighting factor was determined according to the coating performance parameters, and the optimal coating deposition process parameters were obtained by using the normalization method and the weight factor method to evaluate the coating performance parameters. The maximum value of the objective function was 0.687887. The optimum process parameters were current frequency 300Hz, voltage 44v, efficiency 30%, rotate speed 150 r/min.

(3) Through composite coating design, the performance of the coating can be improved. Composite coating can achieve multiple functions such as wear resistance, friction reduction, corrosion resistance, etc. Using the composite coating SKH51+ WC+B83, the value of the coating had gradient wear resistance, SKH51 had a better shape and lower roughness, and its Ra was 1.086 μm . Among them, the WC coating had the best wear resistance among all the schemes, and the abrasion width was 586.12 μm . B83 coating had a very stable friction coefficient of 0.12, which was 48% lower than that of WC coating. The surface of the in-situ reaction coating produced higher hardness TiC, ZrC, and NbC, which effectively improved the wear resistance of the surface coating. Because of the deposition process, the amount of carbide generation on the surface was less than that of WC coating, and the wear resistance was worse than that of WC coating. However, the surface friction coefficient was lower, which can reduce the friction of the coating.

(4) Soft low-temperature metal ESD deposition used RC discharge circuit and gas vibration processing technology to obtain better surface quality. A smaller discharge capacitor can reduce the discharge energy and control the discharge

energy. The electrode did not need to be cooled for a long period of time and could be deposited continuously. When the discharge energy was greater than the melting energy, the ESD coating would be able to deposit. When the discharge energy was less than the melting energy, the electrode did reciprocating friction on the deposited surface. In the process, the air pressure is in the range of 0.45-0.62MPa, the proper distance of the electrode was guaranteed, and the handle knob was opened to the maximum, it can generate a stable vibration frequency of 310~350hz. The pneumatic impact is more stable, and a better deposition effect can be obtained.

(5) Graphene oxide and sodium silicate gel coating can effectively improve the surface quality of the coating with less roughness. It is a new research to modify the surface of ESD with nanomaterials. It was low in cost, very effective in improving surface quality, and easily recognized by the industry. Through the research on the performance of graphene oxide gel, it is found that the friction coefficient was 0.17, the grinding width was 1283.02 μm , the surface quality was the lowest, and the bonding force was 16.57~20.35N.

CHAPTER 4. INDUSTRIAL APPLICATIONS OF COMPOSITE COATINGS

4.1 Industrial background

Wear and tear cannot be avoided. Any mechanical device has a lifespan. The life of machinery is extended by remanufacturing. Remanufacturing is an advanced form of reuse in the circular economy advocated by industry. The scope of remanufacturing processes can be classified into restorative remanufacturing and upgraded remanufacturing. In industrial production, enterprises put forward higher requirements for industrial equipment to extend the life of core components and improve product performance. Surface processing technologies are important means of remanufacturing process. Since the surface engineering was limited by the original processing technology and material, it could not be emphasized by the enterprises. With the emergence of new materials, new processes and new technologies, more and more companies paid attention to surface repair. Through the repair of some key parts, it can match the overall requirements of the equipment. The output value of the global remanufacturing industry has exceeded 100 billion US dollars. The United States and the European Union attach great importance to the remanufacturing industry, and their related products in the field of construction machinery and automobiles account for a large proportion of the world. Remanufacturing has become a new direction for the future development of machinery manufacturing industry.

In February 2013, the Southeast automobile company took the lead in proposing a "battery quick-change model" based on chassis battery replacement. In

2015, new energy electric vehicle company took the lead in producing this kind of electric vehicles and put them into taxi operation. The battery was an important component, accounting for more than 60% of the total cost. One year later, there were a small number of problems with the sliding pin shaft locking mechanism of battery boxes. At that time, the company did not pay attention to it, thinking that it was a problem with the processing technology of the battery box. It was only the replacement of the failed parts. But, the problem recurred after a year. The maintenance workload of workers had increased rapidly. Even after the failure of the orifice plate, the original battery box needs to be replaced. These problems led to much higher maintenance costs. Company paid attention to this issue. Therefore, it hoped to find a relatively low-cost and quick maintenance method, which can ensure the super-long service life and high reliability of the locking mechanism.

4.2 Problem description

The chassis quick-change battery box was fixed by the locking mechanism. When the battery box was lifted up by the lifting device, the pin shaft of the locking member was pulled by the square push block to move, and the locking mechanism was opened, as shown in Fig. 4.1. The surface of the pin shaft underwent reciprocating sliding friction. After a long time, it caused surface wear. After one year of use, some automatic locking devices failed to return normally. Through a large number of failed battery box investigations, the friction between the pin shaft and the orifice plate led to out-of-tolerance dimensions and the fit deterioration. Furthermore, the surface roughness becomed larger, and the frictional force increased. The failure modes of the parts mainly include extrusion

deformation and failure of the pin shaft to rebound, as shown in Fig. 4.2. In the use of electro-galvanized coating process or lubricant method, the problem had not been fundamentally improved. After 2 months, the problem reappeared. Therefore, according to the requirements of the company, the remanufacturing design and repair of the pin shaft locking mechanism were carried out.



Fig. 4.1 – Chassis Replacement Battery Box: a - Replacement Battery Box ;
b - Replacement Equipment

Since the equipment was in an open environment, lubricants and greases were not effective. Dry friction occurred on the surface of the pin shaft, the surface wear mechanism is adhesive wear, abrasive wear, and corrosive wear after the zinc coating wear. The battery shell was made of 20g or q235 material, the orifice plate and the pin shaft were made of 45 steel materials.

It can be seen from Fig. 4.3 that the pin shaft cannot rebound, it was found that the galvanized layer on the surface of the sliding pin was corroded due to wear. In the initial state of corrosion (Fig. 4.3a), it can be seen that the corrosion spreads outward from the galvanized layer. With the accumulation of time, the surface of the pin shaft was completely corroded, as shown in Fig. 4.3b. After being corroded,

the surface quality was reduced after repeated wear in Fig. 4.3c. In the second stage, it appeared that the pin could not rebound properly. According

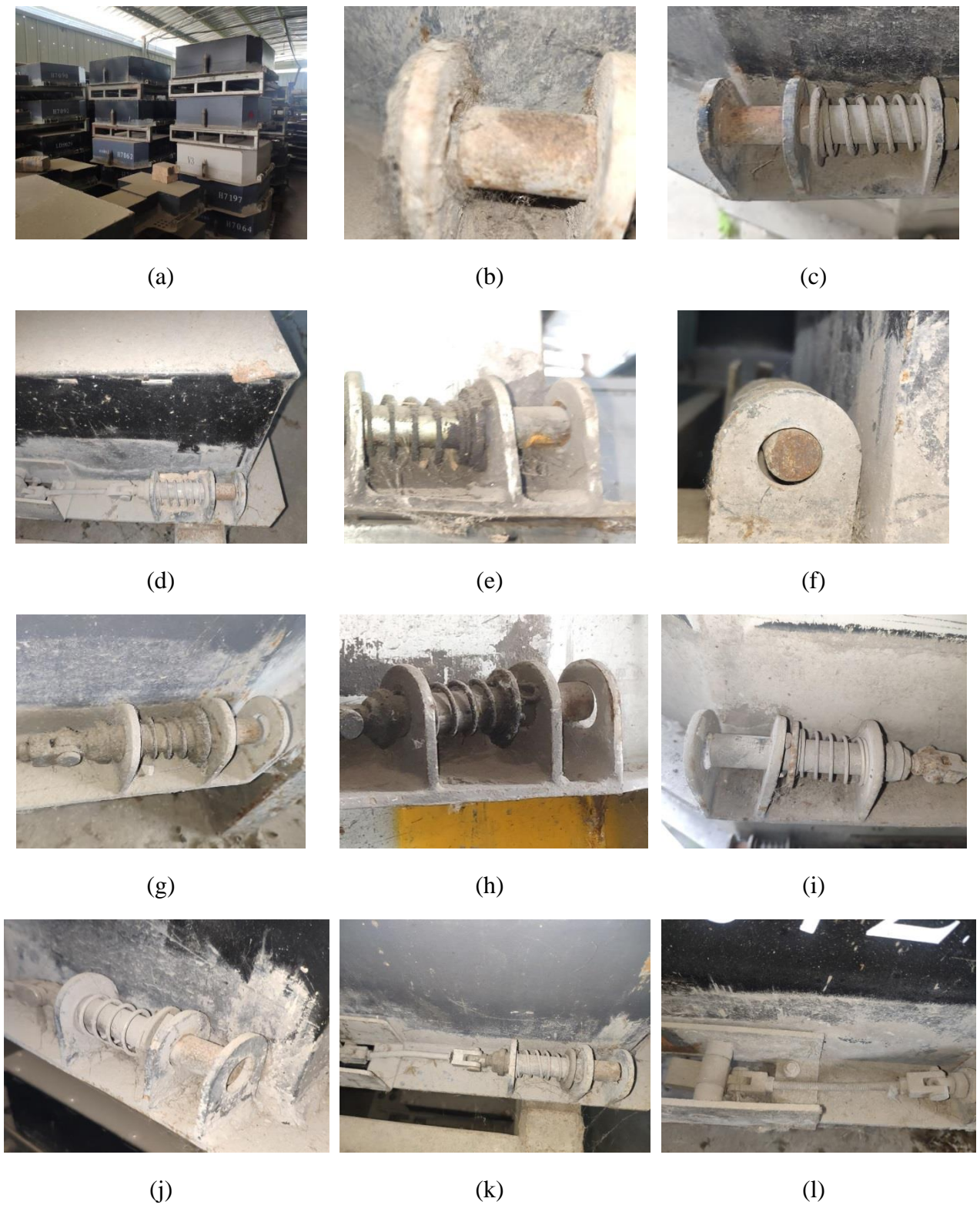


Fig. 4.2 – The failed battery box and the lock mechanism corrosion wear: a-the failed battery boxes; **Wear:** b- wear 1; c- wear 2; d- wear 3; e- wear 4; f- wear 5; **Out of tolerance leads to deformation:** g- extrusion deformation 1; h- extrusion

deformation 2;i- extrusion deformation 3;j- extrusion deformation 4;k- extrusion deformation 5;l- extrusion deformation 6.

to the design requirements, the replacement battery box has no failure within 8 years. Therefore, it is positive to increase the wear resistance of the pin shafts. However, if the spring stiffness was increased, the battery box structure would need to be redesigned. Otherwise, the use of larger stiffness springs cannot be installed manually. These two methods make it difficult for companies to accept this solution.

Therefore, the repair solution of the sliding pin shaft of the lock mechanism was proposed.

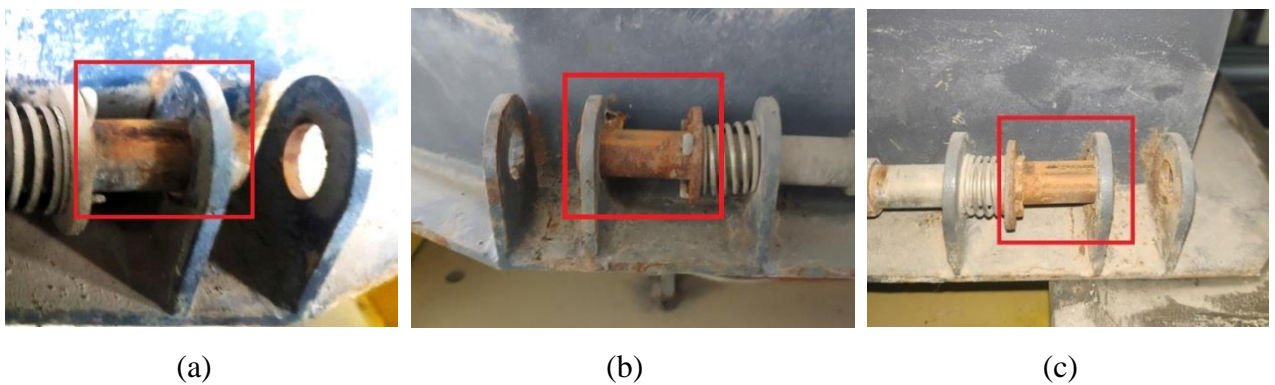


Fig. 4.3 – Three stages of pin shaft corrosion wear: a- initial wear; b- full-scale corrosion; c- wear after corrosion.

4.3 Analysis of experimental causes

The pin shaft did not rebound properly, mainly because the surface corrosion increased, which resulted in an increase in friction. 45 steel that was the same material as the pin shaft, was selected as the sample. The samples were corroded in water for 14 days, and placed in humidity air for oxidation for more than two months, and the thickness of the oxide layer increased. The thickness of the oxide layer was $27.5\mu\text{m}$ to $55.5\mu\text{m}$, as shown in Fig. 4.4. No.45 steel plates of surface corrosion were used as laboratory objects, and 6mm size of ZrO_2 friction balls

which had a surface accuracy of G10 were used as counter grinding materials. After the pre-test found that, at the beginning of the test, the maximum coefficient of friction f reached 0.7982 in Fig. 4.5. At this time, the pressure was 14.43 N. It showed that the surface corrosion increased surface friction, which was the main reason for the inability to enter into the hole. Because the galvanized coating of round pins was not sufficiently abrasion-resistant, the surface abrasion was caused, which further increased the progress of corrosion. Therefore, the surface wear resistance should be firstly improved, and then the wear resistance after corrosion should be considered secondly.



Fig. 4.4 – Surface corrosion morphology of 45 steel

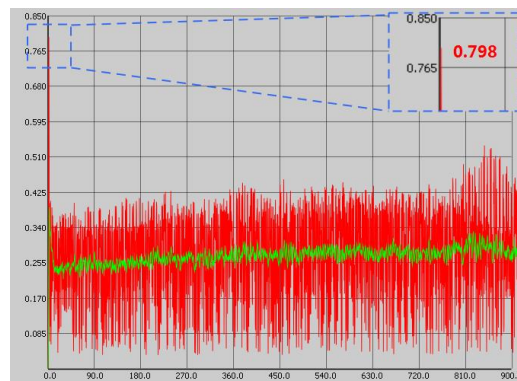


Fig. 4.5 – Corrosion morphology of 45 steel

4.4 Design of the replacement battery box

4.4.1 Basic theory of static analysis

Static analysis involves statics and mechanics of materials. Statics is an important branch of rigid body mechanics, which does not consider the mechanics

of large deformation and plastic changes of parts. It constitutes rigid body mechanics together with kinematics and dynamics. It was first proposed by Varignon in 1725. Static mechanics has a wide range of applications in engineering and technology. Mechanics of materials is the study of the mechanical properties of various parts structures under the selection of materials. The Italian scientist Galileo first proposed the mechanics of materials. Linear calculations were performed on materials under the continuity assumption, the homogeneity assumption and the isotropy assumption. In mechanics of materials, its strength theory is relatively well developed. For example, maximum tensile stress theory, strain theory, maximum shear stress theory and shape change energy density theory. These theories have been widely used in industry.

4.4.2 Modelling of the battery box

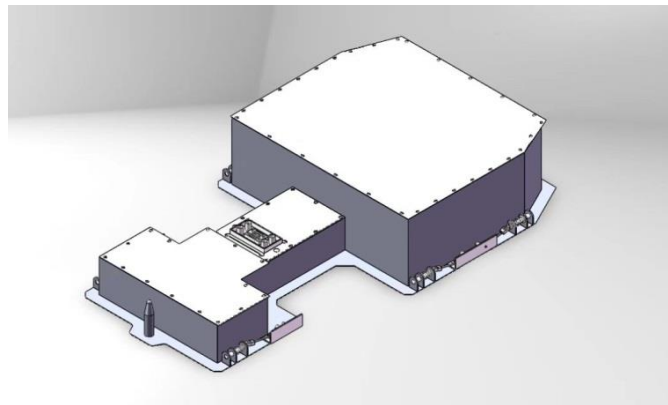


Fig. 4.6 – 3D structural diagram of the battery box

The battery box should be simplified to arrive at a reasonable structure, which was the key to this design. In the beginning period of the project, the battery box was modeled separately by Ansys Workbench software. In the later stage of the optimized structural design, feature points could not be extracted and parametric structural design could not be carried out. Sequential step-by-step

derivation of experimental data can only be carried out by modification of individual parameters. Therefore, three-dimensional modeling software was used to model the battery box. The battery box was assembled to parameterize the structure, as shown in Fig. 4.6.

4.4.3 Strength calculation of pin shafts

When the structural strength of the battery case was calculated, the calculation was based on the first strength theory[197]. The data can be obtained by measuring the battery box. The inside of the battery box was composed of two parts of the battery, the first part was the front small battery pack, and the second part was the rear main battery pack. The overall mass of the battery box containing batteries was about 230kg. The mass of the battery in the front small box was 18kg, the mass of the battery in the rear large box was 186kg, and the weight of the battery box and other accessories was 26kg.

$$S_1 = a_1 \times b_1 = 0.299 \times 0.159 = 0.047541\text{m}^2 \quad (4.1)$$

In Equation (4.1): S_1 -the contact area of the small box of the battery box; a_1 - the length of the battery box front cell; b_1 -the width of the cell at the front of the battery box.

The normal stress on the front small battery box is:

$$\sigma_1 = \frac{G_1}{S_1} = \frac{18 \times 9.8 \times 10^3}{0.047541} = 3.71 \times 10^7 \text{ Pa} \quad (4.2)$$

In Equation (4.2): σ_1 —the stress on the battery at the front of the battery box; G_1 —Gravity on the battery at the front of the battery box.

According to the value of the required stress of the commonly used materials in engineering, the permissible axial compressive stress of low alloy steel is obtained as follows : $[\sigma]=230MPa$. Therefore, $\sigma_1 \leq [\sigma]$ can be obtained, and the small front box meets the strength requirements.

$$S_2 = a_2 \times b_2 = 0.364 \times 0.307 = 0.111748m^2 \quad (4.3)$$

In Equation (4.3): S_2 - Rear large box floor area; a_2 -Length of the rear big box body; b_2 -Width of the rear big box body.

The normal stress on the rear large box is:

$$\sigma_2 = \frac{G_2}{S_2} = \frac{186 \times 9.8 \times 10^3}{0.111748} = 1.63 \times 10^7 Pa \quad (4.4)$$

In Equation (4.4): σ_2 - Stresses on the rear of the battery box; G_2 - Gravity force on the rear of the battery box.

According to the required stress value of the engineering materials consulted, the allowable axial compressive stress of the low alloy steel is $[\sigma]=230MPa$. Thus it can be obtained that $\sigma_2 \leq [\sigma]$, the large rear box meets the strength requirements.

The stress on the pin shaft is:

$$\tau = \frac{G/n}{S} = \frac{230 \times 9.8 / 6}{(14.5 / 2 \times 10^{-3})^2 \pi} = 2.276 MPa \leq [\tau] = \frac{350}{2.5} = 130 MPa \quad (4.5)$$

In Equation (4.5): n - the number of pin shaft on the battery; G - gravity of battery at the front of the battery box; S - Shear area of the pin shaft.

The battery box gravity is considered according to the dynamic load, and the stress of the pin shaft is:

$$\tau = \frac{G/n}{S} = \frac{230 \times 9.8 / 6}{(14.5 / 2 \times 10^{-3})^2 \pi} = 2.276 MPa \leq [\tau] = \frac{350}{3.5 \sim 5} = 70 \sim 100 MPa \quad (4.6)$$

As shown in Equation (4.6), strength meets requirements. There are no defects in the design strength of battery box.

4.5 Coating solutions of the pin shaft

If the pin shaft is replaced with a wear-resistant material, such as stainless steel, the manufacturing cost will increase by more than 5 times during the processing, as shown in Fig. 4.7. These difficult-to-machine materials have higher requirements on the cutting tool, and the delivery time is longer when there are not many orders. Instead, the remanufacturing method was used. The original galvanized coating process was removed and the composite coating was reasonably selected, which reduced costs and extended the life of the equipment. It reduced the pollution caused by electroplating and realized green processing.

Composite coating was designed to reduce wear. According to the previous composite coating design scheme, and the pin shafts were deposited according to the experimental scheme, as shown in Table 4.1. The common material of 45 steel was selected for the pin shafts. Scheme 1, SKH51 coating was used as a protective layer to increase the surface wear resistance and impact toughness. Scheme 2, SKH51 coating was used as the bottom layer and WC coating was used as the top layer, WC had better abrasion resistance and formed a gradient coating to increase the abrasion resistance of the SKH51 coating. Scheme 3, SKH51 coating was used as the bottom layer, WC coating was used as the middle layer, and B83 anti-friction material was selected to increase the coating thickness in order to reduce the surface roughness. Scheme 4, SKH51 coating was used as the base layer, and graphene oxide and sodium silicate were deposited on the coating to form GO

gel coating, which meant that it can improve the surface quality, reduce the effect of friction on the coating, and improve the corrosion resistance. Silicate is not only a good adhesive, but also inhibits the corrosion of steel and the corrosion of non-ferrous metals, which are aluminum, copper and their alloys. Silicates are effective in preventing the attack of chloride ions.

Table 4.1 – Industrial Coating Scheme

Scheme	Coating	Number of Coating Layers
1	SKH51	1
2	SKH51+WC	2
3	SKH51+WC+B83	3
4	SKH51+GO	2

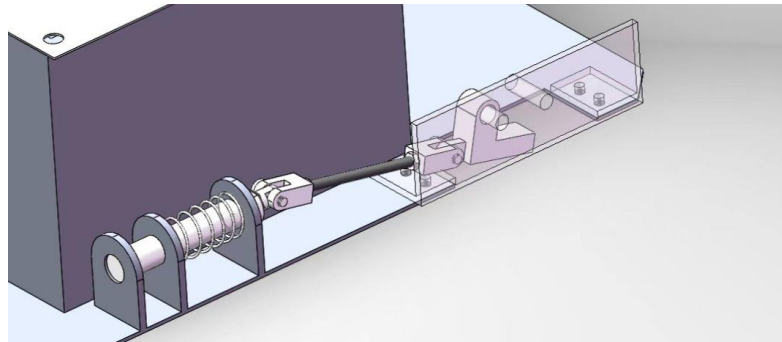


Fig. 4.7 – Pin shaft assembly diagram

The surface was polished with No. 240, No. 400 and No. 600 sandpaper respectively, and the surface was cleaned with anhydrous alcohol. A high-speed ESD repair machine HMT9500 (Shengzao Co., Ltd., China) was used to deposit the coating on the pin shaft surface using 2.5mm SKH51 rod as the electrode. Argon gas (15Mpa) was used as the protective gas on the deposited surface of the pin shaft. The pin shaft was fixed, and the inline oblique line deposition process was repeatedly done on the surface. The deposition parameters were taken as the optimum parameters above in section 3.4. The multilayer coating deposition was

carried out separately, as shown in Table 4.2. For scheme 1 and scheme 4, the full coverage of the coating was carried out. Semi-coverage coating was selected for scheme 2 and scheme 3. For scheme 1 and scheme 4, the full coverage of the coating was carried out. Semi-coverage coating was selected for scheme 2 and scheme 3. Among them, B83 coating adopted micro-capacitor and pneumatic impact for surface deposition, which had obtained a better surface quality. The GO gel material was mechanically stirred, and then the SKH51 coated surface was coated by the dropper, and which was suspended in a drying and heating chamber for baking at a certain temperature for 120 minutes. Because GO gel was easy to flow on the pin shafts, a secondary coating was applied after the surface was dry and then the coating was baked.

Table 4.2 – Coating deposition morphology of the pin shaft

Scheme	Coating	Coating deposition morphology
1	SKH51	
2	SKH51+ WC	
3	SKH51+ WC+B8 3	

4 SKH51+
GO



In order to avoid corrosion expansion, and the wear between the spring and the washer was reduced. Electro-spark carburizing of the gasket were carried out. Deposition of Ti lay and graphite layer were carried out respectively in Table 4.3. In terms of rust prevention, Ti and graphite double-layer coating was better than pure graphite coating. Moreover, Ti coating had better corrosion resistance. In-situ reaction generates TiC material, which can increase the wear resistance of Ti coating to a certain extent.

Table 4.3 – Coating deposition morphology of the gasket

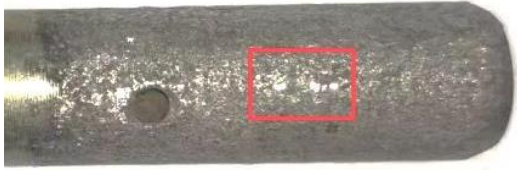
Scheme	Coating	Coating layer	Coating deposition morphology
1	carburisation	1	
2	Ti+ carburisation	2	

4.6 Abrasion resistance test

After 500 times of battery replacement experiments, it was found from the worn surface, as shown in Table 4.4. For scheme 1, the area of the wear scar was larger at the front end of the pin shaft due to the SKH51 on the curved surface.

Scheme 1, SKH51 coating was deposited on the curved surface, the area of the abrasion spot was larger in the front of the pin shaft. Scheme 2, it adopted SKH51+WC double coating process, there was no wear spot on the surface of the pin shaft, only slight scratches. The wear resistance was improved significantly. Scheme 3, the SKH51+WC+B83 three-coating process was used, there were small wear spots on the shiny surface without scratches, which showed that B83 has a good anti-friction effect. Scheme 4: the SKH51 and GO double-coating process was used, scratches appeared on the working surface of the pin shaft, and there were flakes of coating peeling off at the end of the pin shaft, mainly because the deposited coating was too thin. The impact caused peeling off at the chamfer of the pin shaft, which indicated that the coating had poor impact resistance. By comparison, SKH51, Go double-coating process was adopted with lower cost and better anti-corrosion effect, but the impact resistance was poor.

Table 4.4 – Wear morphology of pin shaft surface

Scheme	Coating	Wear morphology
1	SKH51	
2	SKH51 +WC	
3	SKH51 +WC+B 83	



In terms of wear morphology, SKH51+WC+B83 coating had the best wear resistance and friction reduction effects, and B83 coating had the best anticorrosion performance. Therefore, it was recommended that enterprises adopted the SKH51+WC+B83 scheme.

As can be seen from Table 4.5, the original programme cost of 8480 hryvnia according to a car for four years, the coating with argon protection was reduced to 2940 hryvnia, and without argon protection was reduced to 2400 hryvnia, which can save the company 5540~6080 hryvnia. The company has 83 electric taxis in operation. It can save 460,000 hryvnia in four years. Annual savings will be 115,000 hryvnia.

Table 4.5 – Evaluation of Coating Cost Savings per vehicle

Material	Number of pin shafts	Price of the pin shaft kit (UAH)	service life (year)	Maintenance (UAH)	Total(UAH)	Single year cost(UAH)
45 steel	6	280	1.5	1500	3180	2120
304 stainless steel	6	1500	4		9000	2250
45steel+ SKH51+GO coatings	6	355	2	1500	3630	1815
45 steel + SKH51+WC+B83 (No argon gas)	6	400	4		2400	600
45 steel+ SKH51+WC+B83 (Argon gas protection)	6	490	4		2940	735

4.7 Technical suggestions

The coating of the pin shaft of the replaceable battery box directly affected the normal operation. Reasonable coating deposition process was the guarantee of coating quality. The functional design of the coating is the guarantee of the performance. Composite coating has better multi-purpose. But, because the coating deposition time is long, it may be changed from full coating to partial coating to reduce the processing time and processing cost, which can improve the production efficiency.

(1) It is recommended that enterprises replace the electroplating coated zinc coating and choose the more environmentally friendly ESD deposition coating. The coating quality of the pin shaft directly affects the service life. Before the deposition process, attention should be paid to the removal of oil stains on the surface of the pin shaft for acid selection, and grinding of oxidized skin. Suitable surface roughness helps the implementation of the deposition.

(2) Composite coating can always meet a variety of use requirements, according to the needs of industry to choose a reasonable coating structure. The number of coating layers should not be too many, generally no more than three layers.

(3) Since the ESD coating have the defects, and the coating is not continuous, Coating deposition of higher quality process was reasonable selected, which reduces the surface roughness and reduces the friction.

(4) In the working process due to the pin is curved surface, too high argon gas pressure cannot play a good and effective protective effect. The protective gas pressure can be reduced appropriately to prevent the surface from being oxidized.

(5) ESD is combined with a variety of processes. It can effectively reduce the cost of coating, which is an effective way for industrial application. Through the application of graphene oxide gel coatings, the surface roughness can be reduced, and the manufacturing cost can be effectively reduced. which is also a hot spot that the industry will pay attention in the future.

4.8 Summary

This chapter briefly introduces the application of the ESD process in the battery-swapping electric vehicle industry, summarizes and analyzes the test results of the four coating schemes, and determines the best industrial application scheme according to the field wear resistance test. For part of the automatic locking device normal cannot return to the position, the composite coating solution was proposed on the pin shaft, which meet the requirements of abrasion resistance, but also had a smaller friction, but also had a certain degree of corrosion resistance. This solution was composed of three coatings: SKH51 coating, WC coating and B83 coating. It can effectively reduce the cost of plating, reduce the pollution of the plating process and achieve a long life expectancy of the parts. This method is cheap, easy to operate and easy to maintain, and which is recognized by enterprises. This is expected to help the enterprise save 115,000 UAH every year.

CONCLUSIONS

On the basis of the obtained results and their interpretation, the following conclusions can be drawn:

1. When using Taguchi's orthogonal method, according to the abrasion width, the optimal parameters of the surface carburizing process of steel 45 have been set: the efficiency of 50%, the voltage of 35 V, the current frequency of 180 Hz, and the operating time of 360 s. As a result, the average wear width was 268.206 μm , and the wear depth was 2.999 μm , which is 59.96% less than for steel 45 without carburizing.

2. Using the method of normalization and the method of weighting coefficients to estimate the operating parameters of the coating at the maximum value of the objective function of 0.687887, the optimal parameters of the process of electro-spark deposition of the SKH51 coating on the surface of steel 45, namely, the current frequency of 300 Hz, the voltage of 44 V, the efficiency of 30%, and the rotation speed of 150 rpm have been determined.

3. While comparing the composite coatings of different composition, as an optimal solution, there has been recognized the composite coating formed according to the scheme of SKH51+WC+B83. With the gradient coating of SKH51+ WC, the value of the coating had a gradient wear resistance, the coating of SKH51 had a better morphology and lower roughness ($R_a = 1,086 \mu\text{m}$.) The WC coating had the best wear resistance among all the schemes, and the wear width was 586.12 μm . The B83 coating had a very stable friction coefficient of 0.12, which was 48% lower than that of the WC coating.

Coating SKH 51+ WC+B83 has a good wear resistance and low coefficient of friction, long service life and high reliability. Since the material of B83 is the outer layer of the composite coating of SKH51+ WC+B83, the wear mechanism of the optimal coating is mainly plastic deformation accompanied by slightly polishing.

4. To obtain a better surface quality when providing for a deposition of a soft low-temperature metal by the ESD method, it is necessary to use an RC-discharge circuit and the technology of gas-vibration processing, which makes it possible to control the discharge energy, not to cool the electrode for a long period of time, and to carry out a continuous process of applying a deposition. When the discharge energy is getting greater than the melting energy, the ESD coating would be able to deposit. When the discharge energy is getting less than the melting energy, the electrode performs reciprocating friction on the deposited surface. While processing, the air pressure is in the range of 0.45~0.62MPa, the proper distance of the electrode is to be guaranteed. In this case, a stable vibration frequency is of 310~350 Hz. The pneumatic impact is more stable, and a better deposition effect can be obtained. The mechanism of pneumatic deposition is to control energy through the number of impact discharges per unit time, which reduces the traditional electrode impact force and reduces the deformation of the low-temperature soft metal electrodes. In such a manner, it can enhance the quality of the surface deposition.

5. Graphene oxide gel coating can reduce coating friction and surface roughness. It has a certain wear resistance. It is a new research to modify the

surface of ESD coatings with Nano-materials. It was low in cost, very effective in improving surface quality, and easily recognized by the industry. Through the research on the performance of graphene oxide gel, it has been found that the friction coefficient is 0.17, the grinding width is 1283.02 μ m, the surface quality is the lowest, and the bonding force is of 16.57~20.35N.

6. The ESD process has been applied in the automotive industry to discharge batteries of electric vehicles. Since some locking devices cannot return normally, a solution of SKH51+WC+B83 composite coating on the pin shaft surface of the locking mechanism for the lifting device of a battery for an electric car was proposed. It can effectively reduce costs, reduce pollution during the electro-spark deposition coating process and to ensure a long service life of the remanufactured parts. This method is cheap, easy to operate and easy to maintain, and it is recognized by enterprises. This is expected to save the company 115,000 UAH per year.

REFERENCES

- [1] P. Dašić, F. Franek, E. Assenova, and M. Radovanović, "International standardization and organizations in the field of tribology," *Industrial Lubrication Tribology International*, vol. 55, no. 6, pp. 287-291, 2003.
- [2] H. P. Jost, "Tribology micro & macro economics: A road to economic savings," *Tribology Lubrication Technology*, vol. 61, no. 10, pp. 18-22, 2005.

- [3] L. Jianbin, "Investigation on the origin of friction and superlubricity," *Science Bulletin*, vol. 65, no. 27, p. 13, 2020.
- [4] H. Shuodong, "On-site repair technology for 660MW turbogenerator rotor journal damage," (in Chinese), *China Equipment Engineering*, no. 012, pp. 76-78, 2022.
- [5] L. Yanpeng, "Remanufacturing and fatigue life prediction of large turbogenerator rotor shafts," Master, North University of China, 2020.
- [6] Z. Yushuan, "Application of surfacing welding deposition repair technology in maintenance," (in Chinese), *China Metal Bulletin*, no. 7, p. 197+199, 2019.
- [7] G. A. Christopoulos and A. N. Safacas, "Upgrade of a kiln drive system for cement industry," in *The XIX International Conference on Electrical Machines-ICEM 2010*, 2010, pp. 1-5: IEEE.
- [8] M. Satter, A. Ebadi, K. Aghaie, M. Fotovati, and A. Piroozan, "Wear of gears: a case study at Shiraz Cement Plant," *Wear*, vol. 162, pp. 1054-1058, 1993.
- [9] C. Xiangdong, "The method of correcting deviation and preventing rail gnawing of bridge cranes," *Plant Maintenance Engineering*, no. 12, pp. 104-106, 2023.
- [10] S. Junjie, H. Zhaoqiang, and H. Rui, "Cause analysis and treatment of rail gnawing and wheel rim wear of bridge crane cart," *Mining Equipment*, no. 06, pp. 146-148, 2023.

- [11] S. Changquan, L. Yumei, W. Jing, and L. Guangdong, "Causes and treatment methods of rail gnawing by bridge cranes," *Special equipment safety technology*, no. 3, pp. 40-42, 2023.
- [12] Z. Jinhuan and L. Chunling, "Interpretation of the adjustment of "New Energy Vehicle Industry Development Plan (2021-2035)", " *Automotive Technologist*, no. Z1, pp. 32-34, 2021.
- [13] Y. Junyu, Z. Dandan, and F. Gang, "Exploration of construction machinery remanufacturing under the background of double carbon," *Construction Machinery Maintenance*, no. 03, pp. 44-47, 2022.
- [14] D. Shiyun and Y. Shixing, "Development status and prospect of laser remanufacturing technology," *Surface engineering & remanufacturing*, vol. 21, no. 06, pp. 17-26, 2021.
- [15] W. Fei, Z. Chao, Z. Yinyu, and L. Kai, "Research status of surface coating technology," *Hot working technology*, vol. 46, no. 10, pp. 21-24+29, 2017.
- [16] J. L. Reynolds Jr, R. L. Holdren, and L. E. Brown, "Electro-spark deposition: electro-spark deposition is a viable process suitable for applying overlays and restoring part dimensions with little effect on the substrate microstructure," *Advanced Materials Processes*, vol. 161, no. 3, pp. 35-38, 2003.
- [17] B. I. Stavitskii, "Glimpses of the history of electrospark machining of materials," *Surface Engineering and Applied Electrochemistry*, vol. 46, no. 2, pp. 178-191, Apr 2010.
- [18] M. Berndtsson, "Circular economy and sustainable development," ed, 2015.

- [19] P. Schröder, A. Lemille, P. J. R. Desmond, Conservation, and Recycling, "Making the circular economy work for human development," vol. 156, p. 104686, 2020.
- [20] A. P. Velenturf, P. J. S. P. Purnell, and Consumption, "Principles for a sustainable circular economy," vol. 27, pp. 1437-1457, 2021.
- [21] B.-S. Xu, "Progress of remanufacturing engineering and future technology expectation," *Advances in Manufacturing*, vol. 1, no. 1, pp. 8-12, 2013.
- [22] C. Lei, Y. Du, M. Zhu, W. Huo, H. Wu, and Y. Zhang, "Microstructure and mechanical properties of in situ TiC/Ti composites with a laminated structure synthesized by spark plasma sintering," *Materials Science Engineering: A*, vol. 812, p. 141136, 2021.
- [23] C. Liu *et al.*, "A review on remanufacturing assembly management and technology," *The International Journal of Advanced Manufacturing Technology*, vol. 105, pp. 4797-4808, 2019.
- [24] X. Binshi, "Surface Engineering Development and Remanufacturing Engineer," *Journal of Tongji University*, vol. 29, no. 9, pp. 1085-1091, 2001.
- [25] B. S. J. K. E. M. Xu, "The remanufacturing engineering and automatic surface engineering technology," vol. 373, pp. 1-10, 2008.
- [26] Q. Ke, H.-c. Zhang, G. Liu, and B. Li, "Remanufacturing engineering literature overview and future research needs," in *Glocalized Solutions for Sustainability in Manufacturing: Proceedings of the 18th CIRP International Conference on Life Cycle Engineering*, Technische Universität

- Braunschweig, Braunschweig, Germany, May 2nd-4th, 2011*, 2011, pp. 437-442: Springer.
- [27] L. Zhu *et al.*, "Recent research and development status of laser cladding: A review," *Optics Laser Technology*, vol. 138, p. 106915, 2021.
- [28] E. Birger, G. Moskvitin, A. Polyakov, and V. Arkhipov, "Industrial laser cladding: current state and future," *Welding International*, vol. 25, no. 03, pp. 234-243, 2011.
- [29] H. Assadi, H. Kreye, F. Gärtner, and T. Klassen, "Cold spraying—A materials perspective," *Acta Materialia*, vol. 116, pp. 382-407, 2016.
- [30] S. An, B. Joshi, A. L. Yarin, M. T. Swihart, and S. S. Yoon, "Supersonic cold spraying for energy and environmental applications: One - step scalable coating technology for advanced micro - and nanotextured materials," *Advanced Materials*, vol. 32, no. 2, p. 1905028, 2020.
- [31] W. Sun *et al.*, "Post-process treatments on supersonic cold sprayed coatings: A review," *Coatings*, vol. 10, no. 2, p. 123, 2020.
- [32] B. Wu, B.-s. Xu, B. Zhang, X.-d. Jing, and C.-l. Liu, "Automatic brush plating: An update on brush plating," *Materials Letters*, vol. 60, no. 13-14, pp. 1673-1677, 2006.
- [33] J. Hu *et al.*, "Effect of annealing treatment on microstructure and properties of Cr-coatings deposited on AISI 5140 steel by brush-plating," *Coatings*, vol. 8, no. 5, pp. 193-202, 2018.

- [34] W. Wachtler, "Brush plating in production," in *AESF SUR FIN-PROCEEDINGS*, 1998, pp. 401-406: American Electroplaters & Surface Finishers Society INC.
- [35] E. Katinas, V. Jankauskas, N. Kazak, and V. Michailov, "Improving abrasive wear resistance for steel Hardox 400 by electro-spark deposition," *Journal of Friction and Wear*, vol. 40, pp. 100-106, 2019.
- [36] R. Johnson, "Principles and applications of electro-spark deposition," Westinghouse Hanford Co., Richland, WA (USA)1987.
- [37] Z. Zhengchuan, L. Guanjun, I. Konoplianchenko, V. Tarellyk, G. Zhiqin, and D. Xin, "A review of the electro-spark deposition technology," *Bulletin of Sumy National Agrarian University. The series: Mechanization Automation of Production Processes*, no. 2 (44), pp. 45-53, 2021.
- [38] N. Radek, J. Pietraszek, and A. Szczotok, "Technology and application of electro-spark deposited coatings," in *26th International Conference on Metallurgy and Materials*, Brno, Czech Republic, EU, 2018, pp. 1432-1437.
- [39] V. Tarellyk, O. Gaponova, O. Myslyvchenko, and B. Sarzhanov, "Electrospark deposition of multilayer coatings," *Powder Metallurgy Metal Ceramics*, vol. 59, pp. 76-88, 2020.
- [40] G. Sheldon and R. Johnson, "Electro-spark deposition: a technique for producing wear resistant coatings," Hanford Engineering Development Lab., Richland, WA (USA)1984.

- [41] S. AOSHIMA, "Review of Electro-Spark Deposition Process," *Journal of The Japan Society of Electrical Machining Engineers*, vol. 34, no. 77, pp. 30-35, 2000.
- [42] J. Gould, "Application of electro-spark deposition as a joining technology," *Welding Journal*, vol. 90, no. 10, pp. 191-197, 2011.
- [43] Y. Zhang, K. Yang, and J. Zhao, "Experimental research and numerical simulation of weld repair with high energy spark deposition method," *Metals*, vol. 10, no. 7, p. 980, 2020.
- [44] V. B. Tarelnyk, O. P. Gaponova, Y. V. Konoplianchenko, V. S. Martsynkovskyy, N. V. Tarelnyk, and O. O. Vasylenko, "Improvement of quality of the surface electroerosive alloyed Layers by the combined coatings and the surface plastic deformation. I. Features of formation of the combined electroerosive coatings on special steels and alloys," *Metallofizika I Noveishie Tekhnologii*, vol. 41, no. 1, pp. 47-69, 2019.
- [45] V. B. Tarelnik *et al.*, "Electrospark graphite alloying of steel surfaces: technology, properties, and application," *Surface Engineering and Applied Electrochemistry*, vol. 54, no. 2, pp. 147-156, 2018.
- [46] B. Lazarenko and N. Lazarenko, "About the inversion of metal erosion and methods to fight ravage of electric contacts," 1943. WEI-Institute, Moscow in Russian
- [47] L. Zhang and J. Shao, "Research status and development trend of electro-spark surface deposition technology," (in Chinese), *Equipment Manufacturing Technology*, no. 8, pp. 76-79, 2017.

- [48] A. Verkhoturov, S. Kirilenko, I. Podchernyaeva, N. Siman, L. Shvedova, and I. Timofeeva, "Electrospark alloying of metal surfaces with group 4 transition metal nitrides.[TiN, ZrN, HfH]," *Poroshkovaya Metallurgiya (Kiev)*, vol. 4, pp. 80-84, 1981.
- [49] K. Keutel, H. Fuchs, H. Mecke, and C. Edelmann, "Modified pulse arc deposition for reducing of droplet emission," in *Proceedings ISDEIV. 18th International Symposium on Discharges and Electrical Insulation in Vacuum (Cat. No.98CH36073)*, 1998, vol. 2, pp. 562-565.
- [50] M. H. Staia *et al.*, "Characterization and wear behavior of pulsed electrode surfacing coatings," *Wear*, vol. 251, no. 1, pp. 1051-1060, 2001.
- [51] Y. NAGLYI, "Electro-spark hardening of cutting tools," *Soviet Engineering Research*, vol. 3, no. 11, p. 106, 1983.
- [52] B. Muralidharan and H. Chelladurai, "Experimental analysis of electro-discharge deposition process," *The International Journal of Advanced Manufacturing Technology*, vol. 76, no. 1, pp. 69-82, 2015.
- [53] J. Wang, Z. Zhang, N. Yan, G. LI, M. TANG, and Z. FENG, "Interface behavior of WC-4Co coating by electro-spark deposition," *The Chinese Journal of Nonferrous Metals*, vol. 24, no. 11, pp. 2849-2855, 2014.
- [54] V. V. Tarelnik and A. N. Kuchmii, "Electroerosion hardening of metal-cutting tools for machining corrosion-resistant steels," *Chemical and Petroleum Engineering*, vol. 33, no. 1, pp. 100-102, 1997.
- [55] T. You *et al.*, "Research of surface carburizing on titanium alloys by electrospark deposition," *Foundry*, no. 03, pp. 239-241, 2007.

- [56] P. Zhang, E.-L. Zhang, L. Ma, and Z.-H. Cai, "Processing properties of tin ceramic coating prepared by in-situ synthesis electric spark deposition," *Journal of Armored Forces*, vol. 25, no. 4, pp. 74-79, 2011.
- [57] Z. Chen and Y. Zhou, "Surface modification of resistance welding electrodes by electro-spark deposited composite coatings: Part II. Metallurgical behavior during welding," *Surface Coatings Technology*, vol. 201, no. 6, pp. 2419-2430, 2006.
- [58] K. Vishwakarma, O. Ojo, and N. Richards, "Nano-size solidification microconstituents in electro-spark deposited Ni-base superalloy," *Philosophical Magazine Letters*, vol. 95, no. 1, pp. 30-36, 2015.
- [59] S. H. Baghjari, F. M. Ghaini, H. R. Shahverdi, C. Mapelli, S. Barella, and D. Ripamonti, "Laser welding of niobium to 410 steel with a nickel interlayer produced by electro spark deposition," *Materials Design*, vol. 107, pp. 108-116, 2016.
- [60] H. Aghajani, E. Hadavand, N.-S. Peighambaroust, and S. Khameneh-asl, "Electro spark deposition of WC–TiC–Co–Ni cermet coatings on St52 steel," *Surfaces and Interfaces*, vol. 18, p. 100392, 2020.
- [61] B. Chen, X. Fan, X. Tang, and D. Li, "Microstructure and properties of YG10/CD750 double electrode alternating deposition electro-spark deposition coating," *Hot Working Technology*, vol. 47, no. 04, pp. 168-172, 2018.

- [62] J. Tang, "Mechanical and tribological properties of the TiC–TiB₂ composite coating deposited on 40Cr-steel by electro spark deposition," *Applied Surface Science*, vol. 365, pp. 202-208, 2016.
- [63] M.-H. Tsai and J.-W. Yeh, "High-entropy alloys: a critical review," *Materials Research Letters*, vol. 2, no. 3, pp. 107-123, 2014.
- [64] E. P. George, D. Raabe, and R. O. Ritchie, "High-entropy alloys," *Nature reviews materials*, vol. 4, no. 8, pp. 515-534, 2019.
- [65] Y. ZHANG *et al.*, "Research status and prospect of electro-spark deposition technology," (in Chinese), *Surface Technology*, vol. 50, no. 1, 2021.
- [66] Q. Li, T. M. Yue, Z. Guo, and X. Lin, "Microstructure and corrosion properties of AlCoCrFeNi high entropy alloy coatings deposited on AISI 1045 steel by the electrospark process," *Metallurgical and Materials Transactions A*, vol. 44, no. 4, pp. 1767-1778, 2013.
- [67] S. N. Karlsdottir *et al.*, "Phase evolution and microstructure analysis of CoCrFeNiMo high-Entropy alloy for electro-spark-deposited coatings for geothermal environment," *Coatings*, vol. 9, no. 6, p. 406, 2019.
- [68] Y. F. Wang, H. Yan, L. I. Juan, S. Y. Sun, Z. J. Song, and Z. Q. Shi, "Microstructure and corrosion resistance of FeCoCrNiCu high-entropy alloy coating prepared by electro-spark deposition," (in Chinese), *Transactions of the China Welding Institution*, vol. 39, no. 07, pp. 121-124+134, 2018.
- [69] E. I. Zamulaeva, E. A. Levashov, A. E. Kudryashov, P. V. Vakaev, and M. I. Petrzhik, "Electrospark coatings deposited onto an Armco iron substrate with nano- and microstructured WC–Co electrodes: Deposition process,

- structure, and properties," *Surface and Coatings Technology*, vol. 202, no. 15, pp. 3715-3722, 2008.
- [70] Y. Gao, C. Zhao, and J. Yi, "Microstructure and properties of Ni-Cr alloyed coating prepared by electrospark deposition processes," (in Chinese), *Journal of Materials Engineering* vol. 2, no. 3, pp. 74-78, 2012.
- [71] X. Wei *et al.*, "Facile preparation of nanocrystalline Fe₂B coating by direct electro-spark deposition of coarse-grained Fe₂B electrode material," *Journal of Alloys Compounds*, vol. 717, pp. 31-40, 2017.
- [72] Y. Zhang, Z. Chen, X. Wei, L. Wang, Z. Hou, and W. Yang, "Microstructure and properties of chromium carbide based metal-ceramic coatings prepared by electro-spark deposition," (in Chinese), *Rare Metal Materials and Engineering*, vol. 48, no. 2, pp. 601-607, 2019.
- [73] T. Jiang, J. Hu, and J. Zhou, "Effect of middle layer by electro-spark deposition technology on bonding strength of porcelain and cast pure titanium," *Journal of Oral Science Research*, vol. 27, no. 04, pp. 277-280, 2011.
- [74] N. Boshitskaya, I. Podchernyaeva, V. Lavrenko, I. Uvarova, and D. Yurechko, "Combined functional biocoatings on the VT-6 alloy," *Powder Metallurgy and Metal Ceramics*, vol. 52, no. 9-10, pp. 551-559, 2014.
- [75] S. Durdu, K. Korkmaz, S. L. Aktuğ, and A. Çakır, "Characterization and bioactivity of hydroxyapatite-based coatings formed on steel by electro-spark deposition and micro-arc oxidation," *Surface and Coatings Technology*, vol. 326, pp. 111-120, 2017.

- [76] A. Esmaeili, S. A. Ghaffari, M. Nikkhah, F. M. Ghaini, F. Farzan, and S. Mohammadi, "Biocompatibility assessments of 316L stainless steel substrates coated by Fe-based bulk metallic glass through electro-spark deposition method," *Colloids and Surfaces B-Biointerfaces*, vol. 198, p. 111469, 2021.
- [77] N. Radek and K. Bartkowiak, "Performance properties of electro-spark deposited carbide-ceramic coatings modified by laser beam," *Physics Procedia*, vol. 5, pp. 417-423, 2010.
- [78] Y.-x. Gao and J.-b. Wang, "Effects of laser remelting on microstructure and wear properties of Ni -based coating prepared by electrospark deposition," *Materials Protection*, vol. 54, no. 1, pp. 54(1): 112-115, 120., 2021.
- [79] C. Chen, Y. Tang, and Y. Xu, "Ultrasonic ESD deposition device and its process research," in *Proceedings of the 14th China Special Processing Academic Conference*, 2011, pp. 598-602.
- [80] H. Zhao, C. Gao, X.-y. Wu, B. Xu, Y.-j. Lu, and L.-k. Zhu, "A novel method to fabricate composite coatings via ultrasonic-assisted electro-spark powder deposition," *Ceramics International*, vol. 45, no. 17, pp. 22528-22537, 2019.
- [81] L. M. Felix, C. C. F. Kwan, and N. Y. Zhou, "The effect of pulse energy on the defects and microstructure of electro-spark-deposited inconel 718," *Metallurgical and Materials Transactions A*, vol. 50, no. 9, pp. 4223-4231, 2019.

- [82] J. Liu, R. Wang, and Y. Qian, "The formation of a single-pulse electrospark deposition spot," *Surface and Coatings Technology*, vol. 200, no. 7, pp. 2433-2437, 2005.
- [83] V. B. Tarel'nyk, O. P. Gaponova, Y. V. Konoplyanchenko, N. S. Yevtushenko, and V. O. Herasymenko, "The analysis of a structural state of surface layer after electroerosive alloying. II. Features of formation of electroerosive coatings on special steels and alloys by hard wear-resistant and soft antifriction materials," *Metallofizika I Noveishie Tekhnologii*, vol. 40, no. 6, pp. 795-815, 2018.
- [84] V. B. Tarel'nik, V. S. Martsinkovskii, and A. N. Zhukov, "Increase in the reliability and durability of metal impulse end seals. Part 1," *Chemical and Petroleum Engineering*, vol. 53, no. 1-2, pp. 114-120, 2017.
- [85] B. Lazarenko and N. Lazarenko, "Technological characteristics of electrospark machining of current conducting materials," *Electrospark Machining of Metals*, vol. 2, no. 1, 1964.
- [86] N. Pereira, "Measuring the RC time constant with Arduino," *Physics Education*, vol. 51, no. 6, p. 065007, 2016.
- [87] S. Dunford, "Calculating the time constant of an rc circuit," *Undergraduate Journal of Mathematical Modeling: One+Two*, vol. 2, no. 2, pp. 1-11, 2010.
- [88] H. L. Andersen, L. Djuandhi, U. Mittal, and N. J. A. E. M. Sharma, "Strategies for the analysis of graphite electrode function," vol. 11, no. 48, p. 2102693, 2021.

- [89] Y. Qi and S. J. J. J. o. T. E. S. Harris, "In situ observation of strains during lithiation of a graphite electrode," vol. 157, no. 6, p. A741, 2010.
- [90] V. Holubets, V. Dovhunykh, M. Pashechko, S. Kornii, and Y. S. J. M. S. Shpulyar, "Friction behavior of electric-spark coatings under the conditions of boundary lubrication," vol. 56, pp. 43-49, 2020.
- [91] V. Tarel'nik *et al.*, "Electrospark graphite alloying of steel surfaces: technology, properties, and application," vol. 54, pp. 147-156, 2018.
- [92] M. Sathish, N. Radhika, and B. Saleh, "A critical review on functionally graded coatings: Methods, properties, and challenges," *Composites Part B: Engineering*, vol. 225, p. 109278, 2021.
- [93] H. Bai *et al.*, "A review on wear-resistant coating with high hardness and high toughness on the surface of titanium alloy," *Journal of Alloys Compounds*, vol. 882, p. 160645, 2021.
- [94] G. Udupa, S. S. Rao, and K. Gangadharan, "Functionally graded composite materials: an overview," *Procedia Materials Science*, vol. 5, pp. 1291-1299, 2014.
- [95] R. Fathi *et al.*, "Past and present of functionally graded coatings: Advancements and future challenges," *Applied Materials Today*, vol. 26, p. 101373, 2022.
- [96] V. Tarelnyk *et al.*, "Application of wear-resistant nanostructures formed by ion nitriding & electrospark alloying for protection of rolling bearing seat surfaces," in *2022 IEEE 12th International Conference Nanomaterials: Applications & Properties (NAP)*, 2022, pp. 01-08: IEEE.

- [97] V. Tarelnyk *et al.*, "New sulphiding method for steel and cast iron parts," in *IOP Conference Series: Materials Science and Engineering*, 2017, vol. 233, no. 1, p. 012049: IOP Publishing.
- [98] O. P. Gaponova *et al.*, "Technological features for controlling steel part quality parameters by the method of electrospark alloying using carburezer containing Nitrogen—Carbon components," *Materials*, vol. 15, no. 17, p. 6085, 2022.
- [99] M. Petrzhik *et al.*, "From bulk metallic glasses to amorphous metallic coatings," *Metastab. Nanocryst. Mater*, vol. 24, no. 25, p. 101, 2005.
- [100] M. S. Khan *et al.*, "The influence of in-situ alloying of electro-spark deposited coatings on the multiscale morphological and mechanical properties of laser welded Al–Si coated 22MnB5," *Materials Science Engineering: A*, vol. 839, p. 142830, 2022.
- [101] A. A. Burkov, S. Pyachin, M. Ermakov, and A. Syuy, "In situ synthesis and characterization of Fe-based metallic glass coatings by electrospark deposition technique," *Journal of Materials Engineering Performance*, vol. 26, pp. 901-908, 2017.
- [102] H. Zhao, C. Gao, C. Guo, B. Xu, X.-Y. Wu, and J.-G. Lei, "In-situ TiC-reinforced Ni-based composite coatings fabricated by ultrasonic-assisted electrospark powder deposition," *Journal of Asian Ceramic Societies*, vol. 11, no. 1, pp. 26-38, 2023.
- [103] A. Sheveyko, K. Kuptsov, M. Antonyuk, A. Bazlov, and D. Shtansky, "Electro-spark deposition of amorphous Fe-based coatings in vacuum and in

- argon controlled by surface wettability," *Applied Surface Science Materials Letters*, vol. 318, p. 132195, 2022.
- [104] V. Tarel'nyk, O. P. Haponova, and Y. V. Konoplianchenko, "Electric-spark alloying of metal surfaces with graphite," *Progress in Physics of Metals*, vol. 23, no. 1, pp. 27-58, 2022.
- [105] D. Karavaev, E. Matygullina, M. Doshchennikov, and D. Sinyushov, "Wear resistance of steel parts after electrospark alloying by graphite electrodes," *Russian Engineering Research*, vol. 39, no. 10, pp. 889-891, 2019.
- [106] O. Shevchenko, "Ultrasound effect on electrospark cementation process," in *IOP Conference Series: Materials Science and Engineering*, 2020, vol. 966, no. 1, p. 012071: IOP Publishing.
- [107] L. Chen, H.-M. Meng, L.-L. Huang, and J.-Y. Liu, "Microstructure and wear property of multi-layer YG8 ESD coating on 45 steel," *Transactions of Materials and Heat Treatment*, vol. 34, no. 11, pp. 170-175, 2013.
- [108] Y. Dai *et al.*, "Surface hardening behavior of advanced gear steel C61 by a novel solid-solution carburizing process," *Metals*, vol. 12, no. 3, p. 379, 2022.
- [109] K. Nakayama, "An overview of the excess carburizing process," *International Journal of Materials Product Technology*, vol. 7, no. 3, pp. 245-256, 1992.
- [110] B. Edenhofer, D. Joritz, M. Rink, and K. Voges, "Carburizing of Steels," in *Thermochemical surface engineering of steels*: Woodhead Publishing, 2015, pp. 485-553.

- [111] J. Padgurskas *et al.*, "Tribological properties of coatings obtained by electro-spark alloying C45 steel surfaces," *Surface Coatings Technology*, vol. 311, pp. 90-97, 2017.
- [112] I. Konoplianchenko *et al.*, "Mathematical modeling a process of strengthening steel part working surfaces at carburizing thereof by electroerosive alloying method," in *AIP Conference Proceedings*, 2018, vol. 2017, no. 1, p. 020008: AIP Publishing LLC.
- [113] K. Kuptsov, A. Sheveyko, D. Sidorenko, and D. Shtansky, "Electro-spark deposition in vacuum using graphite electrode at different electrode polarities: Peculiarities of microstructure, electrochemical and tribological properties," *Applied Surface Science*, vol. 566, p. 150722, 2021.
- [114] C. Weiwei, Z. Ying, K. Hui, Q. Ping, W. Ruijun, and H. Xiaoou, "Study on thickness of WC-8co reinforcing layer deposited by new EDM system on TC1 alloy surface," *New Technology & New Process*, vol. 5, no. 3, pp. 93-94,112, 2007.
- [115] A. Mikhailyuk and A. Gitlevich, "Application of graphite in electrospark technologies," *Surface Engineering and Applied Electrochemistry*, vol. 46, no. 5, pp. 424-430, 2010.
- [116] Y. Liu, J. Qu, X. Cai, W. Zhang, and S. Zhang, "Experimental study on electro-spark additive/subtractive repair for worn cemented carbide," *Machines*, vol. 11, no. 3, p. 333, 2023.

- [117] T. Zhu, P. Shipway, and W. Sun, "The dependence of wear rate on wear scar size in fretting; the role of debris (third body) expulsion from the contact," *Wear*, vol. 440-441, p. 203081, 2019.
- [118] H. Xiang, F. Ke, Y.-f. Tan, X.-l. Wang, and T. Hua, "Effects of process parameters on microstructure and wear resistance of TiN coatings deposited on TC11 titanium alloy by electrospark deposition," *Transactions of Nonferrous Metals Society of China*, vol. 27, no. 8, pp. 1767-1776, 2017.
- [119] L. Krishnia *et al.*, "Comparative study of thermal stability of filled and un-filled multiwalled carbon nanotubes," *Advanced Materials Letters*, vol. 7, no. 3, pp. 230-234, 2016.
- [120] W. Cai, F. Meng, X. Gao, and J. Hu, "Effect of QPQ nitriding time on wear and corrosion behavior of 45 carbon steel," *Applied Surface Science*, vol. 261, pp. 411-414, 2012.
- [121] J. Li, Z. Cao, L. Liu, X. Liu, and J. Peng, "Effect of microstructure on hardness and wear properties of 45 steel after induction hardening," *Steel Research International*, vol. 92, no. 4, p. 2000540, 2021.
- [122] A. BALTUŠNIKAS and R. Levinskas, "XRD analysis of carbide phase in heat resistant steels," *Materials Science*, vol. 12, no. 3, pp. 192-198, 2006.
- [123] N. Sharma, R. Khanna, Y. K. Sharma, and R. D. Gupta, "Multi-quality characteristics optimisation on WEDM for Ti-6Al-4V using Taguchi-grey relational theory," *International Journal of Machining Machinability of Materials*, vol. 21, no. 1-2, pp. 66-81, 2019.

- [124] K. Banker, U. Prajapati, J. Prajapati, and P. Modi, "Parameter optimization of electro discharge machine of AISI 304 steel by using taguchi method," *International Journal of Application or Innovation in Engineering Management*, vol. 3, no. 8, pp. 20-24, 2014.
- [125] A. Raj, J. P. Misra, and D. Khanduja, "Modeling of wire electro-spark machining of inconel 690 superalloy using support vector machine and random forest regression approaches," *Journal of Advanced Manufacturing Systems*, vol. 21, no. 03, pp. 557-571, 2022.
- [126] C. Reséndiz-Calderón, L. Farfan-Cabrera, J. Oseguera-Peña, and G. Rodríguez-Castro, "Wear and friction of boride layer in CoCrMo alloy under different micro-abrasion modes (rolling and grooving abrasion)," *Materials Letters*, vol. 279, p. 128500, 2020.
- [127] W. M. Haynes, D. R. Lide, and T. J. Bruno, *CRC handbook of chemistry and physics*. CRC press, 2016.
- [128] G. Rolland *et al.*, "Coating toughness estimation through a Laser Shock Testing in Ni-Cr-B-Si-C Coatings," *Materials Science Forum*, vol. 941, pp. 1886-1891, 2019.
- [129] Z. R. Liu, Y. X. Xu, B. Peng, W. Wei, L. Chen, and Q. Wang, "Structure and property optimization of Ni-containing AlCrSiN coatings by nano-multilayer construction," *Journal of Alloys Compounds*, vol. 808, p. 151630, 2019.
- [130] N. Karunathilaka, N. Tada, T. Uemori, R. Hanamitsu, and M. Kawano, "Effect of contact pressure applied on tool surface during cold forging on

- fatigue life of tool steel," *Procedia Manufacturing*, vol. 15, pp. 488-495, 2018.
- [131] C. Wu, W. Chen, and L. Chen, "Effects of cryogenic treatment on mechanical property and microstructure of JIS SKH51 high-speed steel," in *IOP Conference Series: Materials Science and Engineering*, 2015, vol. 103, no. 1, p. 012022: IOP Publishing.
- [132] H. Aghajani, E. Hadavand, N.-S. Peighambaroust, and S. Khameneh-asl, "Electro spark deposition of WC–TiC–Co–Ni cermet coatings on St52 steel," *Surfaces Interfaces*, vol. 18, p. 100392, 2020.
- [133] Y. Kayali and Ş. Talaş, "Investigation on wear behavior of steels coated with WC by ESD technique," *International Journal of Surface Science*, vol. 57, pp. 106-112, 2021.
- [134] W. WANG, M. DU, X. ZHANG, and M. GENG, "Microstructure and tribological properties of WC-Ni matrix cermet coatings prepared by electrospark deposition on H13 steel substrate," *Acta Metall Sin*, vol. 57, no. 8, pp. 1048-1056, 2021.
- [135] W. Zhao, H. Su, W. He, X. Wang, X. Cui, and S. Luo, "Defect Control of Electro-spark Deposition WC–Co Coatings via Adjusting Pulse Energy and Deposited Layer Number," *Journal of Materials Engineering Performance*, vol. 32, no. 3, pp. 1402-1411, 2023.
- [136] M. Onan, O. Şahin, E. Yıldırım, and Ş. Talaş, "Effect of WC based coatings on the wear of CK45 sheet metal forming dies," *International Journal of*

- Surface Science Engineering Failure Analysis*, vol. 15, no. 4, pp. 265-280, 2021.
- [137] K. Worasaen, P. Suwanpinij, and K. Tuchinda, "Effect of cryogenic treatment on the microstructure modification of SKH51 steel," *Applied Science Engineering Progress*, vol. 16, no. 1, pp. 5588-5603, 2022.
- [138] S.-H. Yao, Y.-L. Su, W.-H. Kao, and T.-H. Liu, "Tribology and oxidation behavior of TiN/AlN nano-multilayer films," *Tribology international*, vol. 39, no. 4, pp. 332-341, 2006.
- [139] M. Khadem and D.-E. Kim, "Friction and wear behaviors of bare and diamond-like carbon/chromium bi-layer coated SKH51 steel at low temperatures," *Surface Coatings Technology*, vol. 412, p. 127018, 2021.
- [140] M. Jahan, M. Anwar, Y. Wong, and M. Rahman, "Nanofinishing of hard materials using micro-electrodischarge machining," *Proceedings of the Institution of Mechanical Engineers, Part B: Journal of Engineering Manufacture*, vol. 223, no. 9, pp. 1127-1142, 2009.
- [141] W. Darmawan, I. Rahayu, D. Nandika, and R. Marchal, "The importance of extractives and abrasives in wood materials on the wearing of cutting tools," *BioResources*, vol. 7, no. 4, pp. 4715-4729, 2012.
- [142] K.-J. Chen, F.-Y. Hung, T.-S. Lui, and Y.-R. Shih, "Wear inducing phase transformation of plasma transfer arc coated tools during friction stir welding with Al alloy," *Journal of Engineering Sciences*, vol. 2019, 2019.

- [143] W.-C. Yang, S.-H. Chon, C.-M. Choe, and J.-Y. Yang, "Materials selection method using TOPSIS with some popular normalization methods," *Engineering Research Express*, vol. 3, no. 1, p. 015020, 2021.
- [144] J. Landes, Z. Zhou, K. Lee, and R. Herrera, "Normalization method for developing curves with the function," *Journal of Testing Evaluation*, vol. 19, no. 4, pp. 305-311, 1991.
- [145] T. Dragičević and M. Novak, "Weighting factor design in model predictive control of power electronic converters: An artificial neural network approach," *IEEE Transactions on Industrial Electronics*, vol. 66, no. 11, pp. 8870-8880, 2018.
- [146] G. B. Kilic and M. Cakan, "The analysis of the impact of individual weighting factor on individual scores," *Assessment Evaluation in Higher Education*, vol. 31, no. 6, pp. 639-654, 2006.
- [147] N. Mohd Abbas, D. G. Solomon, and M. Fuad Bahari, "A review on current research trends in electrical discharge machining (EDM)," *International Journal of Machine Tools and Manufacture*, vol. 47, no. 7-8, pp. 1214-1228, 2007.
- [148] Z. Zhengchuan, V. Tarellyk, I. Konoplianchenko, L. Guanjun, D. Xin, and Y. Hua, "Research on the Characterization of Ag+Cu+B83 Composite Coatings on the Surface of Tin Bronze by Electro-spark Deposition," in *2021 IEEE 11th International Conference Nanomaterials: Applications & Properties (NAP)*, 2021, pp. 1-8.

- [149] M. Kazemi, S. Ahangarani, M. Esmailian, and A. Shanaghi, "Investigation on the corrosion behavior and biocompatibility of Ti-6Al-4V implant coated with HA/TiN dual layer for medical applications," *Surface and Coatings Technology*, vol. 397, p. 126044, 2020.
- [150] M. Perju, A. Sandu, P. Vizureanu, C. Nejneru, C. Tugui, and D. Burduhos-Nergis, "Microstructural Analysis of Ti/W/WC Deposition by ESD Method," *Acta Phys. Pol. A*, vol. 138, pp. 214-217, 2020.
- [151] T. Al-Quraan, V. Tokaruk, O. Mikosianchyk, R. Mnatsakanov, N. Kichata, and N. O. Kuzin, "Influence of Continuity of Electric Spark Coatings on Wear Resistance of Aluminum Alloy," *Tribology in Industry*, vol. 43, no. 4, pp. 603-614, 2021.
- [152] X. Wei, Z. Chen, J. Zhong, and Y. Xiang, "Feasibility of preparing Mo₂FeB₂-based cermet coating by electrospark deposition on high speed steel," *Surface Coatings Technology*, vol. 296, pp. 58-64, 2016.
- [153] W. Wang, M. Du, X. Zhang, C. Luan, and Y. Tian, "Preparation and properties of Mo coating on H13 steel by electro spark deposition process," *Materials*, vol. 14, no. 13, p. 3700, 2021.
- [154] M. Salmaliyan, F. M. Ghaeni, and M. Ebrahimnia, "Effect of electro spark deposition process parameters on WC-Co coating on H13 steel," *Surface Coatings Technology*, vol. 321, pp. 81-89, 2017.
- [155] E. A. Levashov, E. I. Zamulaeva, A. E. Kudryashov, P. V. Vakaev, M. I. Petrzhik, and A. Sanz, "Materials science and technological aspects of

- electrospark deposition of nanostructured WC - Co coatings onto titanium substrates," *Plasma Processes Polymers*, vol. 4, no. 3, pp. 293-300, 2007.
- [156] A. Sharma and V. Dwivedi, "Effect of milling parameters on surface roughness: An experimental investigation," *Materials Today: Proceedings*, vol. 25, pp. 868-871, 2020.
- [157] S.-s. Kim and Y.-j. Jeong, "Fiber laser welding of dissimilar metal combinations for fuel irradiation capsule fabrication," in *International Congress on Applications of Lasers & Electro-Optics*, 2018, vol. 2018, no. 1, p. P109: Laser Institute of America.
- [158] A. K. Valeeva, I. S. Valeev, and R. Fazlyakhmetov, "Effect of structure of B83 babbitt on its wear," *Journal of Friction and Wear*, vol. 35, pp. 311-315, 2014.
- [159] N. Barykin, R. Fazlyakhmetov, and A. K. Valeeva, "Effect of the structure of babbitt B83 on the intensity of wear of tribocouplings," *Metal science and heat treatment*, vol. 48, pp. 88-91, 2006.
- [160] M. Zawrah, "Synthesis and characterization of WC-Co nanocomposites by novel chemical method," *Ceramics international*, vol. 33, no. 2, pp. 155-161, 2007.
- [161] C. Li, A. Ohmori, and Y. Harada, "Formation of an amorphous phase in thermally sprayed WC-Co," *Journal of Thermal Spray Technology*, vol. 5, pp. 69-73, 1996.
- [162] M. Erfanmanesh, H. Abdollah-Pour, H. Mohammadian-Semnani, and R. Shoja-Razavi, "Kinetics and oxidation behavior of laser clad WC-Co and

- Ni/WC-Co coatings," *Ceramics International*, vol. 44, no. 11, pp. 12805-12814, 2018.
- [163] Y. Ozbek, N. Canikoğlu, and M. Ipek, "The surface properties of WC-Co-Cr based coatings deposited by high velocity oxygen fuel spraying," *Acta Physica Polonica A*, vol. 131, no. 1, pp. 186-189, 2017.
- [164] Z. Zhang, I. Konoplianchenko, V. Tarellyk, G. Liu, X. Du, and H. Yu, "The characterization of running-in coatings on the surface of tin bronze by electro-spark deposition," *Coatings*, vol. 12, no. 7, p. 930, 2022.
- [165] A. K. Valeeva and I. S. Valeev, "Investigation of SnSbCu coatings, electrodeposited on bronze and copper," *Letters on Materials*, vol. 6, no. 2, pp. 122-125, 2016.
- [166] Z. Zhang, I. Konoplianchenko, V. TARELNYK, L. Guanjun, D. Xin, and Y. Hua, "The characterization of soft antifriction coating on the tin bronze by electro-spark alloying," *Materials Science* vol. 29, no. 1, pp. 40-47, 2023.
- [167] E. Yurchenko, I. Rushika, V. I. Agafii, and A. I. Dikumar, "Al-Sn nanostructured coatings on aluminum surfaces using electrospark alloying and their wear behavior," *Journal of Mechanical Energy Engineering*, vol. 2, 2018.
- [168] D. H. Shreve, "Signal processing for effective vibration analysis," *IRD Mechanical Analysis*, pp. 1-11, 1995.
- [169] G. Betta, C. Liguori, A. Paolillo, and A. Pietrosanto, "A DSP-based FFT-analyzer for the fault diagnosis of rotating machine based on vibration

- analysis," *IEEE Transactions on Instrumentation Measurement*, vol. 51, no. 6, pp. 1316-1322, 2002.
- [170] H.-C. Lin and Y.-C. Ye, "Reviews of bearing vibration measurement using fast Fourier transform and enhanced fast Fourier transform algorithms," *Advances in Mechanical Engineering*, vol. 11, no. 1, 2019.
- [171] Q. Liu, J. Wang, L. Li, Y. Zhang, and C. Yu, "Calculation of electric spark discharge energy and its energy loss," *High Voltage Engineering*, vol. 40, no. 4, pp. 1255-1260, 2014.
- [172] H. B. Han and Y. P. Guo, "Study on Electrosark Depositing & Welding Power Supply," *Advanced Materials Research*, vol. 314, pp. 165-170, 2011.
- [173] P. Topală, L. Slătineanu, O. Dodun, M. Coteață, and N. Pînzaru, "Electrosark deposition by using powder materials," *Materials Manufacturing Processes*, vol. 25, no. 9, pp. 932-938, 2010.
- [174] S. K. Tang, "The process fundamentals and parameters of electro-spark deposition," University of Waterloo, 2009.
- [175] A. V. Ribalko, O. Sahin, and K. Korkmaz, "A modified electrosark alloying method for low surface roughness," *Surface and Coatings Technology*, vol. 203, no. 23, pp. 3509-3515, 2009.
- [176] V. Gadalov, D. Romanenko, V. Samoilov, A. Nikolaenko, and S. Grigor'ev, "Procedure of evaluating the surface roughness of the electrosark coating after burnishing with mineral ceramics," *Russian Journal of Non-Ferrous Metals*, vol. 53, pp. 348-350, 2012.

- [177] G. V. Kirik, O. P. Gaponova, V. B. Tarelnyk, O. M. Myslyvchenko, and B. Antoszewski, "Quality analysis of aluminized surface layers produced by electrospark deposition," *Powder Metallurgy and Metal Ceramics*, vol. 56, no. 11, pp. 688-696, 2018.
- [178] P. D. Enrique *et al.*, "Enhancing fatigue life of additive manufactured parts with electrospark deposition post-processing," *Additive Manufacturing*, vol. 36, p. 101526, 2020.
- [179] M. Dovzhik, V. Tarelnik, V. Marcinkovsky, and A. Pavlov, "Restoring machine parts by electroerosive doping and applying polymer composites," in *Selected problems of surface engineering and tribology*, 2016, pp. 87-98.
- [180] W. Yu, L. Sisi, Y. Haiyan, and L. Jie, "Progress in the functional modification of graphene/graphene oxide: A review," *RSC advances*, vol. 10, no. 26, pp. 15328-15345, 2020.
- [181] Y. Zhu *et al.*, "Graphene and graphene oxide: synthesis, properties, and applications," *Advanced materials*, vol. 22, no. 35, pp. 3906-3924, 2010.
- [182] O. C. Compton and S. T. Nguyen, "Graphene oxide, highly reduced graphene oxide, and graphene: versatile building blocks for carbon - based materials," *Small*, vol. 6, no. 6, pp. 711-723, 2010.
- [183] M. Wojtoniszak *et al.*, "Synthesis, dispersion, and cytocompatibility of graphene oxide and reduced graphene oxide," *Colloids Surfaces B: Biointerfaces*, vol. 89, pp. 79-85, 2012.

- [184] L. Tong *et al.*, "Enhanced corrosion and wear resistances by graphene oxide coating on the surface of Mg-Zn-Ca alloy," *Carbon*, vol. 109, pp. 340-351, 2016.
- [185] H. Im and J. Kim, "Thermal conductivity of a graphene oxide-carbon nanotube hybrid/epoxy composite," *Carbon*, vol. 50, no. 15, pp. 5429-5440, 2012.
- [186] V. V. Neklyudov, N. R. Khafizov, I. A. Sedov, and A. M. Dimiev, "New insights into the solubility of graphene oxide in water and alcohols," *Physical Chemistry Chemical Physics*, vol. 19, no. 26, pp. 17000-17008, 2017.
- [187] X. Liu *et al.*, "Self-assembled S, N co-doped reduced graphene oxide/MXene aerogel for both symmetric liquid-and all-solid-state supercapacitors," *Journal of Power Sources*, vol. 516, p. 230682, 2021.
- [188] L. Stobinski *et al.*, "Graphene oxide and reduced graphene oxide studied by the XRD, TEM and electron spectroscopy methods," *Journal of Electron Spectroscopy Related Phenomena*, vol. 195, pp. 145-154, 2014.
- [189] P. Mikhaylov, M. Vinogradov, I. Levin, G. Shandryuk, A. Lubenchenko, and V. Kulichikhin, "Synthesis and characterization of polyethylene terephthalate-reduced graphene oxide composites," in *IOP Conference Series: Materials Science and Engineering*, 2019, vol. 693, no. 1, p. 012036: IOP Publishing.
- [190] A. Kumar, A. M. Sadanandhan, and S. L. Jain, "Silver doped reduced graphene oxide as a promising plasmonic photocatalyst for oxidative

- coupling of benzylamines under visible light irradiation," *New Journal of Chemistry*, vol. 43, no. 23, pp. 9116-9122, 2019.
- [191] J. Huang, C. Zong, H. Shen, Y. Cao, B. Ren, and Z. Zhang, "Tracking the intracellular drug release from graphene oxide using surface-enhanced Raman spectroscopy," *Nanoscale*, vol. 5, no. 21, pp. 10591-10598, 2013.
- [192] M. Nakamizo, R. Kammereck, and P. Walker Jr, "Laser Raman studies on carbons," *Carbon*, vol. 12, no. 3, pp. 259-267, 1974.
- [193] R. Sun, C. Chen, W.-J. Ling, Y.-N. Zhang, C.-P. Kang, and Q. Xu, "Watt-level passively Q-switched mode-locked Tm: LuAG laser with graphene oxide saturable absorber," *Acta Physica Sinica*, vol. 68, no. 10, p. 104207, 2019.
- [194] R. Askarnia, B. Ghasemi, S. R. Fardi, and E. Adabifiroozjaei, "Improvement of tribological, mechanical and chemical properties of Mg alloy (AZ91D) by electrophoretic deposition of alumina/GO coating," *Surface Coatings Technology*, vol. 403, p. 126410, 2020.
- [195] J. Valli, U. Makela, and A. Matthews, "Assessment of coating adhesion," *Surface Engineering*, vol. 2, no. 1, pp. 49-54, 1986.
- [196] A. Shugurov *et al.*, "Study of crack resistance of TiAlN coatings by scratch testing," *Physical Mesomechanics*, vol. 20, pp. 185-192, 2017.
- [197] R. L. Norton, *Machine design*. Prentice Hall, 2010.

APPENDICES

APPENDIX A. List of publications on the topic of the dissertation and information on the approbation of the results of the dissertation

List of publications in which the main scientific results of the dissertation are published:

1. **Du Xin**, Konoplianchenko Ie., Tarelnyk V. Electrosark deposition in remanufacturing engineering, prospect of development and application Mechanization and Automation of Production Processes.2021, 1 (43),8-12, DOI: <https://doi.org/10.32845/msnau.2021.1.2>(PhD participant in carrying out of investigation, review and editing, preparation of article for printing).
2. **Du Xin**, Research on wear resistance of carbonized 45 steel by electro-spark deposition technology , Bulletin of Sumy National Agrarian University. The series: Mechanization and Automation of Production Processes.2022, 3 (49),11-18.DOI: <https://doi.org/10.32845/msnau.2022.3.2> (PhD participant in carrying out of experimental researches, processing of results, preparation of article for printing).
3. Zhengchuan, Z., Konoplianchenko E. B., Tarelnyk B. B., Guanjun, L., **Xin, D.**, Yao, J., & Zhaoyang, S. (2022). Industry Application of the Coatings on the Bearing Bush by Electro Spark Alloying Technology. Scientific Bulletin of Ivano-Frankivsk National Technical University of Oil and Gas, 2022,1(52), 15–23. DOI: [https://doi.org/10.31471/1993-9965-2022-1\(52\)-15-23](https://doi.org/10.31471/1993-9965-2022-1(52)-15-23) (PhD participant in carrying out of experimental researches, processing of results).

4. Zhang Zhengchuan, Liu Guanjun, Ie. Konoplianchenko, V. Tarellyk, Ge Zhiqin, **Du Xin**. A review of the electro-spark deposition technology. Bulletin of Sumy National Agrarian University, The Series: Mechanization and Automation of Production Processes. 2021, 2(44), 45-53. DOI: <https://doi.org/10.32845/msnau.2021>. (PhD participant in carrying out of investigation, review and editing).

5. **Xin D**, Tarellyk V. Konoplianchenko Ie. Research on SKH51+WC+B83 composite gradient coating by ESD method, Sciences Of Europe. 2023, 127, 102-110. DOI: <https://doi.org/10.5281/zenodo.10039444> (PhD participant in carrying out of investigation, review and editing, preparation of article for printing).

6. **Xin D**, Tarellyk V. Performance analysis of GO gel composite coating on electro-spark deposited surfaces, International Science Journal of Engineering & Agriculture. 2023, 2(5), 20-30. DOI: <https://doi.org/10.46299/j.isjea.20230205.03> (PhD participant in carrying out of investigation, review and editing, preparation of article for printing).

7. Zhang Zhengchuan, Ievgen Konoplianchenko, Viacheslav Tarellyk, Liu Guanjun, **Du Xin**, Yu Hua. The Characterization of Soft Antifriction Coating on the Tin Bronze by Electro-spark Alloying. Materials Science (Medžiagotyra). 2023, 29(1), 40-47. (PhD participant in carrying out of experimental researches, processing of results).

DOI: <http://dx.doi.org/10.5755/j02.ms.30610> (**Scopus Q3, Web of Science**)

8. Zhang Zhengchuan, Viacheslav Tarellyk, Ievgen Konoplianchenko, Liu Guanjun, **Du Xin**, Ju Yao. The Characterization of Tin Bronze Substrates Coated by Ag+B83 through Electro-spark Deposition Method. *Surface Engineering and Applied Electrochemistry*. 2023, 59(2), 220-230. (PhD participant in carrying out of experimental researches, processing of results).

DOI:<https://doi.org/10.3103/S1068375523020187> (**Scopus Q3, Web of Science**)

9. Zhang Zhengchuan, Viacheslav Tarellyk, Ievgen Konoplianchenko, Liu Guanjun, Wang Hongyue, **Du Xin**, Ju Yao, Li Zongxi. New evaluation method for the characterization of coatings by electroerosive alloying. *Materials Research Express*. 2023, 10(3), 036401. (PhD participant in carrying out of experimental researches, processing of results).

DOI:<https://doi.org/10.1088/2053-1591/acc15b> (**Scopus Q1, Web of Science**)

10. Zhang Zhengchuan, Ievgen Konoplianchenko, Viacheslav Tarellyk, Liu Guanjun, **Du Xin**, Yu Hua. The Characterization of Running-In Coatings on the Surface of Tin Bronze by Electro-spark Deposition. *Coatings*. 2022, 12(7), 930-945. (PhD participant in carrying out of experimental researches, processing of results, preparation of article for printing).

DOI:<https://doi.org/10.3390/coatings12070930> (**Web of Science Q2, Scopus Q2**)

11. **Du Xin**, Tarellyk V. Study on the properties of electro-spark deposited SKH51+WC gradient coating on 45 steel. *Proceedings of the 2nd International*

scientific and practical conference. CPN Publishing Group. Tokyo, Japan. 2023. 207-213. ISBN 978-4-9783419-2-1. (PhD participant in carrying out of experimental researches, processing of results)

12. **Du Xin**, Tarelnyk V., Konoplianchenko Ie. Study on the deposition property of SKH51 transitional coatings by TAGUCHI orthogonal array method, Proceedings of the 10th International scientific and practical conference, Barca Academy Publishing. Madrid, Spain. 2023. 117-122. ISBN978-84-15927-34-1 (PhD participant in carrying out of experimental researches, processing of results)

13. **Du Xin**, Tarelnyk V. Research on performance of SKH51+WC+B83 composite coatings in locking mechanism of electric vehicle, Proceedings of the 10th International scientific and practical conference, Barca academy publishing, Madrid, Spain. 2023. 123-128. ISBN 978-84-15927-34-1 (PhD participant in carrying out of experimental researches, processing of results)

14. **Du Xin**, Ievgen Konoplianchenko, Viacheslav Tarelnyk, Development directions and perspectives of eds technologies. The 27th International Scientific and Practical Conference, Sumy, Ukraine. 2021. 214-217. (PhD participant in carrying out of experimental researches, processing of results)

15. **Xin D**, Tarelnyk V., Konoplianchenko Ie., Zhaoyang Song. The orthogonal design of wc-8co reinforcement thickness on experimental analysis. The 10th International scientific and practical conference (December 25-27, 2022), Lviv, Ukraine. 2022. 347-352. ISBN 978-966-8219-86-3 (PhD participant in carrying out of experimental researches, processing of results, preparation of article for printing)

16. **Xin D.** Technology of deposition of power lines of road transport systems. Збірник тез доповідей VI Міжнародної науково-практичної конференції «Автомобільний транспорт та інфраструктура» (19–21 квітня 2023 року). Національний університет біоресурсів і природокористування України. Київ. 2023. 144-145. ISBN 978-617-8102-96-8. (PhD participant in carrying out of experimental researches)

17. **Du Xin**, Viachesla Tarelnyk, Ievgen Konoplianchenko, Song Zhaoyang. Simplified model of wear parameters for electro-spark coatings. Proceedings of the XXXIV International Scientific and Practical Conference (August 29 – September 01, 2023). Warsaw, Poland. 2023. 169-173. ISBN 979-8-89145-197-1. (PhD participant in carrying out of experimental researches, processing of results)

18. **Xin D**, Tarelnyk V., Konoplianchenko I., Zhaoyang Song. Calculation and analysis of single pulse energy for electro-spark deposition of low temperature alloy. Proceedings of the 12th International scientific and practical conference. CPN Publishing Group. Osaka, Japan. 2023. 63-67. ISBN 978-4-9783419-1-4 (PhD participant in carrying out of experimental researches, processing of results)

19. Zhang Zhengchuan, Viacheslav Tarelnyk, Ievgen Konoplianchenko, Liu Guanjun, **Du Xin**, Yu Hua. Research on the Characterization of Ag+Cu+B83 Composite Coatings on the Surface of Tin Bronze by Electro-spark Deposition (2021) Proceedings of the 2021 IEEE 11th International Conference on "Nanomaterials: Applications and Properties", NAP 2021, 1-8. (PhD participant in carrying out of experimental researches, processing of results)

DOI: <https://doi.org/10.1109/NAP51885.2021.9568514> (SCOPUS)

20. Zhang Zh., Konoplianchenko Ie.V., Tarellyk V.B., **Du X.** The future research direction of the ESD deposition technology. *Машинобудування очима молодих: прогресивні ідеї – наука – виробництво: матеріали XX Міжнародної науково-технічної конференції (м. Суми, 29 вересня – 1 жовтня 2021 року) / редкол.: В. О. Залога, В. О. Іванов. – Суми: Сумський державний університет, 2021. 21-23. (PhD participant in carrying out of investigation, review and editing). (SCOPUS)*

21. V. Tarellyk, O. Gaponova, V. Martsynkovskyy, I. Konoplianchenko, V. Melnyk, V. Vlasovets, A. Sarzhanov, N. Tarellyk, **D. Xin**, Y. Semirnenko, S. Semirnenko, T. Voloshko, O. Semernya. Energy Dispersive X-Ray Microanalysis of Part Surface Layer Carburized by Electric Spark Alloying. 2020 IEEE 10th International Conference Nanomaterials: Applications & Properties (NAP), Sumy, Ukraine, 2020, pp. 01TFC13-1-01TFC13-9, (PhD participant in carrying out of experimental researches, processing of results) DOI: <https://doi.org/10.1109/NAP51477.2020.9309618>. (SCOPUS)

APPENDIX B. Documents on the implementation of the results of the dissertation

Certification

Du Xin completed the industry practical application of new repairable coating in the industrial equipment. The new environmental protection technology of new repair anti-wear coating was implemented, and the process design, manufacture, installation and commissioning were carried out. In the electric vehicle, the key components of the replaceable battery can be replaced to reduce wear and improve the life of the product. The new coating technology has low maintenance cost and convenient production, and the stability and reliability of repaired key parts are obviously improved. The scientific results are valuable for industry.

Hereby certify.

XinXiang New Energy Electric Vehicle Co., Ltd.



May 20, 2023